Non-canonical functions of the MDM2 oncoprotein

Dissertation

for the award of the degree

"Doctor rerum naturalium"

of the Georg-August-Universität Göttingen

within the doctoral program

International Max Planck Research School for Molecular Biology

of the Georg-August University School of Science (GAUSS)

submitted by

Valentina Manzini

from Marino, Italy

Göttingen, 2022

Thesis Committee

Prof. Dr. Matthias Dobbelstein

Institute of Molecular Oncology, Göttingen Center for Molecular Biosciences

Prof. Dr. Argyris Papantonis

Institute of Pathology, University Medical Center Göttingen

Prof. Dr. Markus Bohnsack

Department of Molecular Biology, University Medical Center Göttingen

Members of the Examination Board

1st Referee

Prof. Dr. Matthias Dobbelstein

Institute of Molecular Oncology, Göttingen Center for Molecular Biosciences

2nd Referee

Prof. Dr. Argyris Papantonis

Institute of Pathology, University Medical Center Göttingen

Further members of the Examination Board

Prof. Dr. Markus Bohnsack

Department of Molecular Biology, University Medical Center Göttingen

Prof. Dr. Heidi Hahn

Institute for Human Genetics, University Medical Center Göttingen

Prof. Dr. Melina Schuh

Department of Meiosis, Max Planck Institute for Biophysical Chemistry, Göttingen

Dr. Jochen Rink

Department of Tissue Dynamics and Regeneration, Max Planck Institute for Biophysical Chemistry, Göttingen

Date of oral examination: 8 March 2022

Declaration

Herewith I declare that I prepared the dissertation titled **“Non-canonical functions of the MDM2 oncoprotein”** in my own capacities with no other sources and aids than quoted.

Valentina Manzini

Göttingen, January 2022

Table of Contents

List of Figures ……vi
Abbreviations……..vii
ABSTRACT……x
1 INTRODUCTION 1
1.1 The transcription factor *TP53* 1
1.1.1 p53 structure and regulation 1
1.1.2 Stress signals inducing p53: DNA damage and ribosomal stress 2
1.1.3 p53 canonical target genes and cellular outcomes 3
1.2 MDM2 as effector protein of p53-dependent responses 5
1.2.1 The p53/MDM2 negative feedback loop 5
1.2.2 Expression and structure of MDM2 7
1.3 Canonical and non-canonical functions of MDM2 8
1.4 Interactions of MDM2 with ribosomal proteins regulate cellular processes in response to nucleolar stress 9
1.4.1 The nucleolus is the site of ribosome biogenesis and a major stress sensor 9
1.4.2 Ribosome biogenesis requires the activity of all three RNA Polymerases 11
1.4.3 Pre-rRNA processing in humans 13
1.4.4 MDM2 interacts with ribosomal proteins in response to ribosomal stress 15
1.5 The role of MDM2 in DNA replication 16
1.5.1 DNA replication is a highly plastic and complex process 16
1.5.2 MDM2 can regulate DNA replication speed and PARP1 levels 18
1.6 Other non-canonical functions of MDM2 19
1.6.1 MDM2 can regulate gene expression and chromatin modifications 19
1.6.2 MDM2 and DNA damage repair 19
1.7 Scope of the thesis 20
2. MANUSCRIPT 1 21
2.1 INTRODUCTION 23
2.2 RESULTS 24
2.3 DISCUSSION 38
2.4 SUPPLEMENTARY DATA 40
2.5 METHODS 44

3. MANUSCRIPT 2 55
3.1 INTRODUCTION 57
3.2 RESULTS 59
3.3 DISCUSSION 74
3.4 SUPPLEMENTARY DATA 77
3.5 METHODS 83
4. DISCUSSION 89
4.1 MDM2, together with RPL5 and RPL11, inhibits RNA Pol III activity 89
4.2 MDM2 is an inhibitor of transcription 91
4.3 P53 activation induces nucleolar stress 92
4.4 MDM2 induction and cell death 93
4.5 MDM2 accumulation increases replication speed 95
4.6 MDM2 and DNA damage 97
4.7 Conclusions and further perspectives 98
5. APPENDIX 99
6. REFERENCES 103
7. ACKNOWLEDGMENTS 114

List of Figures

Figure 1: p53 structure……...2

Figure 2: the p53 pathways is activated upon cellular stress or chemical inhibition of the MDM2/p53 interaction……..6

Figure 3: structure of MDM2 and known interactions……..…8

Figure 4: the nucleoli are the site of rRNA synthesis……...10

Figure 5: ribosome biogenesis required the activity of all three RNA Polymerases……12

Figure 6: pre-rRNA processing in human cells is an intricate sequence of processing steps……13

Figure 7: DNA fork reversal and re-start…….....17

Abbreviations

µg	Microgram
µl	Microliter
µM	Micromolar
5-FU	5-fluorouracil
APAF-1	Apoptosis-peptidase activating factor-1
APS	Ammonium persulphate
ARF	Alternative Reading Frame
ATM	Ataxia Telangiectasia Mutated
ATR	Ataxia Telangiectasia And Rad3-Related
BAX	BCL2-associated X Protein
BCA	Bicinchoninic acid
BF	Bayes Factor
CDK	Cyclin-dependent kinase
CDK9i	CDK9 inhibitor
cDNA	Complementary DNA
ChIP	Chromatin Immunoprecipitation
C_t, C_T	Threshold cycle
CTD	C-terminal domain
Ctrl	Control
ddH_2O	Double-distilled H_2O
DFC	Dense fibrillar component
DMEM	Dulbecco's Modified Eagle Medium
DMSO	Dimethyl sulfoxide
DSB	DNA double-strand breaks
DTT	Dithiotreitol
EDTA	Ethylenediaminetetraacetic acid
EdU	5-ethynyl-2'-deoxyuridine
EtOH	Ethanol
ETS	External transcribed spacer
FBL	Fibrillarin
FBS	Fetal bovine serum
FC	Fibrillar center
GAPDH	Glyceraldehyde-3-phosphate dehydrogenase

GC	Granular component
GSK-3b	Glycogen synthase kinase-3b
H3	Histone 3
HCl	Hydrochloric acid
HRP	Horseradish peroxidase
HSC	Hematopoietic stem cell
i.a.	Among other things (Latin *inter alia*)
i.e.	That is (Latin *id est*)
IC_{50}	Half maximal inhibitory concentration
IGS	Intergenic spacer
IRBC	Impaired Ribosome Biogenesis Checkpoint
ITS	Internal transcribed spacer
KCl	Potassium chloride
KDM	Histone lysine demethylase
MDM2	Murine double minute 2 homolog
miRNA	microRNA
mRNA	Messenger RNA
mTOR	Mammalian target of rapamycin
NCL	Nucleolin
NES	Nuclear export signal
NLS	Nuclear localization signal
NML	Nucleomethylin
NOLS	Nucleolar localization signal
NOR	Nucleolar organizer region
NPM	Nucleophosmin
ns	Not significant
PAGE	Polyacrylamide gel electrophoresis
PARP	Poly(ADP-ribose) polymerase
PBS	Phosphate buffered saline
PIC	Pre-initiation complex
pRb	Retinoblastoma protein
PRC2	Polycomb Repressor Complex 2
PROTAC	Proteolysis targeting chimera
PUMA	p53-upregulated mediator of apoptosis
rDNA	Ribosomal DNA

rev	Reverse
RING	Really Interesting New Gene
RISC	RNA-induced silencing complex
ROI	Region of interest
ROS	Reactive oxygen species
RNA Pol (I,II,III)	RNA polymerase (I,II,III)
RP	Ribosomal protein
rRNA	Ribosomal RNA
RT	Room temperature
RT-qPCR	Real-time quantitative PCR
SDS	Sodium dodecyl sulphate
siRNA	Small interfering RNA
SL1	Selectivity factor 1
snoRNA	Small nucleolar RNA
snoRNP	Small nucleolar ribonucleoprotein complex
SNP	Single nucleotide polymorphism
snRNA	Small nuclear RNA
SSU	Small subunit
SUV39H1	Suppressor of variegation 3-9 homolog 1
TAD	Transactivation domain
TBP	TATA-binding protein
TIF1-A	Transcription initiation factor 1A
Tris	Tris(hydroxymethyl)-aminomethan
tRNA	Transfer RNA
TTF-1	Transcription termination factor 1
UBF	Upstream binding factor

ABSTRACT

The tumour suppressor gene *TP53* is mutated in ~50% of human cancers. The p53 protein is a transcription factor which is induced by several cellular stresses, such as ribosomal stress and DNA damage. Expression of its target genes leads to cell cycle arrest, apoptosis, or senescence. MDM2 is one of these target genes and acts as a negative regulator by binding to p53, leading to its proteasomal degradation and inhibition. MDM2 and p53 are thus linked by a negative feedback loop which provides cells with an additional layer of regulation. In recent years, several non-canonical functions of the E3 ubiquitin ligase MDM2 have been uncovered which do not involve the negative regulation of p53. In this thesis we investigated two of these non-canonical roles, in the context of ribosome biogenesis and DNA replication.

Firstly, we employed the proteolysis targeting chimera (PROTAC) strategy to deplete MDM2 in proliferating cells, in the presence of p53 activation. We found that MDM2 accumulation inhibits RNA Polymerase III activity and reduces the levels of nascent 5S rRNA, an essential component of the ribosomes, through interaction with the ribosomal proteins RPL5 and RPL11. Prolonged p53 activation and MDM2 accumulation, *via* treatment with the cis-imidazoline analog Nutlin-3, led to disrupted ribosome biogenesis and diminished RNA Pol I activity, independent of external stresses.

Secondly, we showed that MDM2 represses fork reversal, a protective mechanism that reverses DNA replication forks in the presence of DNA damage. MDM2 accumulation also increased the progression of of DNA replication forks, and depletion of either the helicase RECQ1, or the primase-polymerase PRIMPOL, reversed this effect. Poly- (ADP-ribose) polymerase 1 (PARP1) was previously shown to prevent premature restart of reversed forks through inhibition of RECQ1. Here, we identified MDM2 as a novel interaction partner of PARP1 which mediates its proteasomal degradation and inhibition.

Taken together, MDM2 performs at least two additional functions, on top of antagonizing p53. It dampens the synthesis of an entire class of RNAs, i.e. Polymerase III transcripts, and it prevents a protective mechanism for DNA replication forks. We speculate that these non-canonical functions of MDM2 might contribute to cell death in the context of p53 activation.

1 INTRODUCTION

1.1 The transcription factor *TP53*

The p53 tumour suppressor, encoded by the *TP53* gene, is one of the most frequently mutated protein in human cancers. More than half of all human cancers present a p53 mutation, while the rest inactivate wild type p53 by viral proteins or by amplification of its negative regulators (Horn and Vousden, 2007a). Since its discovery in 1979, p53 has also become the most intensively studied molecule in biomedical research, with an astonishing 37,896 publications containing the term “p53” in their title (as of January 2022, from PubMed). Even after more than 40 years of research, we are far from understanding the fine mechanisms driving this complex network. The reason behind such complexity comes from the fine-tuning of p53 activation and expression of its target genes, which is often very context specific (Horn and Vousden, 2007a; Smeenk et al., 2008). The cellular outcomes upon p53 activation are regulated at different levels, which can be divided in: 1. the nature of stress signals, 2. the set of proteins, including p53 itself, which regulates p53 activity and stability, 3. the p53-target genes induced.

1.1.1 p53 structure and regulation

P53 has a molecular weight of 53 kDa and it is composed of several domains, as shown in Figure 1. The N-terminal region is highly acidic and contains several hydrophobic residues crucial for protein-protein interactions. This domain comprises of two Transactivation Domains (TAD1 and TAD2) that can bind transcriptional co-regulators (Candau et al., 1997). Among others, this region is essential for interaction with p53-negative regulators MDM2 and MDMX (Wallace et al., 2006), positive regulators as well as histone acetyltransferases p300/CBP (Lill et al., 1997) and receptor SMAD2/3 (Cordenonsi et al., 2003). Between amino acids 60-90 there is a proline-rich domain that can regulate transactivation of p53 and induction of apoptosis (Edwards et al., 2003).

The central domain of p53, from residue 102 to residue 292, consists of a DNA binding domain which specifically binds to p53 response elements (p53RE). These elements are characterized by two palindromic sequences RRRCWWGYYY (R = A, G; Y = C, T; W = A, T) separated by a variable spacer (Smeenk et al., 2008). Since this region is essential for induction of tumour suppressor genes, it is the most highly mutated in cancers. The majority of such mutations are missense mutations, also denominated “hotspot mutation”, which alter the amino acid sequence and disrupts binding to DNA (Baugh et al., 2018).

The carboxyl terminus of p53 contains a tetramerization domain (Tet) and an unstructured and basic C-terminal domain (CTD). The Tet domain allows formation of the active p53 tetramer from two homodimers, which can bind DNA and activate gene expression (Chène, 2001). The CTD can regulate p53 function by adopting different conformation upon interaction with different partners (Sullivan et al., 2018). Moreover, this region also harbours a nuclear localization signal (NLS) and a nuclear export signal (NES) which regulates the cellular localization of p53.

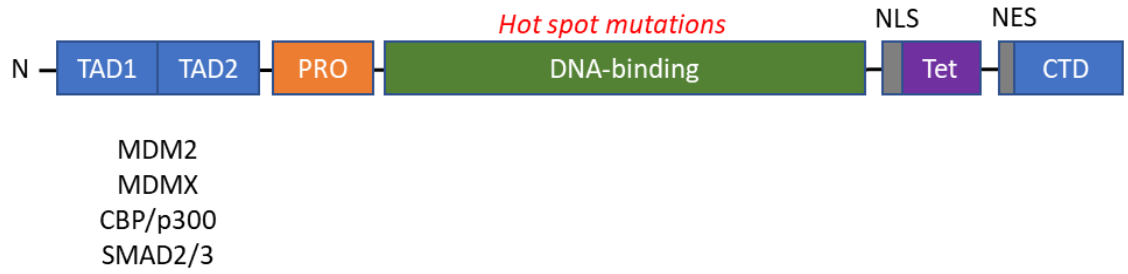

Figure 1: p53 structure

P53 is a multi-domain protein composed of two transactivation domains (TAD), a proline stretch (PRO), a central DNA-binding domain, a tetramerization domain (Tet) and a c-terminal domain (CTD). The central DNA-binding domain harbours the majority of p53 mutations found in cancers, and such “hotspot” mutations usually deactivate p53 binding to the DNA. The C-terminal region of the protein also contain a nuclear localization signal (NLS) and a nuclear export signal (NES).

1.1.2 Stress signals inducing p53: DNA damage and ribosomal stress

A variety of diverse cellular stresses, both extrinsic and intrinsic, can stabilize and activate p53. DNA damage, reactive oxygen species (ROS), ribosomal stress, oncogenes activation and hypoxia are some of the stimuli that have been shown to activate the p53 pathway (Horn and Vousden, 2007b). DNA damage strongly induces a p53 response through the ATM/ATR kinases, which phosphorylates both p53 and MDM2 (Shieh et al., 1997; Siliciano et al., 1997). Phosphorylation of the amino terminal of p53 disrupts its interaction with MDM2, thus limiting proteasomal degradation of p53. Moreover, phosphorylation of MDM2 also disrupts this interaction and enhances MDM2 degradation (Gannon et al., 2012; Meek and Hupp, 2010), further stabilizing p53. Moreover, p53 activation has also been shown to prevent DNA damage by supporting DNA replication (Klusmann et al., 2016). Another strong inducer of the p53 protein is disruption of ribosome biogenesis, also known as “ribosomal stress” or “nucleolar stress” (Holmberg Olausson et al., 2012; Russo and Russo, 2017; Yang et al., 2018). The nucleoli are the site of ribosome biogenesis and RNA Polymerase I transcription. When ribosome biogenesis is deregulated by oncogenes activation or pharmacological inhibition of RNA Pol I, ribosomal proteins (RP) leak from the nucleoli to the nucleoplasm and bind MDM2,

sequestering it from p53 (Russo and Russo, 2017). Alternatively, ARF has been also shown to recruit MDM2 in the nucleoli, which ultimately leads to p53 activation (Weber et al., 1999).

All these stress signals result in loss of fidelity in cellular duplication and can activate p53 through different pathways. The fact that evolution has opted for a single, central cellular node to respond to so many stresses is puzzling. Indeed, the p53 gene is mutated about 50% of the time in cancers (Soussi, 2005). Why is there not an alternative pathway, that could limit the vulnerability of p53 to mutations? We currently cannot answer this question, but we can speculate; having one protein coordinating so many processes might be simply the most efficient and fast way to respond to a wide range of stresses, while having separate pathways could add complexity and therefore, slow down the response.

1.1.3 p53 canonical target genes and cellular outcomes

Once the p53 protein accumulates in response to stress signals, it can tetramerize and bind to p53 responsive elements in the genome. Different types of stress inputs seem to result in different transcriptional outcomes by p53 (Zhao et al., 2000). Dozens of p53-target genes have been identified, with high variability across cell lines; however, a core transcriptional program of ~100 genes has been recently identified which is preserved across cell types (Andrysik et al., 2017). P53-target gene expression is necessary to prevent tumour progression through induction of cell cycle arrest, senescence, apoptosis, and DNA repair.

Although p53 is known as a “guardian of the genome”, its activation is extremely toxic to cells in the absence of stress. Therefore, p53 levels must be tightly regulated and kept low in the absence of cellular stresses. This is achieved by expression of MDM2, an E3 ubiquitin ligase which ubiquitinates p53 leading to its proteasomal degradation. MDM2 is induced by p53 itself, which means these proteins are linked by a negative feedback loop. MDM2 depletion has been shown to be lethal in mice, confirming it’s essential role in inhibiting p53 (Jones et al., 1995).

Among the core p53-induced genes, $p21^{Cip1}$ (*CDKN1A*) is responsible for cell cycle arrest in G1 following p53 activation (Gartel et al., 1996). P21 is a cyclin-dependent kinase inhibitor capable of inhibiting CDK2, CDK1 and CDK4/6 by directly interacting with them, therefore regulating progression from G1 to S phase (Gartel et al., 1996). In the absence of p21, formation of CDK/Cyclin complexes allows for proper ATP binding and kinase activity, which allows them to phosphorylate a negative regulator of gene expression, the Rb (retinoblastoma) protein. Rb is usually found in a complex with the E2F transcription factors family, thereby inhibiting its binding to DNA target genes (Nevins et al., 1997). Upon phosphorylation by

CDK/cyclin, Rb is released from E2F, which is then free to activate gene expression and induce G1 to S phase progression.

Another cellular consequence of p53 activation is induction of apoptosis. This is mainly achieved through expression of pro-apoptotic BH3-only proteins BCL2 Binding Component 3 (BBC3, commonly known as PUMA) and Phorbol-12-Myristate-13-Acetate-Induced Protein 1 (PMAIP1, commonly known as NOXA) (Bennett, 1999). BH3-only proteins bind and inhibit with pro-survival BCL-2 protein, which then leads to release and activation of pro-apoptotic effectors BAX and BAK. These factors cause mitochondrial outer membrane permeabilization (MOMP), release of cytochrome C and consequential activation of caspases. Interestingly, PUMA seems to contribute more strongly to induction of apoptosis compared to NOXA, with few exceptions (Jeffers et al., 2003; Villunger et al., 2003). This suggests that different cytotoxic stimuli and the type of tissue might affect the relative contributions of PUMA and NOXA in induction of apoptosis. Moreover, in non-transformed cells, only combined loss of PUMA and NOXA confers full protection against induction of apoptosis *via* γ-radiation or DNA damage-inducing chemotherapeutics, suggesting that NOXA can compensate for PUMA (Michalak et al., 2008). However, this is not the case for tumour cells, where p53 activation does not always lead to cell death, and where depletion of PUMA and NOXA is not always protective against apoptosis. Response to p53 is highly context-dependent, varying across cell lines, even when derived from the same tumour identity (Kastenhuber and Lowe, 2017).

Regarding induction of apoptosis, there are several possible explanations for such variability:

1) In cancer cells, p53 has been shown to also induce expression of other pro-apoptotic genes such as BIM, BAX and APAF-1 (Kannan et al., 2001; Li et al., 2012; Mirjolet et al., 2000), suggesting that several factors might be involved. BIM in particular might act in synergism with PUMA and NOXA, since depletion of all three factors was as protective as depletion of p53, at least in lymphoma cells (Happo et al., 2010).

2) P53 activation has been shown to induce caspase-independent pathways of cell death, which do not require activity of pro-apoptotic factors. For example, p53 induces ferroptosis by repressing expression of SLC7A11, a member of the cystine/glutamate antiporter and the main target for the drug Erastin (Jiang et al., 2015). Moreover, p53 also plays a role in necroptosis, a regulated form of necrosis which can be induced by oxidative stress. P53 can directly cause mitochondrial swelling and permeabilization, in BAX/BAK double knockout MEFs (Vaseva et al., 2012).

3) Other p53-target genes, which are not described as strictly anti-apoptotic, might be inducing cell death in response to p53, and such target genes are cell line specific. For example MDM2

overexpression has been shown to be very toxic in cells, also in the absence of p53 (Bohlman and Manfredi, 2014).

In general, the mechanistic basis determining cell fate in response to p53 induction (cell cycle arrest, senescence, or apoptosis) are unknown, and a big question in the field remains: why is p53 activation and gene expression so context-dependent, and what are the mechanisms determining such specificity?

1.2 MDM2 as effector protein of p53-dependent responses

MDM2 is the negative regulator of p53, and as such it has always been considered as an oncogene (Zhao et al., 2014). However, beside its canonical role in degrading p53, recent studies have revealed several non-canonical functions of MDM2, some of these being tumour-suppressor. MDM2 has been shown to regulate replication, chromatin modifications and DNA repair (Bohlman and Manfredi, 2014; Fåhraeus and Olivares-Illana, 2014). Due to its complex interactome, MDM2 can be described as a regulatory hub; depending on which protein MDM2 interacts with, it can have different effector functions (Fåhraeus and Olivares-Illana, 2014). The next sections will focus on some of these effector functions.

1.2.1 The p53/MDM2 negative feedback loop

Before going into the specifics of the MDM2 effector functions, it is important to understand its complex relationship with p53. P53 can transcriptionally induce MDM2 expression, and in return MDM2 ubiquitinates and degrades p53. Moreover, MDM2 can also ubiquitinate itself, keeping its own levels low. These proteins are therefore linked by a negative feedback loop (Figure 2), and this is essential to avoid cytotoxicity of p53 in unstressed cells (Picksley and Lane, 1993).

Experimentally, the MDM2/p53 axis can be investigated using *cis*-imidazoline analogs, such as Nutlin-3a, which inhibit the interaction between MDM2 and p53, thus leading to its activation and expression of target genes, including MDM2 itself (Figure 2) (Khoo et al., 2014). Nutlin-3a binds to the hydrophobic domain of MDM2, which is also the interaction region with p53, thus disrupting their interaction and leading to p53 accumulation and activation. The advantage of this strategy is that p53 can be activated without induction of external stresses (such as DNA damage), which makes it easier to distinguish cellular effects due to activation of p53 compared to activation of other stress pathways.

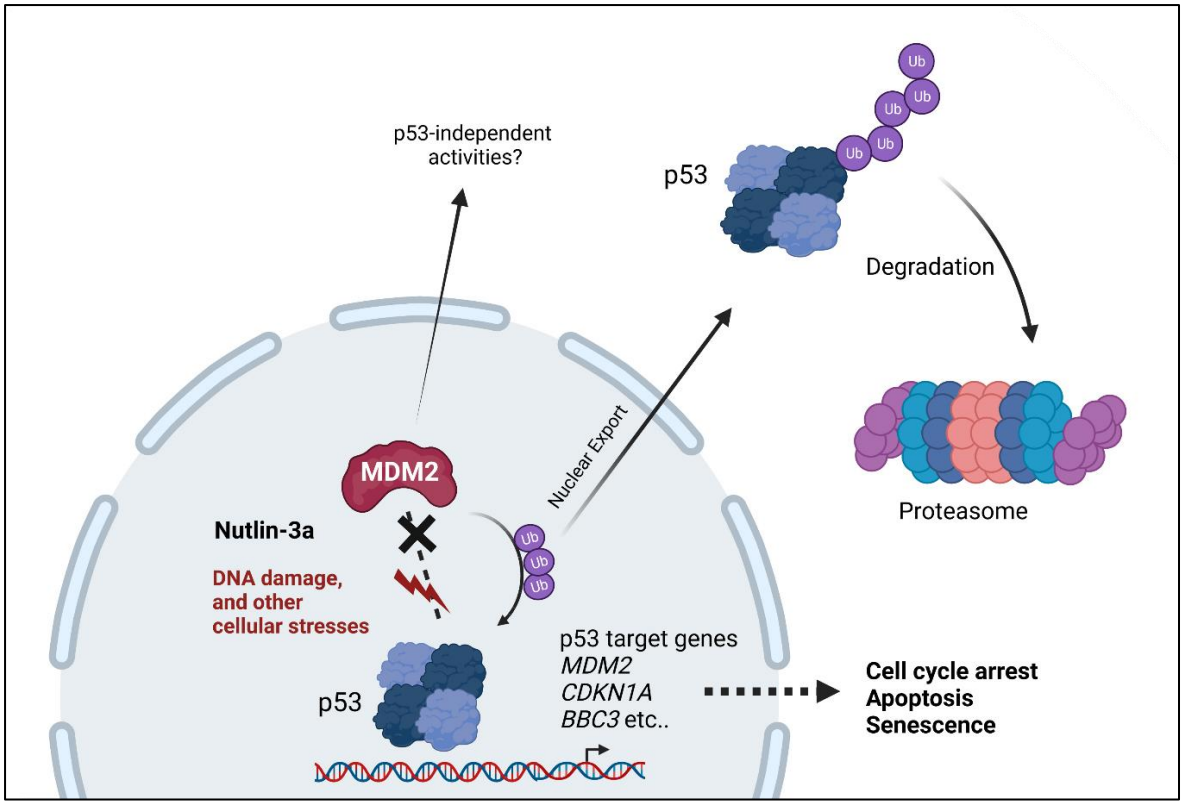

Figure 2: the p53 pathway is activated upon cellular stress or chemical inhibition of the MDM2/p53 interaction

In unstressed cells, MDM2 binds and poly-ubiquitinates p53, leading to its proteasomal degradation and preventing induction of cell cycle arrest or apoptosis in the absence of stress. Upon cellular stresses such as DNA damage, hypoxia or ribotoxic stress, the p53 protein accumulates and tetramerizes with other p53 proteins, leading to target genes expression including *MDM2*. Upon post-translational modification of both p53 and MDM2, the interaction between them is disrupted, and MDM2 cannot ubiquitinate and degrade p53, thus enabling p53 accumulation and activation. Similarly, Nutlin-3a binds the hydrophobic pocket of MDM2, thus preventing its interaction with p53, and enabling p53-target genes expression, including *MDM2* itself, but also *CDKN1A/p21* or *PUMA/BBC3* in the absence of external stresses. P53 and MDM2 are thus linked by a negative feedback loop where p53 induces expression of *MDM2* and MDM2 keeps p53 levels low in return. Created with BioRender.com.

However, it also makes it quite difficult to study MDM2 functions in cells, since its depletion causes cell cycle arrest, p53 accumulation and activation of its numerous target genes. This is the reason why several non-canonical functions of MDM2 have been underappreciated until recently. However, specific strategies can be used to study MDM2 effector functions in the lab:

1) Employing $p53^{-/-}$ cells, and ectopically overexpressing MDM2 using plasmids. This allows to investigate eventual unknown non-canonical functions of MDM2, which might

also be independent of p53. In this context, transient depletion of MDM2 could also be employed without induction of cell cycle arrest or apoptosis due to p53 activation.

2) Using a Proteolysis targeting chimera (PROTAC) against MDM2. The MD-224 MDM2 PROTAC is composed of two domains connected by a linker: one domain (MI-1061) is composed of a molecule that can act similarly to Nutlins, and can bind the hydrophobic pocket of MDM2; the other domain is the ligand pomalidomide that recruits the E3 ubiquitin ligase machinery Cereblon (Li et al., 2019). This strategy has the advantage of depleting MDM2 very fast, degrading protein levels within hours, which is quite convenient when avoiding prolonged p53 activation that would lead to cell cycle arrest and/or apoptosis. This allows investigation of MDM2 in the context of p53 activation, in proliferating cells.

In cells, stresses such as DNA damage induce post-translational modifications (PTM) on both p53 and MDM2, disrupting their interaction and rapidly accumulating p53 (Siliciano et al., 1997).

1.2.2 Expression and structure of MDM2

The *MDM2* gene has two separate promoters, of which the one upstream is constitutively active, but lowly expressed, and gives rise to a long isoform that is inefficiently translated due to the presence of two open reading frames (Brown et al., 1999). The second promoter, which is inducible by p53, gives rise to a shorter *MDM2* transcript which is more efficiently translated and gives rise to full length MDM2 protein (Brown et al., 1999).

Although MDM2 is a protein composed of only 491 aa, it is composed of several structural and functional domains, (Figure 3). The N-terminal domain comprises a hydrophobic pocket (aa 25-100) which is important for interacting with p53. This domain is also the binding site of many drugs (including Nutlins) that disrupt p53-MDM2 interaction. Towards the central region, there are a NLS (aa 179-185) and a NES (aa 190-202), allowing MDM2 to be localized both in the nucleus and in the cytoplasm. The acidic domain found between aa243-301 partially overlaps with a zinc finger domain (aa 290-335). This region is essential for interaction with many ribosomal proteins (Fåhraeus and Olivares-Illana, 2014). The c-terminal domain of MDM2 is composed of a RING (Really Interesting New Gene) domain, which harbours the E3 ubiquitin ligase activity. This domain is also responsible for binding RNA and contains a nucleolar localisation signal. The very last 9 aa regulate oligomerisation with other MDM2 proteins or with Mdm4 (Uldrijan et al., 2007).

To further add complexity, several regions of MDM2 are intrinsically disordered, and post-translational modifications within such domains might drastically change its conformation,

allowing it to acquire several interacting surfaces (Nicholson and Hupp, 2010). Unfortunately, due to such unstructured regions, it is quite difficult to perform structural studies on MDM2, so the different conformational changes of MDM2 are currently not known. In the past few years, more than 100 proteins have been described to interact with MDM2, making MDM2 effectively a hub protein (Fåhraeus and Olivares-Illana, 2014). This promiscuous nature can be partially explained by its structure and PTMs of MDM2, although it is currently not known how such interactions are regulated to achieve specificity.

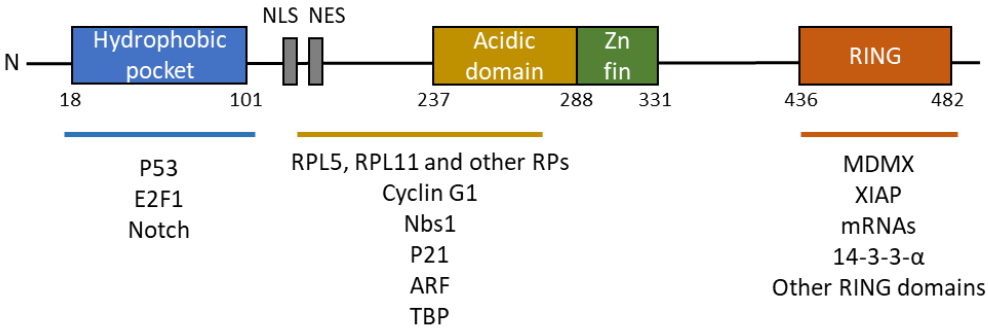

Figure 3: structure of MDM2 and known interactions

MDM2 is a multi-domain protein composed of a hydrophobic pocket, a central acidic domain which partially overlaps with a Zn finger, and a RING domain with E3 ubiquitin ligase activity. A NLS and NES are also present, allowing import/export of MDM2 from the nucleus. MDM2 is also characterized by intrinsically disordered regions which make its structure quite flexible and allows MDM2 to assume multiple conformations. Known interacting partners of MDM2 and their relative binding region are also displayed.

1.3 Canonical and non-canonical functions of MDM2

The canonical and most well understood function of MDM2 is to ubiquitinate and degrade p53. MDM2 ubiquitinates p53 at six C-terminal lysins; this is only possible when p53 is not acetylated (i.e. activated) since these PTMs are mutually exclusive (Liu et al., 2019). MDM2 can also monoubiquitinate p53 at multiple sides, and this leads to re-localization of p53 to the cytoplasm, leading to its inactivation as transcription factor (Brooks and Gu, 2011). It has been proposed that MDM2 alone can monoubiquitinate p53 at multiple sites, while MDM2 heterodimerization with MDM4 is necessary for polyubiquitination of p53 (Gu et al., 2002). This is probably because MDM2, when not heterodimerized, ubiquitinates itself quite fast therefore leading to a shorter half-life. MDM2 can also inhibit p53 transcriptional activity by direct interaction. Upon DNA damage, MDM2 is then released from p53, which is then free to activate gene expression (Linke et al., 2008).

The importance of MDM2 was first observed when trying to create a $MDM2^{-/-}$ mouse line; this was impossible due to embryonic lethality caused by activation of p53 and uncontrolled apoptosis (Jones et al., 1995). This lethality was rescued by knockout of both MDM2 and p53. However, $MDM2^{-/-}p53^{-/-}$ mice showed an increased frequency of sarcomas compared to $p53^{-/-}$ mice alone, but that still retained MDM2. This led to the hypothesis that MDM2 might harbour p53-independent functions or might have other non-canonical roles in the cell independent of degradation of p53. Moreover, MDM2 is rarely mutated in cancer, but frequently overexpressed in sarcomas, with elevated levels associated with poor prognosis (Oliner et al., 2016). However, MDM2 overexpression rarely occurs together with p53 mutation, suggesting that retaining MDM2 activity might benefit cancer cells, possibly due to other non-canonical functions of MDM2 (Bohlman and Manfredi, 2014).

In recent years, several interaction partners of MDM2 have been identified which have been linked to non-canonical functions of MDM2. Some of these interactions are dependent on p53 activation, while others do not require p53 activity at all (Fåhraeus and Olivares-Illana, 2014). The sections below will focus on some of the most studied non-canonical activities of MDM2 in the context of nucleolar stress, ribosomal proteins, DNA replication and repair, transcription, and chromatin modifications.

1.4 Interactions of MDM2 with ribosomal proteins regulate cellular processes in response to nucleolar stress

Events that disrupt ribosome biogenesis, such as oncogenes, UV radiation or RPs imbalance, lead to activation of certain response pathways governed by the nucleolus to make sure the cell homeostasis is preserved. The activation of such response pathways is due to nucleolar or ribotoxic stress, and they can induce p53 activity or not. In the presence of nucleolar stress, several RPs bind MDM2 both in the nucleolus and in the cytoplasm, reinforcing p53 activation. The next paragraphs will further expand on this topic.

1.4.1 The nucleolus is the site of ribosome biogenesis and a major stress sensor

The nucleolus was first identified by microscopy at the beginning in 1830, although their cellular function has been a mystery until 1960s, when it was discovered that nucleoli are the site of rRNA synthesis (Wallace and Birnstiel, 1966). In the past 50 years, nucleoli have emerged as essential organelles involved in many important cellular processes and homeostasis. Nucleolar function is particularly important in proliferating cells since it needs to provide enough ribosomes to meet the requirements for high protein synthesis. Already long time ago, nucleolar size was used as a parameter to determine the proliferation and growth intensity in cancer cells (Stępiński, 2018). From then, it has become evident that an increase in size and number of nucleoli reflects an enhanced rate of proliferation.

From a structural point of view, nucleoli are formed around rDNA repeats in the nucleolar organizing regions (NORs), which are located in the short arms of five acrocentric chromosomes in humans (Mangan et al., 2017). The nucleolus is an organelle which is not enclosed by a membrane; It is a highly dynamic structure where components can diffuse in and out freely. In recent years, the role of liquid-liquid phase separation in forming the nucleoli has been increasingly recognized (Feric et al., 2016). However, it is more probable that the nucleolar structure is maintained by a combination of phase separation and anchoring agents. For example, distal junctions sequences, which are telomeric sequences of NORs containing regions, have been suggested to anchor rDNA to the perinuclear heterochromatin characteristic of nucleoli (Mangan et al., 2017). Moreover, several lamins have also been shown to connect the nucleoli to nuclear matrix and might contribute to maintain nucleolar structure (Sen Gupta and Sengupta, 2017; Martin et al., 2009).

The nucleoli are composed of three substructures with different functions, as shown in Figure 4. The fibrillar centres (FCs) contain rDNA and chromatin associated factors; rRNA transcription occurs at the interface between FCs and the dense fibrillary component (DFC). The DFC is also where early pre-rRNA processing occurs. Finally, the granular component (GC), the most external substructure, is where late processing of pre-rRNA and ribosome assembly takes place (Stępiński, 2018; Yang et al., 2018). This tripartite nucleolar structure strictly depends on rRNA synthesis, and when RNA Pol I is inhibited, the nucleoli disintegrate.

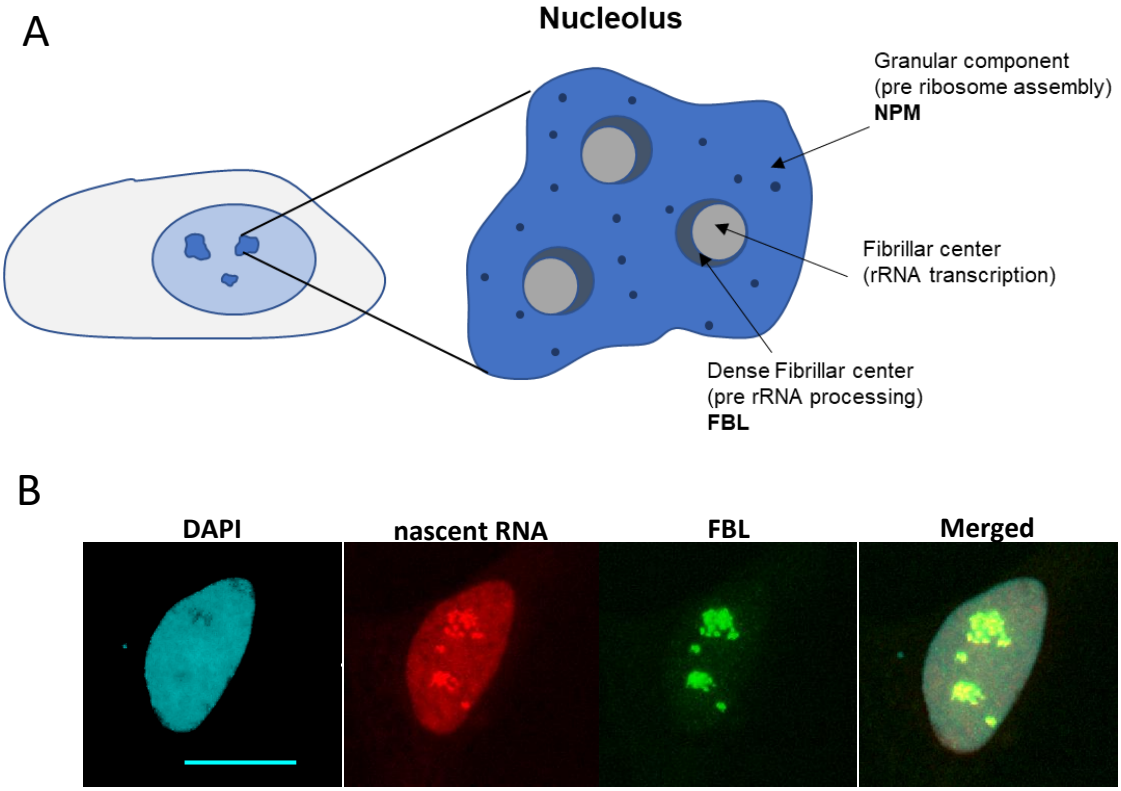

Figure 4: the nucleoli are the site of rRNA synthesis

A) The nucleoli are sub-nuclear organelles which are not enclosed by a membrane. Instead, a combination of protein-protein interactions and phase separation are thought to maintain the nucleolar structure. The nucleolus is the site of rRNA synthesis and processing, as well as where ribosomes are assembled. Structurally, they are composed of three defined regions which are also involved in different steps of ribosome biogenesis: an external granular component where pre-ribosomes are assembled, a dense fibrillar center where pre-rRNA is processed, and an inner fibrillar center where rRNA is transcribed by RNA Pol I.
B) Experimentally, nascent transcription can be visualized via chemical labelling the nascent RNA of live cells using Ethynyl Uridine (EU), as shown in the red channel. Nucleoli can be visualized by staining with known markers, such as Fibrillarin (FBL), which is a protein involved in pre-rRNA modification and it is localized in the dense fibrillar center. In cancer cells, rRNA synthesis can be clearly visualized in the nucleoli.

1.4.2 Ribosome biogenesis requires the activity of all three RNA Polymerases

Proliferating cells, especially cancer cells, require an enormous amount of energy, proteins, and ribosomes to sustain cell growth. Therefore, it is not surprising that cancer cells are particularly “addicted” to ribosome biogenesis. Proliferating cells use 60-80% of cellular energy to produce ribosomes (Pelletier et al., 2018). Until now, several nucleolar proteins involved in this process have been linked to cancer. For example, a wide range of tumours display overexpression of several ribosomal proteins, such as RPLP0, RPLP1 and RPLP2 (Artero-Castro et al., 2011). Aberrant regulation of RNA Pol I is also quite common in cancers (Bohlman and Manfredi, 2014), although it is not known if upregulation of rRNA synthesis is sufficient for malignant transformation.

The biogenesis of eukaryotic ribosomes is a very complex process involving more than 200 proteins and small nucleolar RNAs (snoRNAs) (Bohnsack and Bohnsack, 2019; Henras et al., 2015). This process requires the activity of all three RNA Polymerases. RNA Polymerase I transcribes the 47S pre-rRNA, RNA Polymerase II is responsible for expression of ribosomal and accessory proteins, and RNA Polymerase III produces the final component of ribosomes, the 121nt long 5S rRNA (Goodfellow and Zomerdijk, 2013). Regulation of RNA Pol II has been extensively studied, while RNA Pol I and RNA Pol III are less understood. Contrary to RNA Pol II, both Pol I and Pol III are extremely active and regulated mainly at the initiation step, and they transcribe up to ~80% of total RNA in eukaryotic cells (Goodfellow and Zomerdijk, 2013; Willis and Moir, 2018; Yeganeh and Hernandez, 2020). In humans, there are ~400 rDNA repeats, about 50% of which are transcribed. Pre-initiation complex (PIC) of RNA Pol I is first recruited at the promoter by association of selectivity factor 1 (SL1), when upstream binding factor (UBF) is present (Goodfellow and Zomerdijk, 2013). UBF is a nucleosome-like protein that covers the gene body containing the 47S rDNA, and high UBF levels are linked to high RNA Pol I activity. The chromatin landscape of rDNA repeats is unique because, in actively

transcribed rDNA, active chromatin histone modifications are concentrated at a single region upstream of the spacer promoter, while the rest of the gene body is covered by UBF (Herdman et al., 2017). Another essential protein required for initiation of rRNA synthesis *in vivo* is RNN3 (also known as TIF1A), which is a RNA Polymerase I-specific transcription factor (Drygin et al., 2010).

RNA Pol III transcribes 5S rRNA, tRNAs and several small non-coding RNAs such as 7SL, 7SK and U6 (Yeganeh and Hernandez, 2020). RNA Pol III is composed of 17-subunits, including the catalytic subunit POLR3A, which work together with the transcription factors TFIIIA, TFIIIB and TFIIIC. Three different ways of initiation have been described until now: Class I for 5S rRNA, Class II for tRNA, and Class III for U6 snRNA . In all three cases, TFIIIC recognizes the promoter, which is found internally in the gene body, contrary to protein-coding genes where the promoter is found upstream. It then recruits TFIIIB, which is necessary for completion of the PIC. 5S rRNA synthesis requires an extra transcription factor, TFIIIA, while U6 snRNA requires SNAPc (SNRNA Activating Protein complex). Pol III terminates transcription when it encounters a polyUs stretch (Willis and Moir, 2018).

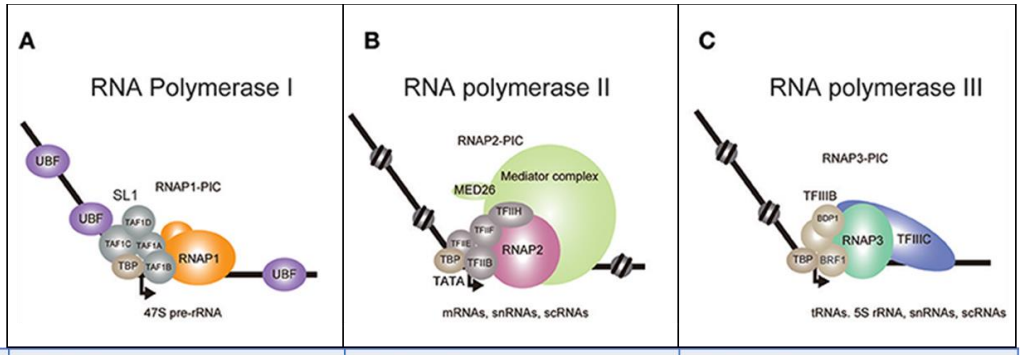

Location	Nucleolus	Nucleoplasm	Nucleoplasm
Synthesis of	Ribosomal (r)RNA	mRNA, snRNAs	tRNA, 5S rRNA and other small RNAs
Regulation	UBF, RNN3	CTD phosphorylation	TFIIIA (5S) TFIIIB (tRNA)
Unique subunit	POLR1A (rpa194)	POLR2A (rbp1)	POLR3A (rpc1)

Figure 5: Ribosome biogenesis requires the activity of all three RNA Polymerases

RNA synthesis in eukaryotes is carried on by three RNA Polymerases. RNA Pol I synthesise a long, single ribosomal 47S (r)RNA which is further processed and modified in the mature 18S, 28S and 5.8S rRNA; it is the most active of the polymerases, producing up to 60% of total RNA in a cell. RNA Pol II produces messenger (m)RNA and small nuclear (sn)RNAs, and it's responsible for up to 15% of RNA synthesis in a cell. RNA Pol III is the second, most active RNA polymerase and it is specialized in synthesis of short and abundant RNAs, such as the 5S rRNA and tRNAs. It also synthesizes U6 snRNAs necessary for splicing. These three molecular machineries share several of their subunits, such as TBP, but they have unique

catalytic subunits namely POLR1A, POLR2A, POLR3A. While RNA Pol II is tightly regulated during the entire transcription process (initiation, elongation and termination) *via* phosphorylation of the C-terminal domain, RNA Pol I and Pol III are mainly regulated at the initiation step through binding of transcription factors. *Modified from Yokoyama et al, 2019*

1.4.3 Pre-rRNA processing in humans

The 47S pre-rRNA undergoes extensive processing and modifications before producing the mature 18S, 28S and 5.8S rRNA. Pre-rRNA processing has been mainly studied in yeast, and while the basic pathway is conserved across all eukaryotes, human ribosome biogenesis is far more complex and less well understood (Bohnsack and Bohnsack, 2019). The first step in the maturation of the 47S pre-rRNA is removal of the external and internal transcribed spacers (ETF and ITS) by endo- and exonucleases (Henras et al., 2015). The resulting 45S pre-rRNA comprises of several cleavage sites which can give rise to different pathways of RNA processing in humans. It is not known how and why human cells utilize alternative pre-rRNA processing pathways, and it's not clear if such variation leads to different pre-rRNA intermediates between different tissues and cell types. An overview of pre-rRNA processing in humans is shown in Figure 6.

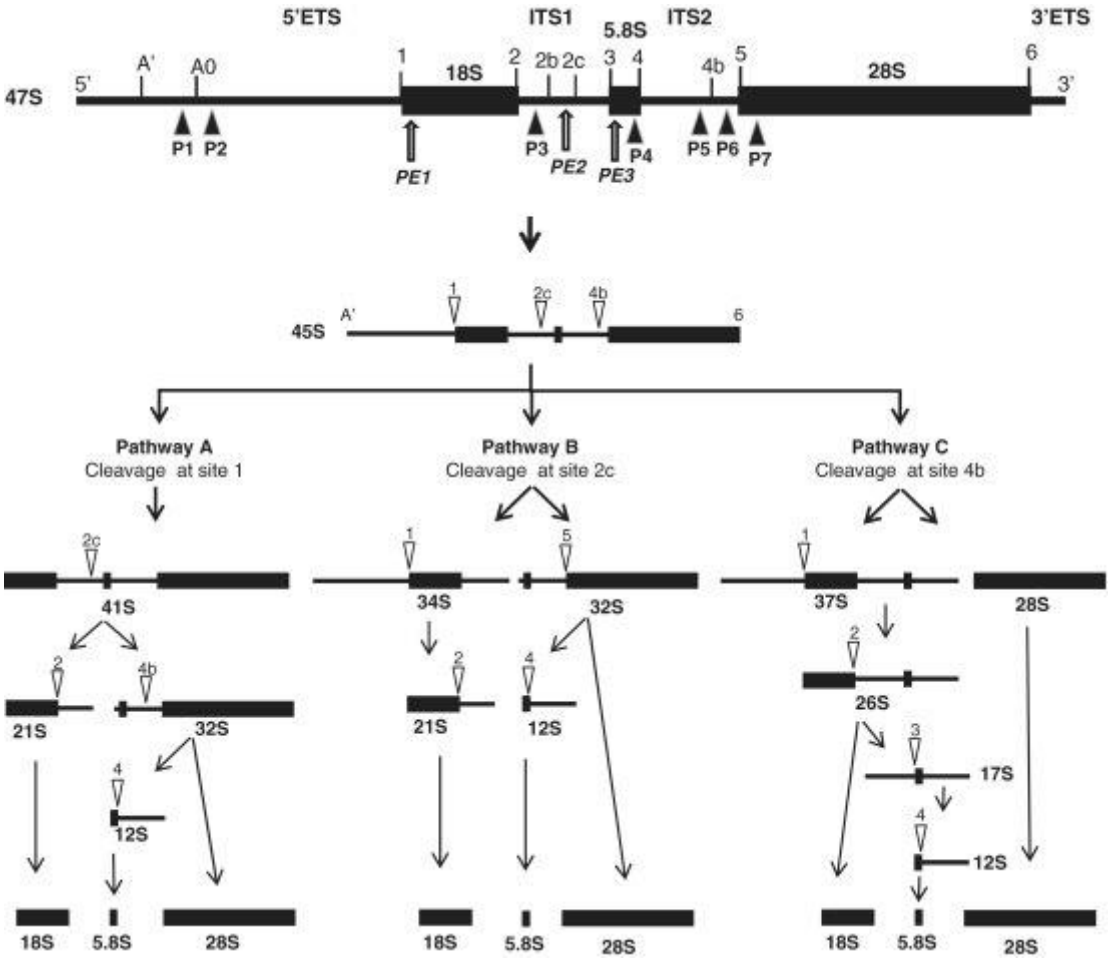

Figure 6: pre-rRNA processing in human cells is an intricate sequence of processing steps

Schematic representation of human pre-rRNA processing pathways. The 47S pre-rRNA is transcribed by RNA Pol I and is cleaved to the 45S pre-rRNA. The 45S can be processed by 3 different pathways, depending on where the first cleavage occurs. The subsequent steps comprises of specific cleaving sites, as shown by white arrowheads (Morello et al., 2011).

Once rRNA has been processed and extensively modified, it is assembled with RPs in the nucleoli to form pre-ribosomes, with the final maturation steps occurring in the cytoplasm. The 18S is integrated with 33 RPs in the 40S small ribosomal subunit (SSU), while 28S, 5.8S and 5S bind 50 RPs to form the 60S large ribosomal subunit (LSU) (Bohnsack and Bohnsack, 2019). The nuclear import/export system is used to transport pre-ribosomes and processing proteins from the nucleoplasm to the cytoplasm. Moreover, RPs need to be imported in the nucleus as soon as they are synthesized, with free RPs being very unstable in the nucleoplasm and cytoplasm. RPs are characterized by their basic charge and a NLS, and they are imported in the nucleus by using non classical pathways (Zemp and Kutay, 2007).

1.4.4 MDM2 interacts with ribosomal proteins in response to ribosomal stress

Proteomic studies have revealed human nucleoli to contain over 4500 proteins, making it an impressive reservoir of proteins which can regulate several cellular processes (Ahmad et al., 2009). The nucleolus plays an important role in maintaining homeostasis, and as such, it can regulate cellular processes in response to stress that disrupts ribosome biogenesis, for example UV light, oncogenes, nutrient starvation, or rRNA repression. This condition, called nucleolar stress, causes leakage of nucleolar proteins to the nucleoplasm, where they can carry extra-ribosomal functions (Yang et al., 2018). RPs are also translocated to the nucleoplasm during nucleolar stress, and several have been shown to interact with MDM2, thus allowing p53 stabilization and induction of cell cycle arrest or apoptosis (Nicolas et al., 2016). The first and best understood RPs-MDM2 complex involves both large ribosomal proteins RPL5 and RPL11. It was shown that RPL5 binding to MDM2 leads to p53 activation, and that Actinomycin D treatment, which inhibits general transcription including rRNA, increased this binding. A complex of MDM2 together with RPL5, RPL11 and RPL23 was identified by immunoprecipitation (Dai and Lu, 2004). Since then, MDM2 has been shown to interact with several RPs from both large and small ribosomal subunit. For example, RPS7 was found to decrease p53 ubiquitination and prolong its half-life, and was shown to be a substrate of MDM2-dependent ubiquitination (Zhu et al., 2009). Later MDM2 was also shown to interact with RPS3 (Yadavilli et al., 2009), RPS27L (Xiong et al., 2011), RPS25 (Zhang et al., 2013),RPL4 (He et al., 2016), RPL26 (Zhang et al., 2010), RPL22 (Cao et al., 2017). Most of these interactions seem to occur in the central domain of MDM2, which comprises of an acidic domain and a zinc finger (Fåhraeus and Olivares-Illana, 2014). Since RPs are strongly basic, it is not surprising that the acidic domain of MDM2 harbours many of these interactions. Nevertheless, the MDM2/RPL5/RPL11 complex has been shown to be the most critical component involved in p53 induction following nucleolar stress, and this can be demonstrated by a large pool of evidence. First, depletion of either RPL5 and RPL11, but not other RPs, leads to nucleolar stress and disruption without inducing p53, demonstrating the absolute requirement of these RPs in stabilization of p53 (Nicolas et al., 2016). Secondly, RPL5 and RPL11 were shown to be more stable and avoid proteasomal degradation in response to stress signals much more, compared to other RPs, and that they can mutually protect each other from proteasomal degradation (Bursać et al., 2012). Knockdown of RPL5 and RPl11 was also shown to attenuate p53 activation by p14ARF, and to be involved in induction of senescence in response to replicative stress (Holmberg Olausson et al., 2012; Nishimura et al., 2015). Moreover, MDM2/RPL5/RPL11 complex was shown to mediate a tumour suppression pathway in response to ribosome biogenesis *in vivo* and independently of p14-ARF (Macias et al., 2010). In this study, mice harbouring several mutations in the acidic domain of MDM2 that disrupted the interaction with RPL5 and RPL11, retained normal p53

response to DNA damage; however, p53 response was lacking in response to nucleolar stress, confirming that RP-MDM2 interactions are an essential component of p53-dependent tumour suppression in response to aberrant ribosome biogenesis.

Sloan *et al.* first described the 5S rRNA to also be a binding partner of MDM2, and together with RPL5 and RPL11, it forms the 5S RNP. The 5S RNP was shown to be required for p53 activation in response to ribosome biogenesis inhibition, and this was the first proof that 5S rRNA is also an essential component of this stress response pathway (Sloan et al., 2013). Moreover, the 5S RNP was shown to accumulate in the nucleoplasm following ribosome biogenesis inhibition, where it probably interacts with MDM2, and that RPL5 is necessary for processing of the 5S pre-rRNA. Interestingly, depletion of any of the components of the 5S RNP abolishes the binding of the others, explaining why RPL5 and RPL11 might be dependent on each other, and are both necessary for proper p53 response (Bursać et al., 2012).

1.5 The role of MDM2 in DNA replication

1.5.1 DNA replication is a highly plastic and complex process

DNA replication is a highly plastic process, which needs to be tightly regulated in pace with the cell cycle. Insults that impair DNA replication can cause replication stress, which can lead to genome instability and mutations. Therefore, DNA replication must proceed at determined speeds to enable activation of the DNA damage response (DDR) and to repair existing errors (Merchut-Maya et al., 2019).

Replication stress is defined as a cellular state where the integrity and quality of DNA synthesis is negatively affected, and prolonged stress could lead to arrested or collapsed forks, excessive acceleration of DNA replication, uncoupled leading-lagging DNA synthesis and ultimately DNA damage (Merchut-Maya et al., 2019).

An essential regulator of replication fork speed is Poly(ADP-ribosylation) (PARylation), which is catalysed by Poly(ADP-ribose) polymerase-1 (PARP1). In response to DNA breaks, PARP1 can PARylate itself or other target proteins and this has been shown to be critical in multiple pathways, such as DNA repair, DNA replication, transcription, and cell death (Lovato et al., 2012). The first indication that PARP1 can regulate fork speed came from studies using chemical inhibitors, which have been investigated as therapeutic agents against cancer. Studies from the Bartek lab showed that PARP inhibition increases fork speed and induces replication stress (Maya-Mendoza et al., 2018), and this depended on p21 expression. They propose a model where PARP1 interacts with p21, and in the absence of DNA damage, this complex prevents inhibition of PCNA-dependent DNA replication. Upon DNA damage and

PARP1 auto-PARylation, p21 is released from the complex and slows down replication by interacting with PCNA. Several studies have also shown that PARP1 can parylate not only p21, but also p53 and this prevents its nuclear export leading to its accumulation and activation (Kanai et al., 2007; Simbulan-Rosenthal et al., 1999). The p53 axis and PARP1 are undoubtedly connected, and further research is necessary to understand how p53-induced target genes affect fork speed and replication in this context.

Recently, the human helicase RECQ1 has been shown to promote restart of reversed forks, and that PARP1 stabilizes forks in the regressed state by inhibiting RECQ1 via PARylation (Berti et al., 2013). Fork reversal is an important protective mechanism that allows DNA replication forks to reverse their curse in the presence of DNA damage, leading to the formation of four-way DNA junctions also named “chicken foot” structures (Quinet et al., 2017). Fork reversal is a two-step pathway, where different proteins are required for either the formation or the restart of reversed forks, and it is currently an active field of research. In the model proposed by the Vindigni lab, PARP1 activation prevents premature restart of reversed forks by inhibiting the human helicase RECQ1, and this represents an ideal molecular switch that coordinates DNA replication restart in the context of genotoxic stress (Figure 7). As a matter of fact, the presence of DNA damage would activate PARP1 enzymatic activity, which would then PARylate and inhibit RECQ1-dependent fork restart, allowing enough time for the DNA damage to be repaired (Neelsen and Lopes, 2015). A schematic view of this mechanism is depicted in Figure 7.

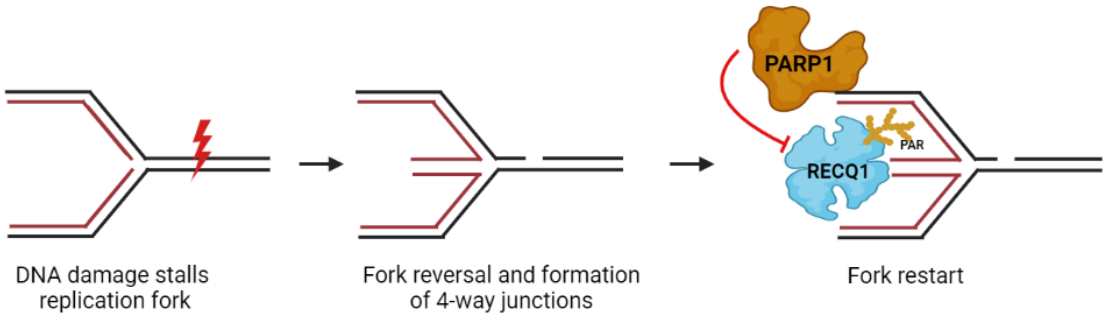

Figure 7: DNA fork reversal and re-start

When the replication fork encounters an obstacle in the leading strand, such as DNA damage, it cannot proceed further and might dissociate from the DNA. To slow down replication and avoid accumulation of ssDNA, the fork can reverse its course to form a 4-way junction (also called chicken foot structure), allowing enough time for the damage to be repaired. The helicase RECQ1 has been shown to promote restart of reversed forks, however PARP1 presence at the fork inhibits early restart by PARylating RECQ1. Created with BioRender.com.

Several proteins have been shown to regulate PARP1 activity and stability (Alemasova and Lavrik, 2019), and recently the E3 ubiquitin ligase CARM1 has been shown to inhibit PARP1 in favour of fork reversal restart (Genois et al., 2021). This raises the question if any other regulatory modules are present at replication forks to govern fork reversal through PARP1 activity.

1.5.2 MDM2 can regulate DNA replication speed and PARP1 levels

As mentioned above, there have been several studies that linked the p53 pathway to PARP1 regulation in the context of DNA replication and repair. P53 activation has been shown to regulate the restart of stalled forks either directly (*via* protein-protein interactions) or indirectly (*via* expression of its target genes). A recent study demonstrated that P53 can directly interact with the replication machinery to enhance the restart of stalled replication forks in cells (Roy et al., 2018). P53 can affect DNA replication also through the expression of its target genes. P21 is one of such target genes, and as already mentioned above, its expression has been shown to inhibit DNA synthesis (Maya-Mendoza et al., 2018). Previous publications from our lab have revealed that p53 activation via Nutlin can enhance DNA replication processivity and progression (Klusmann et al., 2016). In this study, MDM2 depletion decreased fork speed, arguing that expression of MDM2 might be mediating the acceleration of fork speed by p53. Similarly, MDM4 was shown to increase fork progression independently of p53 (Wohlberedt et al., 2020). A follow-up study confirmed the importance of MDM2 in regulation of fork speed through avoidance of R-loops (DNA:RNA hybrids), and that the E3 ubiquitin ligase activity of MDM2 was required to increase replication speed (Klusmann et al., 2018). MDM2 expression prevented R-loops formation, therefore removing obstacles that would impede DNA replication and therefore, the fork speed is enhanced. However, further mechanisms might be involved in the MDM2-dependent fork speed acceleration.

Interestingly, Nutlin treatment and subsequent p53 activation has been shown to degrade and suppress PARP1 in human breast cancer cells (Kobayashi et al., 2020), however the cellular consequences of such event are unknown. The authors show that this degradation was prevented upon MDM2 depletion, arguing that MDM2 might be mediating degradation of PARP1. The authors speculate that MDM2 might be affecting PARP1 levels either by direct interaction or through an allosteric mechanism. This represents a novel link between PARP1 and the p53 axis, and further studies are necessary to understand the implications of such event in the context of fork restart and replicative stress.

1.6 Other non-canonical functions of MDM2

1.6.1 MDM2 can regulate gene expression and chromatin modifications

MDM2 has long been known to affect p53-dependent transcription. For example, MDM2 represses p53-responsive genes by directly interacting with p53 on its target genes promoters and therefore preventing assembly of the transcription machinery (Arva et al., 2005). More than 20 years ago, *in vitro* experiments where MDM2 was incubated with naked DNA revealed that MDM2 represses gene expression (Thut et al., 1997). A possible mechanism explaining MDM2 role in transcription relies in its function as chromatin modifier. MDM2 was found to support chromatin condensation by enhancing trimethylation of Histone 3 at lysine 9 (Chen et al., 2010). Moreover, MDM2 can also regulate chromatin ubiquitination, particularly that of histone H2A and H2B (Minsky and Oren, 2004). Studies from the Dobbelstein lab confirmed this, and found MDM2 to enhance the repressive chromatin modifications H3K27me3 and H2AK199ub1, and this dependent on a functional RING finger domain (Wienken et al., 2016). Specifically, MDM2 suppresses gene expression associated with cell differentiation, independent of p53, and through interaction with the Polycomb Repressor Complex 2.

1.6.2 MDM2 and DNA damage repair

MDM2 overexpression was found to negatively affect genome stability by reducing levels of DNA damage signalling and significantly delay DNA repair (Alt, 2003; Bouska et al., 2008), also independently of p53. Specifically, ATM-mediated phosphorylation of H2AX (yH2AX) was reduced after a short exposure to gamma radiation in cells overexpressing MDM2. In the presence of double-strand breaks (DSB), MDM2 was found to bind Nbs1, a component of the Mre11-Rad50-Nbs1 (MRN) complex. Elevated levels of MDM2 in $p53^{-/-}$ cells also led to chromosome break, but these were prevented when the interacting region of MDM2 with Nbs1 was mutated (Bouska et al., 2008). The authors also found MDM4, structurally related to MDM2, to inhibit DNA break repair by interacting with Nbs1 at chromatin Carrillo et al., 2015a. These results indicate that both MDM2 and MDM4 have conserved and redundant functions to inhibit DNA break repair. *MDM2* transgenic mice expressing ~3-4 fold increased expression, displayed high levels of DNA breaks, fusions, and other chromosomal abnormalities (Lushnikova et al., 2011; Wang et al., 2008). Nutlin treatment has also been shown to induce DNA breaks and activate the DNA damage response, possibly through delay in DNA break repair. Interestingly, this could be rescued by MDM2 depletion (Carrillo et al., 2015). MDM2 overexpression was also shown to confer resistance to DNA damage induction by topoisomerase II poisons by repressing the DSB levels induced by these inhibitors (Senturk et al., 2017). The exact mechanism is not well understood, although the RING domain of

MDM2 was found to be necessary. Further investigations will be necessary to better understand the link between MDM2 and the DNA damage response.

1.7 Scope of the thesis

In this study, we investigated the role of MDM2 in two cellular processes, ribosome biogenesis and DNA replication. We used cancer cell lines that harbour wild type p53 and treat them with various small molecules, in order to induce MDM2 expression. We included cell lines with and without MDM2 amplification to investigate how MDM2 levels affect RNA transcription, the formation of ribosomes, cell viability and DNA replication forks.

1.7.1 MDM2, in a complex with the ribosomal proteins L5 and L11, inhibits RNA Polymerase III and induces nucleolar stress.

We aimed to understand the role of MDM2 overexpression in regulation of non-coding RNA transcription, with particular focus on rRNA synthesis. We used the *cis*-imidazoline analog Nutlin-3a to disrupt the interaction between MDM2 and p53, effectively accumulating both proteins. Moreover, we used the proteolysis targeting chimera (PROTAC) MD-224 to deplete MDM2 upon p53 induction, in proliferating cells, and investigate its direct role in RNA synthesis. We found that MDM2, together with RPL5 and RPL11, inhibits RNA Pol III transcription. In collaboration with the Bohnsack lab, we used a combination of immunofluorescence studies, western blotting, and northern blotting to investigate how prolonged p53 affects ribosome biogenesis and RNA Pol I activity. We found that long Nutlin treatments led to inhibition and displacement of RNA Pol I, nucleolar stress, and disruption in ribosome biogenesis. Depletion of any member of the MDM2/RPL5/RPL11 complex escued RNA Pol III activity, restored RNA Pol I localizaton in the nucleoli, and prevented Nutlin-induced cell death.

1.7.2 MDM2 binds and ubiquitinates PARP1 to enhance DNA replication fork progression

We used a combination of *in vitro* and *in vivo* assay to show that MDM2 poly-ubiquitinates PARP1, causing its proteasomal degradation, and directly interacts with PARP1 in cells, as shown by co-immunoprecipitation and proximity ligation assays. We found a novel role of MDM2 in acceleration of DNA replication, as shown by fiber assays, and this depended on activity of the helicase RECQ1 and the primase-polymerase PRIMPOL. Overexpression of PARP1 restored normal fork progression despite MDM2 overexpression in p53 -/- cells. In collaboration with the Lopes lab, electron microscopy experiments revealed a direct role of MDM2 in reducing the number of four-way junctions, which are DNA structures formed as a consequence of fork reversal.

2. MANUSCRIPT 1

MDM2, in a complex with the ribosomal proteins L5 and L11, inhibits RNA Polymerase III and induces nucleolar stress.

Author list:

Valentina Manzini[1], Jennifer Jansen[1], Vella Nikolova[1], Antje Dickmanns[1], Philipp Hackert[2], Katherine Bohnsack[2], Markus Bohnsack[2], Matthias Dobbelstein[1]

[1] Institute of Molecular Oncology, Göttingen Center of Molecular Biosciences (GZMB), University Medical Center Göttingen, Göttingen, Germany.

[2] Department of Molecular Biology, University Medical Center Göttingen, Göttingen, Germany.

Own contribution: carried out experiments and data analysis for all figures except Figure 1F-G, Figure 4D, Figure 5 B-C and Figure S1. Involved in conceptualization and interpretation of data, figure arrangements and writing the manuscript.

SUMMARY

MDM2 is the negative regulator of the tumor suppressor p53, and as such it is considered an oncogene. Upon nucleolar stress, several ribosomal proteins (RPs) bind MDM2 and prevent it from degrading p53. This process which links ribosomal stress to p53 activation has been described as a crucial tumor-suppressive mechanism. The 5S-RPL5-RPL11 complex, also called the 5S RNP, has been shown to interact with and inhibit MDM2, and its presence is crucial for p53 activation in the presence of defects in ribosome biogenesis. Here we disrupted the MDM2/p53 interaction with non-genotoxic agents to activate p53 and accumulate MDM2. MDM2 induction leads to inhibition of RNA Pol III activity, as shown by decreased 5S pre-rRNA and unprocessed tRNA. MDM2 was also found in proximity of POLR3A, and depletion of either RPL5 and RPL11 prevented this. Prolonged p53 activation led to disrupted ribosome biogenesis and nucleolar stress. Depletion of either MDM2, RPL11 or RPL5, which affects the integrity of the complex, reverted most of these effects. In conclusion, the MDM2-RPL5-RPL11 complex can inhibit RNA Pol III activity also in the absence of externally induced nucleolar stress, and prolonged MDM2 accumulation leads to displacement of POLR1A, inhibition of RNA Pol I and ultimately cell death.

2.1 INTRODUCTION

The tumor suppressor and transcription factor p53 triggers responses to cellular stress, inducing cell cycle arrest or apoptosis (Vogelstein et al., 2000). Among the plethora of p53 target gene products, MDM2 (Mouse double minute 2 homolog) stands out as an E3 ubiquitin ligase which can destabilize p53, resulting in a negative feedback loop (Picksley and Lane, 1993). MDM2 thus acts as an oncogene, and it is overexpressed in human malignancies such as sarcomas (Rayburn et al., 2005). Somewhat counterintuitively, however, MDM2 may also act in a tumour suppressing fashion. For example, loss of MDM2 can stabilize mutant p53 and thus enhance tumour formation in mice (Terzian et al., 2008). Overexpression of MDM2 has been shown to inhibit the G0/G1-S phase transition in both murine and non-transformed human cells (Brown et al., 1998). Such activities of MDM2 might be explained by MDM2-binding proteins (Fåhraeus and Olivares-Illana, 2014). MDM2 is often described as a regulatory hub due to its complex interactome. Structurally, MDM2 harbours both a nuclear localization signal (NLS) and a nuclear export signal (NES) (Roth, 1998). A considerable portion of MDM2 is intrinsically disordered, which makes it flexible and allows for a wide range of interactions (Fåhraeus and Olivares-Illana, 2014).

Oncogene activation can lead to cellular stresses, one of these being nucleolar stress, or ribosomal stress. Nucleoli are the site of ribosome biogenesis, involving hundreds of proteins and RNAs (Bohnsack and Bohnsack, 2019). This process requires the activity of all three RNA Polymerases. RNA Pol I synthesizes the 47S precursor ribosomal RNA (rRNA), which is then cleaved and modified to become mature 18S, 28S and 5.8S rRNAs in the nucleoli. RNA Pol II transcribes the mRNA that encodes ribosomal proteins (RPs) and all accessory proteins required for proper ribosome biogenesis. Finally, RNA Pol III transcribes the 5S rRNA in the nucleoplasm, which is then processed in the nucleoli (Russo and Russo, 2017). Disruption in either the synthesis of rRNA or its processing leads to nucleolar stress, where RPs “leak” from the nucleoli to the nucleoplasm (Yang et al., 2018). Tumor cells have a high demand for ribosome biogenesis, as a result of their fast proliferation. This might result in high susceptibility towards nuclear stress, providing novel opportunities for cancer therapy (Drygin et al., 2010).

Upon nucleolar stress, several RPs bind MDM2, preventing it from degrading p53 and thus triggering p53 activity (Russo and Russo, 2017). The 5S RNP, composed by RPL5, RPL11 and the 5S rRNA, is a prominent example. The 5S rRNA is an essential component of this complex, and its presence is critical for p53 regulation (Sloan et al., 2013). The 5S RNP - MDM2 pathway activates p53 in the response to nucleolar stress induced by oncogenes, nutrient starvation, and chemotherapeutic drugs (Pelava et al., 2016). The depletion of most

ribosomal proteins not only alters the structure of nucleoli but also induces p53; however, depletion of either RPL5 or RPL11 fails to trigger p53, while still disordering the nucleolar structure (Nicolas et al., 2016). This further suggests a central role of these RPs in p53 regulation.

Due to the extremely high metabolic and energetic requirements, ribosome biogenesis must be tightly regulated in response to external cellular stresses, such as DNA damage. We hypothesized that p53 activation might regulate ribosome biogenesis through one of its target genes. MDM2 represented a strong candidate, given its known interaction with ribosomal proteins. We took advantage of the proteolysis targeting chimera (PROTAC) technology to deplete MDM2 in proliferating cells. We found that MDM2 accumulation inhibits RNA Pol III transcription through the 5S RNP. Depletion of either MDM2, RPL5 or RPL11 rescued RNA Pol III activity in this context. Prolonged p53 induction led to disrupted ribosome biogenesis, followed by diminished RNA Pol I activity, nucleolar stress, and cell death.

2.2 RESULTS

MDM2 accumulation inhibits RNA Pol III activity

Since MDM2 has been shown to be in a complex with the pre-existing population of 5S rRNA in response to nucleolar stress (Onofrillo et al., 2017), we asked whether induction of MDM2 without external stresses would affect synthesis of the 5S rRNA. We treated the osteosarcoma wild-type *TP53* cell line SJSA-1 with the MDM2 ligands MI-1061 or Nutlin-3a (from now on referred as Nutlin), or with the MDM2 PROTAC MD-224 for 6h (Figures 1A-D). MD-224 is a heterobifunctional small molecule composed of a MDM2 ligand (MI-1061) and a ligand (lenalidomide) that recruits the E3 ligase ubiquitin machinery Cereblon (Li et al., 2019). This compound can induce p53 transcriptional activity, while specifically degrading MDM2 thus allowing to investigate MDM2 activity in proliferating cells. Both MI-1061 and MD-224 induced p53 activation, as shown by expression of p53-target genes *MDM2* and *CDKN1A* (Figure 1C) and immunoblot analysis of p53 and p21 protein levels (Figure 1D). However, MD-224 specifically depleted MDM2 protein levels without affecting p53 activation compared to MI-1061, and without affecting *MDM2* expression at mRNA level. To quantify pre-5S rRNA, we designed primers that span the cleavage site necessary for processing into the mature 121nt 5S rRNA (Table 2), which allowed us to specifically quantify the levels of unprocessed (thus nascent) 5S rRNA. We used the 144nt 5S DNA sequence described in several previous studies, encoded by the RF00001-230 gene (Kalvari et al., 2018; Szymanski, 2002; Vierna et

al., 2013). Primers against unprocessed tRNA Leu-CAA were designed using a similar strategy as for the 5S rRNA, as described previously (Melnik et al., 2011). To our surprise, the 5S pre-rRNA levels decreased upon p53 induction via MI-1061 and Nutlin but were restored upon MDM2 degradation by MD-224.The same was observed for the nascent tRNA Leu-CAA RNA (Figure 1E). Next, we investigated weather what we observe is a general inhibition of RNA Pol III activity by metabolically labeling nascent RNA, and visualization *via* Northern Blot (Figure 1F). SJSA-1 cells were treated with Nutlin and cells were harvested at different time-points. 5S rRNA synthesis was completely stopped already after 4h Nutlin treatment, while tRNA synthesis decreased over time, until reaching a complete block after 15h of Nutlin treatment.

We proceeded to test whether MDM2 accumulation also inhibits RNA Pol III activity in other two MDM2-amplified cell lines, the liposarcoma cell lines GOT-3 and CRL-3043. qPCR analysis showed a similar trend as previously observed in SJSA-1; both MI-1061 and Nutlin caused a significant decrease in 5S and tRNA Leu-CAA unprocessed RNA, which was reversed upon MDM2 depletion using MD-224 (Figure 1G). qPCR and immunoblot analysis confirmed the efficiency of MD-224 and other treatments in GOT-3 (Figure S1A-B). p53 activation resulted in downregulation of RNA Pol III transcripts also in CRL-3043 (Figure S1C).

In conclusion, p53 induction *via* MI-1061 and Nutlin caused repression of RNA Pol III activity in several cell lines harbouring a MDM2 amplification. Such effect on transcription was reverted upon depletion of MDM2 using MD-224, suggesting MDM2 as the effector mediating RNA Pol III inhibition.

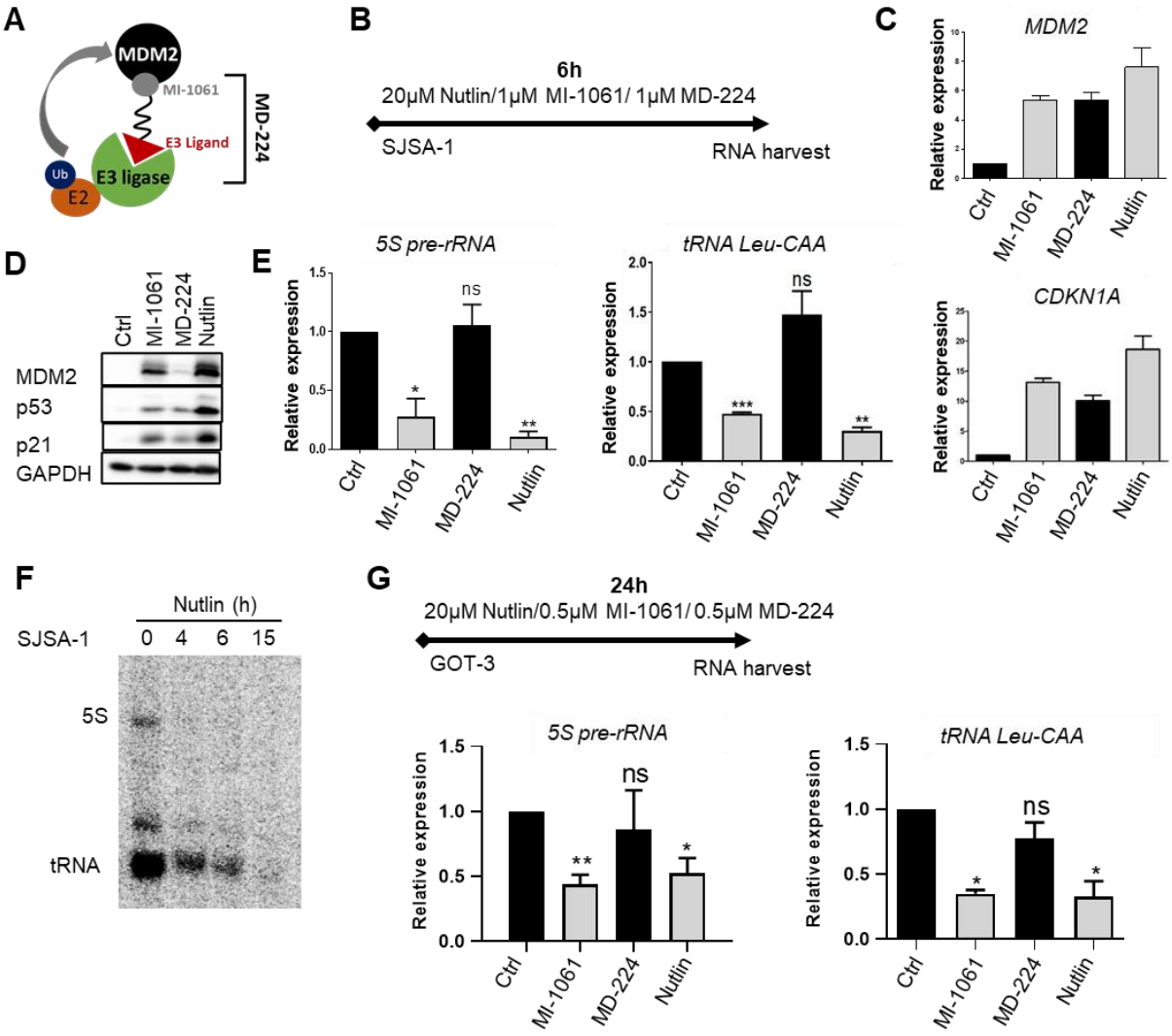

Figure 1: MDM2 accumulation inhibits RNA POL III activity.

A) Scheme depicting the mechanism of action of the MDM2 PROTAC, MD-224.
B) SJSA-1 cells were treated with 20μM Nutlin, 1μM MI-1061 or 1μM MD-224 for 6h prior to harvesting of RNA and analysis via qPCR. N=3.
C) qPCR analysis of p53-target genes MDM2 and p21 upon 6h of treatments shows equal gene expression of both following treatment with either MI-1061, MD-224 or Nutlin, confirming that MD-224 degrades Mdm2 at the protein level without affecting its expression.
D) Western blot analysis of whole cell lysates treated as shown in A. Both Nutlin and MI-1061 induce similar levels of p53 and MDM2. MD-224 still shows strong p53 accumulation, but MDM2 is depleted.
E) Relative expression of unprocessed 5S rRNA and unspliced tRNA Leu-CAA. In both cases, both MI-1061 and Nutlin caused a strong downregulation of unprocessed RNA, which could be rescued upon MDM2 depletion via the PROTAC MD-224. N=3.
F) Metabolic labelling of nascent RNAs upon several time-points of Nutlin confirms a strong repression of nascent 5S rRNA, starting already after 4h of Nutlin treatment.
G) GOT-3 cells were treated for 24h following the scheme in the top panel. qPCR analysis showed a significant decrease in unprocessed 5S rRNA and tRNA Leu-CAA, which

was almost completely rescued upon depletion of MDM2 using the MD-224 PROTAC. N=3.

The MDM2/RPL5/RPL11 complex is found in the proximity of POLR3A and leads to RNA Pol III inhibition

Next, we asked whether MDM2 is found in proximity of the RNA Pol III machinery. We used proximity ligation assays (PLAs) in SJSA-1, targeting both MDM2 and the catalytic subunit of RNA Pol III, POLR3A. Fluorescence signal is observed only when the two proteins are within 40nm from each other, suggesting they are part of a complex or interacting directly (Fredriksson et al., 2002). Fluorescent signal increased steadily upon longer Nutlin treatments and induction of MDM2 (Figure 2A). Even without MDM2 induction by Nutlin, dots above background levels were observed in control cells. PLAs using either one of the two primary antibodies, or none, were performed as negative controls (Figure 2B, Figure S2A). Similar PLA signal was observed between MDM2 and another member of the Pol III initiation complex, BRF1 (Figure S2B). We proceeded to test whether the integrity of the MDM2/RPL5/RPL11 complex is required for proximity to POLR3A. We performed PLAs upon 6h 20μM Nutlin treatment, and depletion of each member of the complex via siRNA (Figure 2C). As expected, PLA signal was almost completely abrogated upon MDM2 knock-down (Figure 2D). Moreover, depletion of either RPL5 or RPL11 strongly decreased the PLA signal, confirming that complex formation is required for MDM2 proximity to POLR3A. Two independent siRNA against RPL5 and RPL11 strongly depleted signal in the nucleus, confirming knock down of the RPs prior assembly in the ribosome (Figure S2C). Depletion of either RPL5 or RPL11 did not affect protein levels of p53 or MDM2, as shown by western blot (Figure S2D). We tested if RPL5 and RPL11 are required for RNA Pol III inhibition by detection of 5S pre-rRNA via qPCR (Figure 2E). Depletion of either RP rescued the synthesis of 5S rRNA, confirming that MDM2/RPL5/RPL11 complex is indeed required for RNA Pol III inhibition. Finally, we asked whether members of the RNA Pol III complex are regulated at the protein level. Immunoblot analysis revealed that both MI-1061 and Nutlin caused downregulation of TFIIIA, a transcription factor required for 5S rRNA synthesis, and POLR3A, confirming inhibition of the RNA Pol III machinery (Figure 2F). In conclusion, we could demonstrate that MDM2 is found in proximity to the RNA Pol III transcription machinery, and that its interaction with RPL5 and RPL11 is required for this co-localization. Depletion of either RPL5 or RPL11 restored 5S rRNA transcription. We could observe depletion of transcription factor TFIIIA and catalytic subunit POLR3A, and this depended on MDM2 accumulation.

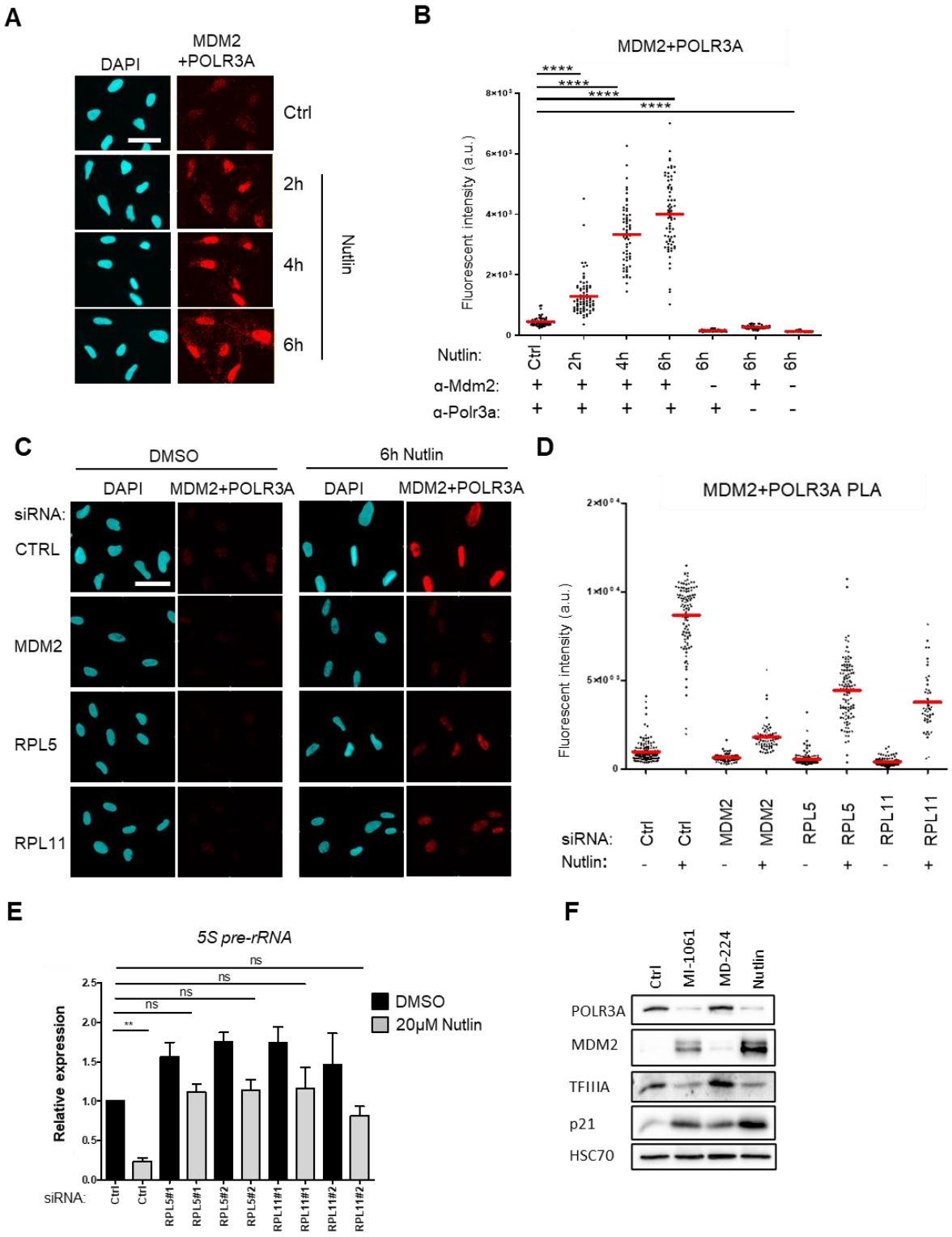

Figure 2: The MDM2/RPL5/RPL11 complex is found in the proximity of RNA Pol III and leads to its inhibition.

A) Representative images of the experimental conditions tested with proximity ligation assay (PLA) between MDM2 and POLR3A upon increasing lengths of Nutlin treatment.

B) Fluorescent intensity of single nuclei coming from PLA signal was determined using DAPI as a mask. Red lines represent mean for each condition. Negative controls omitting one or both antibodies were also included. N=60-80 cells per condition.
C) PLA signal of MDM2 and POLR3A. Depletion of MDM2 disrupts PLA signal almost completely, while RPL5 and RPL11 depletion considerably decreases proximity of MDM2 with POLR3A. N=70-90 cells per condition.
D) qPCR analysis of pre-5S rRNA upon 6h of Nutlin and depletion of either RPL5 or RPL11 by two independent siRNA showed a rescue in 5S pre-rRNA synthesis. N=3.
E) Depletion of MDM2 using MD-224 led to a rescue in TFIIIA protein levels, a transcription factor essential for 5S synthesis.
F) SJSA-1 were treated for 12h with either 1µM of MD-224 or MI-1061, or 20µM of Nutlin. Protein levels of POLR3A and TFIIIA went down upon induction of both p53 and MDM2, but were rescued after depletion of MDM2.

Nutlin treatment leads to global RNA synthesis repression, independent of p21

RNA Pol I and III account for ~80% of the transcriptional output of a proliferating cell, with RNA Pol III being responsible for the transcription of a quarter of this (Willis and Moir, 2018). Therefore, we ought to investigate if MDM2 induction via Nutlin affects global RNA synthesis, or specifically Pol III activity. A fast and easy way to measure the transcriptional activity of a cell, temporally and spatially, can be achieved by labelling cells with the nucleoside analogue 5-Ethynyl Uridine (EU), which is incorporated into nascent RNA. This is followed by the chemoselective ligation of a fluorophore using click chemistry and detection with fluorescence microscopy (Jao and Salic, 2008). We labelled SJSA-1 cells with EU in the last 10min or 4h of a 20h Nutlin treatment (Figure 3A, top panel). When labelling cells with EU for 10min, Nutlin treatment induces a profound repression of RNA synthesis across the whole nucleus (Figure 3A, middle and bottom panel). To our surprise, when labelling cells with EU for 4h, nucleolar transcription seemed to be strongly repressed, as shown by lack of EU signal in the nucleoli. Since RNA Pol I is the only polymerase active in the nucleoli, this suggested a profound inhibition of rRNA synthesis production. We next performed rescue experiments using siRNAs against TP53 and its target genes. As expected, depletion of TP53 completely rescued the repression of RNA synthesis upon Nutlin (Figure 3B-C), excluding possible off-target effects of the drug. MDM2 knock-down also partially rescued RNA synthesis. Interestingly, MDM2 depletion alone led to a decrease in RNA synthesis in the absence of Nutlin, possibly due to the cell cycle arrest caused by p53 induction. The p53-target gene p21 has been found to repress several genes by different mechanisms (Ferrándiz et al., 2012). Since p21 also induces cell cycle arrest in G1, we questioned whether it could also inhibit RNA Pol III and I in such context. We therefore knocked down p21, followed by Nutlin treatment for 15h, and labelled the last 15min with EU. Western blot analysis confirmed depletion of p21 following transfection (Figure 3D), however no rescue in RNA synthesis was observed (Figure 3E).

Long Nutlin treatments causes cell cycle arrest due to p21 induction, while shorter treatments of up to 6h do not affect the cell cycle (Sriraman et al., 2018). However, only a slight repression of global RNA synthesis was observed upon shorter Nutlin treatments (Figure S3A), possibly due to the early inhibition of RNA Pol III as shown in Figure 1F. Nevertheless, degradation of MDM2 in proliferating cells using the MD-224 PROTAC rescued repression of RNA synthesis upon 6h treatments (Figure 3F).

After excluding G1-arrest and p21 activation as a cause of RNA synthesis repression, we asked if induction of apoptosis might be responsible for transcription inhibition. SJSA-1 cells are known to respond to Nutlin with cell death, starting already at 24h (Sriraman et al., 2018). Caspase activation is known to cleave several essential proteins (Julien and Wells, 2017), and Caspase-7 activity has been shown to be enhanced by RNA (Desroches and Denault, 2019). Therefore, we tested if inhibition of caspases rescues RNA synthesis repression. Pan-caspase inhibition using zVAD did not restore transcription (Figure S3B-C), although it inhibited PARP1 cleavage confirming its efficiency (Figure S3D).

In conclusion, MDM2 induction via Nutlin and/or MI-1061 caused a global repression of RNA synthesis, as shown by short EU labelling of 10min. Longer EU labelling (4h EU), representing processed and more “steady state” RNA levels, revealed a strong inhibition of Pol I-dependent nucleolar transcription. RNA synthesis was rescued by depletion of p53 and, partially, by depletion of MDM2 via siRNA. Neither depletion of p21 nor inhibition of caspases was able to restore transcription, excluding G1 arrest or induction of apoptosis as causes of RNA synthesis repression.

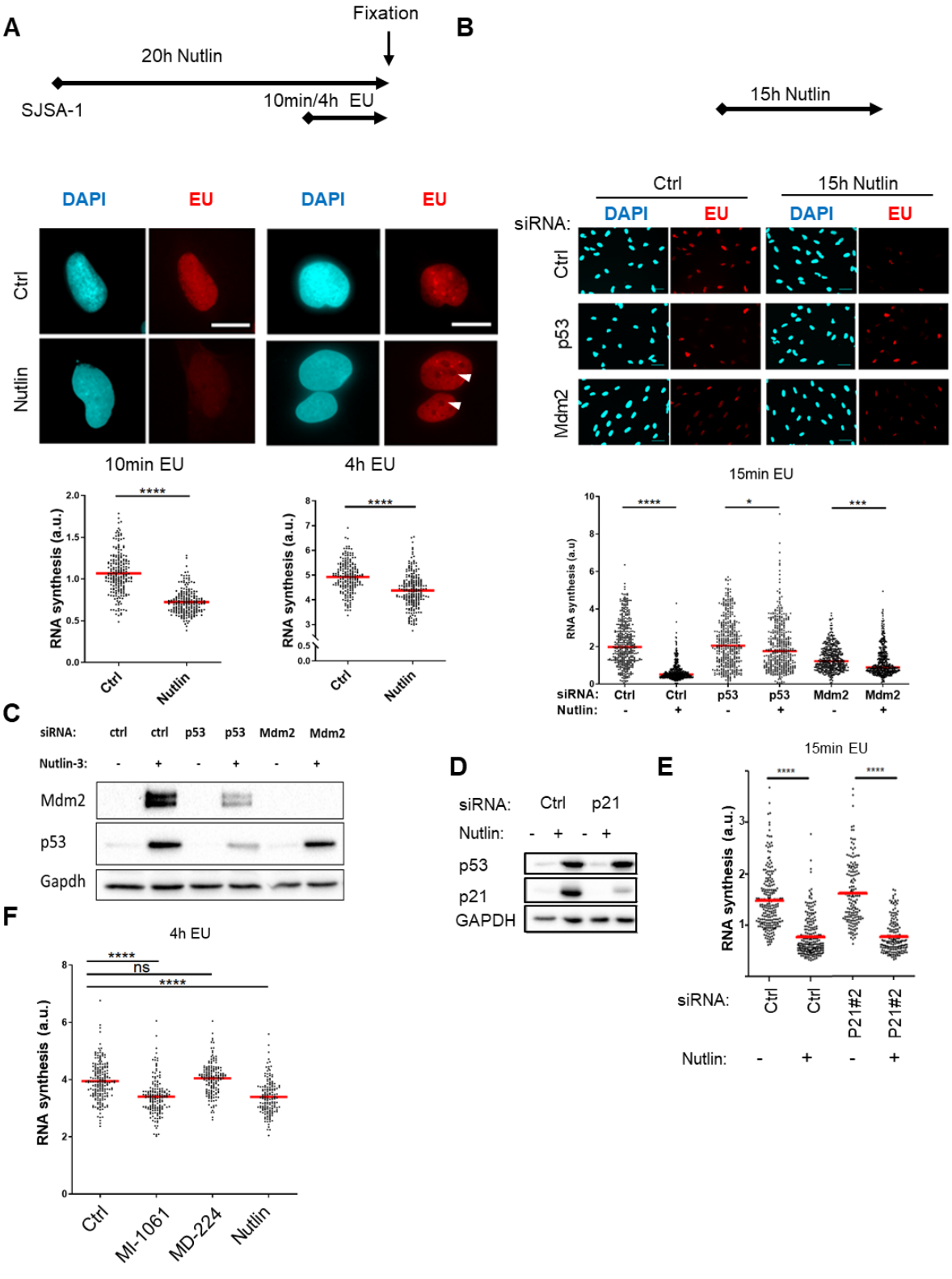
A
Fixation
20h Nutlin
SJSA-1
10min/4h EU
B
15h Nutlin
DAPI
EU
DAPI
EU
Ctrl
Nutlin
10min EU
4h EU
RNA synthesis (a.u.)
****
Ctrl
Nutlin
Ctrl
15h Nutlin
siRNA:
DAPI
EU
DAPI
EU
Ctrl
p53
Mdm2
15min EU
RNA synthesis (a.u)
****
*
***
siRNA: Ctrl Ctrl p53 p53 Mdm2 Mdm2
Nutlin: - + - + - +
C
siRNA: ctrl ctrl p53 p53 Mdm2 Mdm2
Nutlin-3: - + - + - +
Mdm2
p53
Gapdh
D
siRNA: Ctrl p21
Nutlin: - + - +
p53
p21
GAPDH
E
15min EU
****
****
RNA synthesis (a.u.)
siRNA: Ctrl Ctrl P21#2 P21#2
Nutlin: - + - +
F
4h EU
****
ns
****
RNA synthesis (a.u.)
Ctrl
MI-1061
MD-224
Nutlin

Figure 3: Nutlin treatment leads to global RNA synthesis repression, independent of p21.

A) Top: SJSA-1 cells were treated with 20µM of Nutlin form 20h. The final 10min or 4h were labelled also with 1mM Ethynyl Uridine (EU) for consequent analysis of nascent RNA synthesis. Middle: representative images of cells labelled with 10min (left) or 4h EU (right). Bottom: nuclear EU signal was quantified using DAPI as mask and plotted. Red lines represents means. N=150-200 cells per condition.
B) Top: SJSA-1 cells were reverse transfected using siRNA to deplete either p53 or MDM2 for 48h, with the final 15h also being treated with Nutlin. 15min prior to fixation, cells were incubated with EU for labelling of nascent RNA. Middle: representative images of experimental conditions. Bottom: quantification graphs of EU signal of single nuclei. N=400.
C) Immunoblot analysis confirms depletion of p53 and MDM2 following siRNA transfection as shown in B.
D) Immunoblot analysis confirms p21 knockdown.
E) EU assay following p21 depletion via siRNA. N=150.
F) SJSA-1 cells were treated with 1µM MI-1061/MD-224 or 20µM Nutlin for 6h, followed by 10min EU labelling. MDM2 depletion using the MD-224 PROTAC led to a rescue in RNA synthesis compared to MI-1061 and Nutlin. N=150-200.

P53 activation induces nucleolar stress and RNA Polymerase I inhibition in several cell lines harbouring a MDM2 amplification

In order to confirm RNA Pol I inhibition, we treated SJSA-1 cells with Nutlin or BMH-21, an inhibitor that leads to destruction of RNA Polymerase I (Peltonen et al., 2014) (Figure 4A). Immunofluorescence analysis revealed RNA synthesis repression (particularly in the nucleolus) upon BMH-21 treatment, as seen by the EU assay (Figure 4B). Fibrillarin (FBL) is a protein present exclusively in nucleoli, and its translocation into the nucleoplasm is a sign of nucleolar stress (Yang et al., 2018). Treatment with BMH-21 caused leaking of FBL in the nucleoplasm, confirming nucleolar stress as described previously. Interestingly, Nutlin treatment also caused a strong leakage of FBL to the nucleoplasm. Western blot analysis revealed downregulation of major components of the RNA Pol I machinery; the catalytic subunit POLR1A and RNA Pol I-specific transcription factor RRN3 are downregulated both by BMH-21 and Nutlin treatment (Figure 4C). To further investigate the cause for the downregulation of RNA Pol I components, we co-treated SJSA-1 cells with Nutlin and the proteasome inhibitor MG-132 (Figure S4A); this restored protein levels, suggesting protein degradation as the cause of the downregulation. Interestingly UBF, which levels correlate with RNA Pol I activity, was also down regulated upon Nutlin treatment, and was observed to be displaced from the nucleoli at early time points (Figure S4B). Inhibition of the proteasome using MG-132 rescued UBF levels, confirming degradation at the protein level (Figure S4B). Neither FBL nor Nucleophosmin (NPM) were regulated at the protein level; NPM and POLR1A were also shown to translocate to the cytoplasm upon 24h Nutlin treatment, once again

confirming nucleolar stress (Figure 4E, Figure S4C). We reproduced these results also in GOT-3 and CRL3043, two liposarcoma cell lines harbouring an MDM2 amplification (Figure 4 D-F).

Taken together, these data confirm disruption of the RNA Polymerase I machinery and presence of nucleolar stress upon p53 induction.

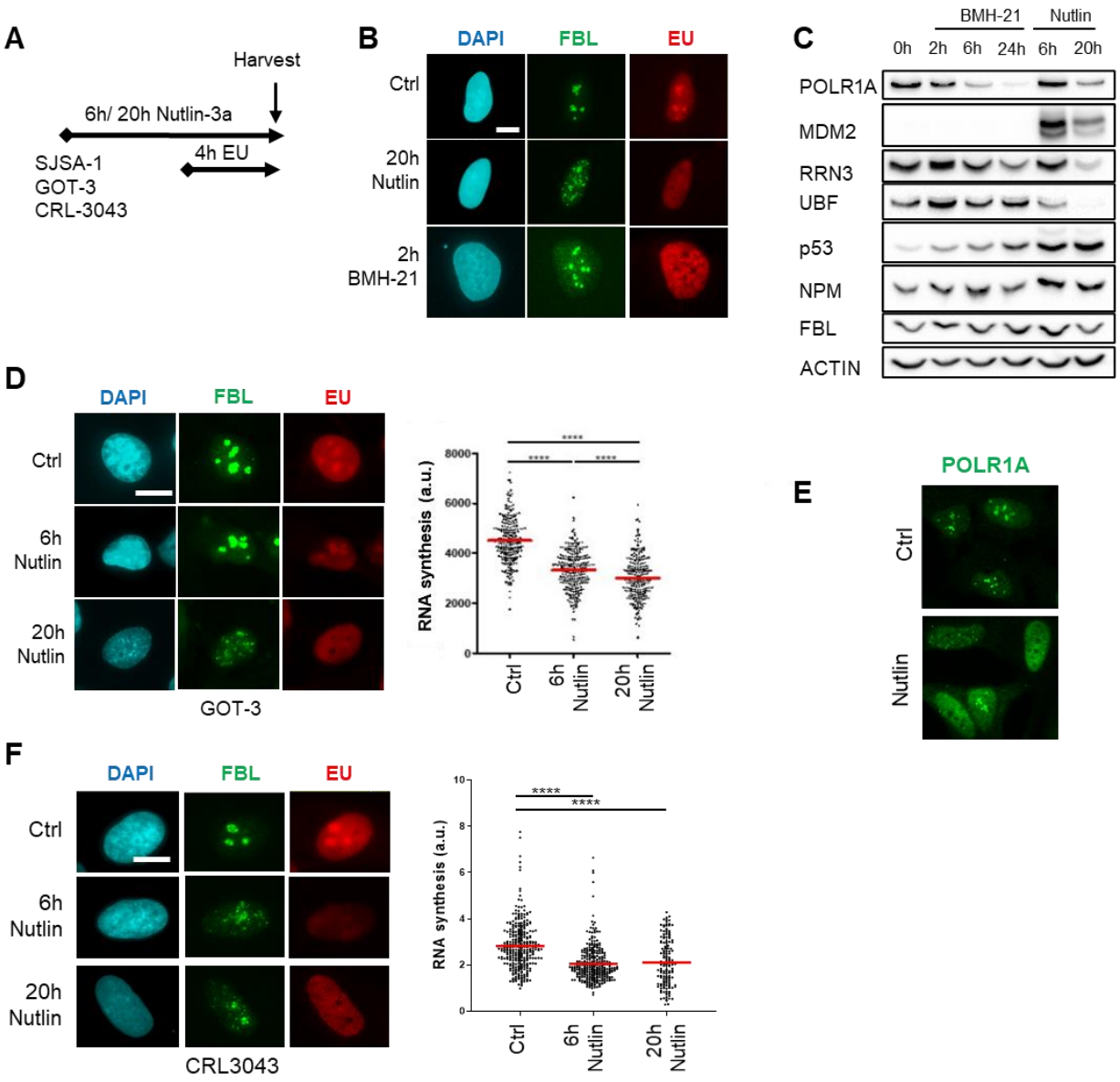

Figure 4: p53 activation induces nucleolar stress and RNA Polymerase I inhibition in several cell lines harbouring an MDM2 amplification

A) Treatment scheme for experiments shown in B-F. SJSA-1 cells were treated with 20µM Nutlin for 20h, with the last 4h also labelled with 1mM Ethynyl Uridine (EU) for detection of nascent RNA.
B) Nucleolar disruption was observed after 20h of Nutlin-3a treatment, as shown by the Fibrillarin (FBL) staining, a nucleolar marker. BMH-21, a RNA POL 1 inhibitor, was

used as control for disruption of rRNA synthesis and nucleolar stress. Scale bar= 10µm.

C) Immunoblot analysis of Nutlin-3a and BMH-21 treated SJSA-1 cells. Both treatments caused a downregulation of POLR1A and RRN3/TFIIA protein levels. UBF downregulation was specific to Nutlin-3a treatment.
D) GOT-3 cells were treated as described in A. EU assay confirmed a downregulation of RNA synthesis, particularly in the nucleoli. FBL was also strongly displaced from nucleoli, confirming nucleolar stress. Scale bar= 20µm.
E) CRL3043 cells were treated as described in A. Both rRNA synthesis repression and nucleolar stress was observed also in this cell line. N=150-300
F) Immunofluorescence analysis revealed a displacement of the catalytic subunit of RNA Pol 1, POLR1A, from nucleoli to the nucleoplasm, confirming RNA Pol 1 complex disruption. Scale bar= 20µm.

MDM2 accumulation leads to RNA Pol I disruption and defects in ribosome biogenesis, also in cell lines without a MDM2 amplification

Since Nutlin treatment led to displacement of POLR1A to the nucleoplasm, we asked if this also depended on complex formation between MDM2 and ribosomal proteins L5 and L11. Depletion of either RP using siRNA prevented displacement of POLR1A from the nucleoli, confirming the involvement of RPL5 and RPL11 in RNA Pol I inhibition (Figure 5A). We next investigated the consequences of RNA Pol I inhibition on ribosome biogenesis. SJSA-1 cells were treated with Nutlin and RNA was harvested at different time points, followed by northern blotting and analysis of steady-state levels of RNA (Figure 5B). BMH-21 was included as control for RNA Pol I inhibition, and caused a profound decrease in 47S pre-rRNA, as expected. On the other hand, Nutlin treatment caused a milder decrease of 47S; instead, accumulation of unprocessed 12S pre-rRNA was observed, suggesting faulty processing of rRNA of the large ribosomal subunit 60S. Due to the very high levels of rRNA synthesis and the highly dynamic nature of pre-rRNA processing, we next opted to metabolically label nascent RNAs prior analysis on northern blot (Figure 5C). Metabolic labelling can detect changes that occur within minutes and allows for a much more sensitive quantification of pre-rRNA. We saw a strong repression in 47S pre-rRNA synthesis at 15h of Nutlin treatment, which can be observed (mildly) at 6h, confirming the EU assay results. 28S production was affected much more than 18S, again suggesting a disruption in the production of the 60S large subunit rather than the 40S small subunit. Finally, we investigated whether these defects in RNA Pol I and III complexes were reproducible in the MCF-7 cell line, which displays normal levels of MDM2 (Figure 5D). Degradation of POLR1A, UBF and TFIIIA was seen also in this cell line, but it was milder and observed at later time points.

In conclusion, we could show that displacement of the catalytic subunit of RNA Pol I caused by Nutlin treatment depends on both RPL5 and RPL11. Prolonged treatments led to defects

in 28S rRNA processing and repression of 47 pre-rRNA synthesis, meaning ribosome biogenesis is impaired.

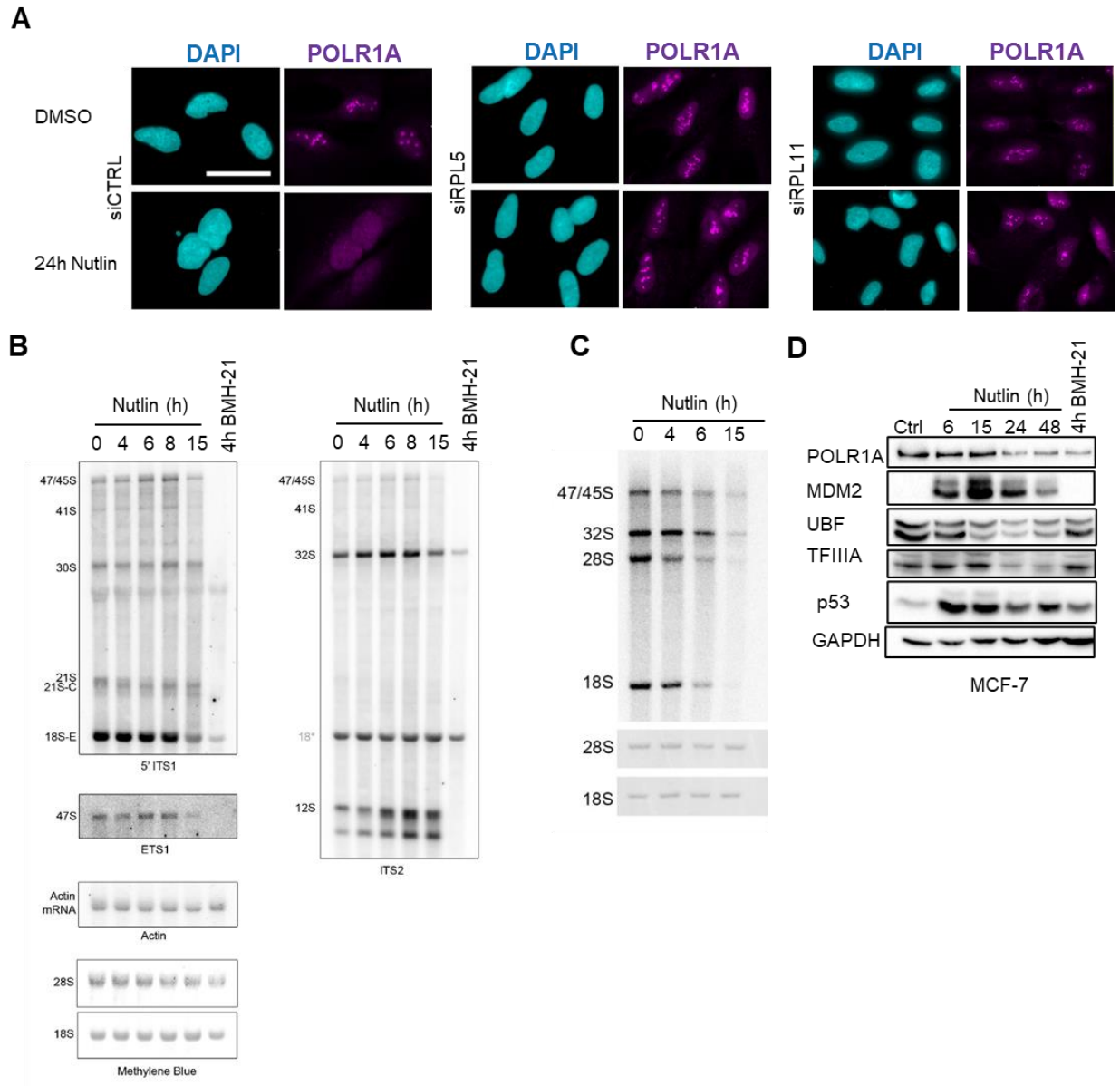

Figure 5: MDM2 accumulation leads to RNA Pol I disruption and defects in ribosome biogenesis, also in cell lines without a MDM2 amplification

A) Representative images of POLR1A displacement from the nucleoli to the nucleoplasm upon Nutlin treatment. Depletion of either RPL5 or RPL11 rescues POLR1A displacement. Scale bar= 40µm.
B) North Blot analysis of rRNA processing upon Nutlin-3a time points. P53/Mdm2 induction via Nutlin leads to accumulation of several pre-RNA, particularly 12S, which suggests disruption in ribosome biogenesis
C) Pulse-chase metabolic labelling of nascent RNAs confirms rRNA synthesis repression at 15h of Nutlin. This is preceded by defects of 28S production and processing.
D) MCF-7 cells, which do not harbour an MDM2 amplification, also show some level of nucleolar stress, as observed by downregulation of nucleolar proteins.

The MDM2/RPL5/RPL11 complex induces cell death in SJSA-1 cells

Most cancer cell lines respond to Nutlin largely by a reversible cell cycle arrest. Only a minority of cell lines, most of which containing an MDM2 amplification, respond with cell death (Shen and G. Maki, 2011). This might suggest that high MDM2 levels are necessary for induction of cell death in response to Nutlin. Nevertheless, some drug candidates similar to Nutlin have entered clinical trials (Khoo et al., 2014); the major concern remains the lack of efficiency of such drugs, since a reversible cell cycle arrest could lead to p53 mutation and resistance. We therefore decided to investigate the role of the 5S RNP-MDM2 complex in Nutlin-induced cell death. We transfected SJSA-1 cells with two independent siRNA against either Mdm2 or Puma, a p53-target genes involved in caspase activation and apoptosis (Callus et al., 2008), for 24h followed by 48h of Nutlin treatment. Much to our surprise, depletion of Mdm2 but not Puma, prevented cell death in response to Nutlin, as shown by cell viability assays (Figure 6A-B). This is surprising also because p53 levels do not seem to be affected by depletion of Mdm2, but rather stay the same upon Nutlin treatment, suggesting a rather important role in cell death for Mdm2 but not p53 (Figure 6C). Interestingly, Puma knock down prevented PARP1 cleavage, confirming inhibition of caspases activity (Figure 6D); however, cells still died, suggesting a caspase-independent type of cell death. We proceeded to test whether RPL5 and RPL11 might also be involved in Nutlin-induced apoptosis. Knock down of RPL5 or RPL11 with two different siRNA prevented cell death upon Nutlin, as shown by brightfield images (Figure 6E). Cell viability assays revealed a strong cell cycle arrest in response to RPL5/RPL11 depletion, but no further decrease in cell number upon Nutlin treatment (Figure 6F). Finally, immunoblot analysis confirmed that RPL5/RPL11 depletion prevents PARP1 cleavage upon Nutlin treatment, demonstrating that the presence of RPL5 and/or RPL11 lead to caspase activation once Mdm2 is induced by Nutlin (Figure 6G).

In summary, we show that Nutlin-induced cell death depends on MDM2, RPL5 and RPL11, and depletion of any of the members of the complex rescues cell viability. Depletion of PUMA did not prevent cell death, although it inhibited caspases activation, suggesting a caspase-independent pathway of cell death induced by Nutlin.

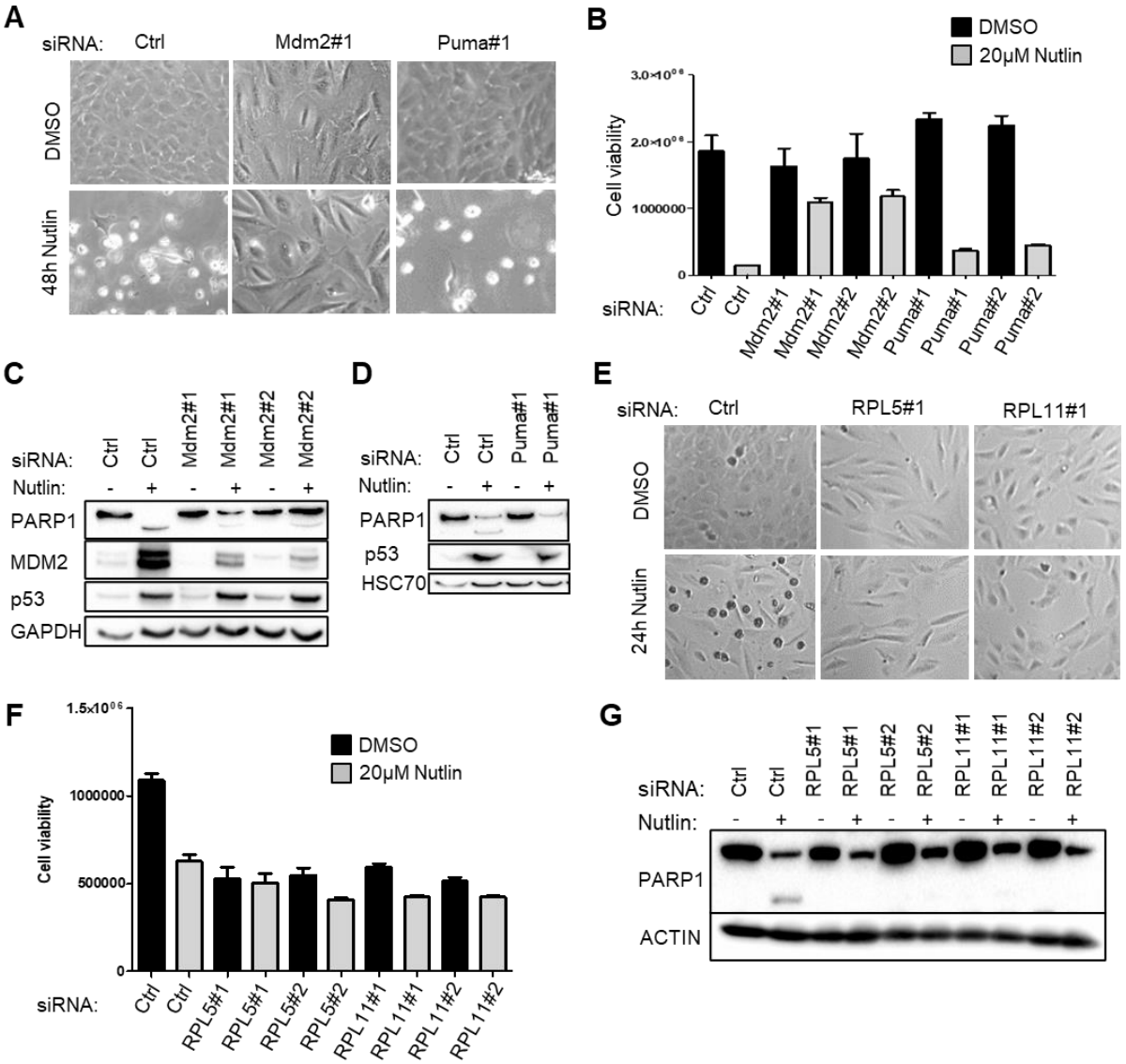

Figure 6: The Mdm2/RPL5/RPL11 complex induces cell death in sarcoma cell lines

A) SJSA-1 cells were transfected with siRNA either against Mdm2 or Puma. Depletion of Mdm2, but not Puma, led to a rescue in cell death.
B) Cell viability was performed measuring the ATP content using the Ultra-Glo recombinant luciferase. Mdm2 knock-downs lead to rescue in cell viability after 48h Nutlin, while depletion of Puma did not.
C) Immunoblot analysis confirms the efficiency of the Mdm2 siRNAs and rescue of PARP1 cleavage upon Mdm2 knockdown, although p53 protein levels are not affected.
D) Immunoblot analysis reveals inhibition of PARP1 cleavage upon PUMA knockdown.
E) A similar rescue of cell death was observed when knocking down either RPL5 or RPL11, as shown by brightfield images.
F) Cell viability quantification after 24h Nutlin treatment and upon depletion of RPL5 or RPL11 by two independent siRNA.
G) Immunoblot analysis confirms that PARP1 is no longer cleaved upon siRNA knockdown of either RPL5 or RPL11.

2.3 DISCUSSION

Our results reveal a novel role of MDM2 in complex with RPL5 and RPL11 in regulating RNA Polymerase III activity. P53 induction via Nutlin caused a fast and strong repression of both type I and type II promoters, and this depended on the presence of MDM2, RPL5 and RPL11. Longer p53 activation led to RNA Pol I repression, nucleolar stress, defects in ribosome biogenesis and ultimately cell death.

We found MDM2 in the proximity of POLR3A, and depletion of either RPL5 or RPL11 reduced such proximity without affecting MDM2 levels (Figure 2C-D). Therefore, RPL5 and RPL11 are necessary for recruitment of MDM2 at RNA Pol III-dependent genes. The exact mechanism remains unknown. The 5S-RNP presents some unique characteristics that differentiate it from other RNPs. First, mammalian cells contain a large pool of free 5S-RPL5 RNPs, representing up to 50% of total 5S rRNA (Madru et al., 2015; Steitz et al., 1988). This suggests extra-ribosomal functions, and the necessity of a fast-responding mechanism upon stress. Both RPL5 and RPL11 can directly interact with the 5S rRNA, and therefore might act as sensors for problems that arise in ribosome biogenesis (Chakraborty et al., 2011). Moreover, RPL5 has been shown to be necessary for the proper processing of 5S rRNA by binding and stabilizing it co-transcriptionally (Sloan et al., 2013). It is tempting to speculate that MDM2 might be recruited in the proximity of RNA Pol III by RPL5 and RPL11 binding nascent 5S rRNA. Depletion of either RPL5 or RPL11 not only rescued 5S rRNA synthesis upon Nutlin treatment, but also seemed to lead to accumulation of unprocessed 5S in the absence of p53 activation (Figure 2E), suggesting that both these proteins are involved in processing of 5S rRNA. Our study shows that both RPL5 and RPL11 are required for inhibition of RNA Pol III by MDM2. This is not surprising, since it has been shown that depletion of any of the components of the 5S rRNA abolishes the binding of the others, explaining why RPL5 and RPL11 might be dependent on each other (Donati et al., 2013), and why depletion of one of them might cause the entire complex to destabilize.

MDM2 has previously been shown to inhibit transcription of RNA Pol II, either by inhibiting transcription factors (Biderman et al., 2012) or by chromatin modifications (Wienken et al 2016). *In vitro* studies from the Tjian laboratory showed that MDM2 represses gene expression, also in the absence of p53 (Thut et al., 1997). Our results further corroborate on this, showing for the first time that MDM2 can also affect transcription of non-coding RNA.

But how could inhibition of RNA Pol III cause such a fast and strong disruption in ribosome biogenesis and Pol I activity? This question remains unexplored in mammalian cells. However, the 5S RNP has certain unique properties that make it an ideal candidate to play a role in a

possible ribosome biogenesis feedback mechanism. First, it links RNA Pol III to all the other RNA polymerases; secondly, the 5S-RNP integrates early into pre-60S particle in the nucleolus, which allows regulation of ribosome biogenesis at early stages (Aubert et al., 2018). Disruption of Pol 3 activity or RPs imbalance would be immediately detected by lack of 5S RNP itself. Disruptions in Pol 1 activity would delay formation of the pre-60S particle, and therefore impede 5S-RNP assembly. Finally, MDM2 could be the final link between many types of different stresses with regulation of ribosome biogenesis. Up until now, MDM2/RPs interactions have been investigated only in response to nucleolar stress as a mechanism to activate p53, leading to cell cycle arrest and cell death *in response* to ribosomal stress (Russo and Russo, 2017). However, not all cellular stresses directly affect ribosome biogenesis, and it is intriguing to speculate that a p53-dependent mechanism might be in act to link other cellular stresses to this highly energy-demanding process. Moreover, MDM2 has been shown to interact with 16 RPs, and depletion of some of these RPs are not important for p53 induction (Liu et al., 2016), arguing that these interactions might play a different role.

Although canonically defined as an oncogene, ectopic expression of MDM2 has been shown to restrict cellular proliferation and tumour development, also in the absence of p53 (Fridman et al., 2003; Jones et al., 1998). Moreover, RP-MDM2 interaction has been shown to act as tumour suppressor in certain settings, for example in c-MYC induced lymphomagenesis (Macias et al., 2010). Our results expand on this by demonstrating that MDM2 act as a tumour suppressor by inhibiting RNA Pol III transcription and disrupting ribosome biogenesis. This is particularly relevant, since the most common alteration of rRNA in tumours are amplification of 5S rDNA (Wang and Lemos, 2017). Future studies will be needed to test whether a possible therapeutic synergism can be achieved combining RNA Pol III inhibition and p53 induction.

2.4 SUPPLEMENTARY DATA

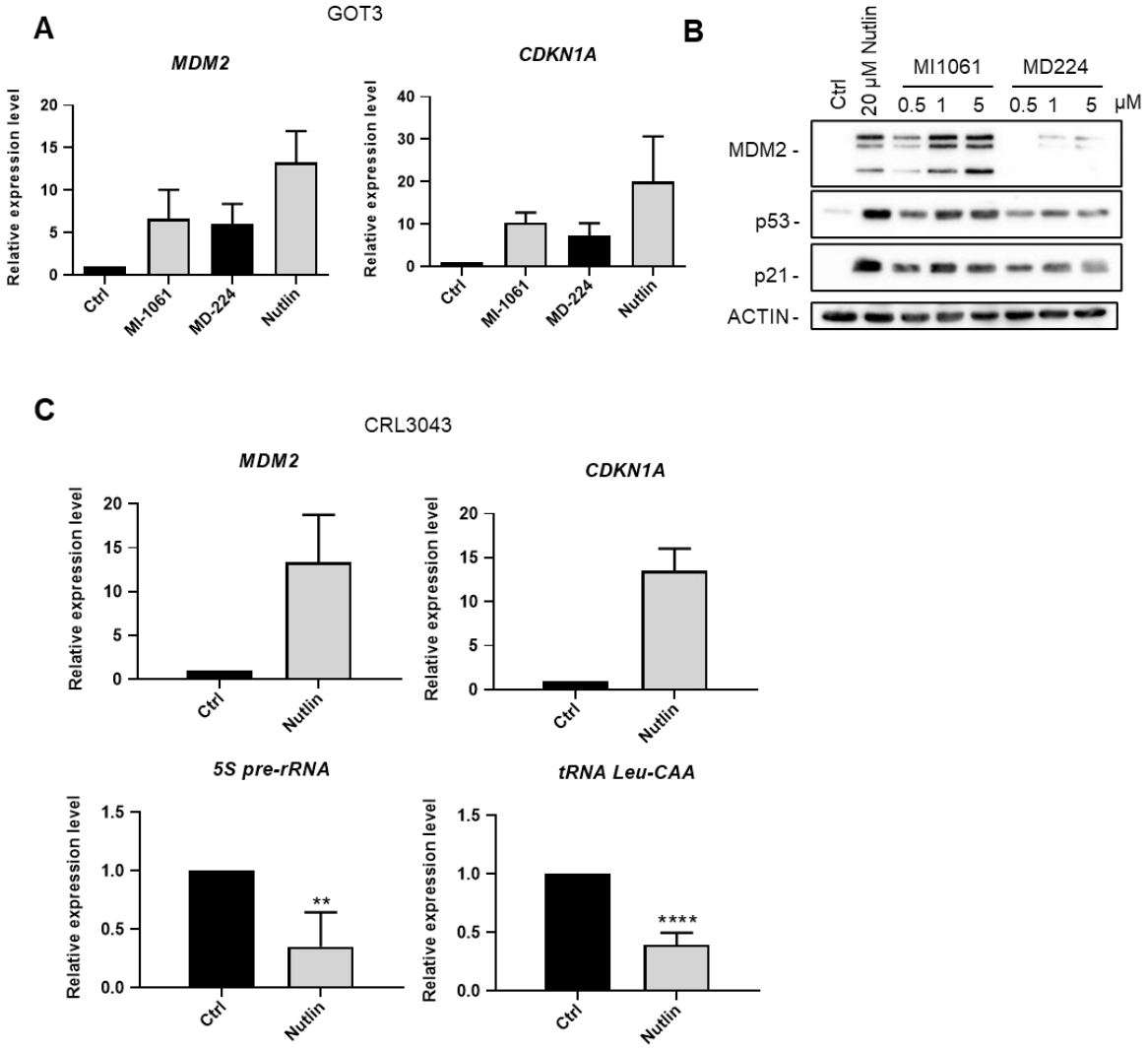

Figure S1: RNA Pol III activity is inhibited upon Mdm2 induction

A) GOT3 cells were treated for 24h with 500nM of either MI-1061 or MD-224, or with 20µM of Nutlin prior to RNA or protein harvesting. qPCR analysis revealed comparable induction of *MDM2* and *CDKN1A* in response to both MI-1061 and MD-224, confirming p53 activation. Nutlin was used as a positive control for p53 activation.

B) Immunoblot analysis of the experiment shown in A. Different concentrations of MI-1061/MD-224 were tested, with 500nM being the most efficient at depleting Mdm2.

C) CRL3043 cells were treated for 6h with 20µM of Nutlin, and qPCR analysis was performed to quantify p53-target genes *MDM2* and *CDKN1A*, and RNA Pol III transcripts. Both 5S pre-rRNA and unspliced tRNA Leu-CAA were downregulated upon Mdm2 induction.

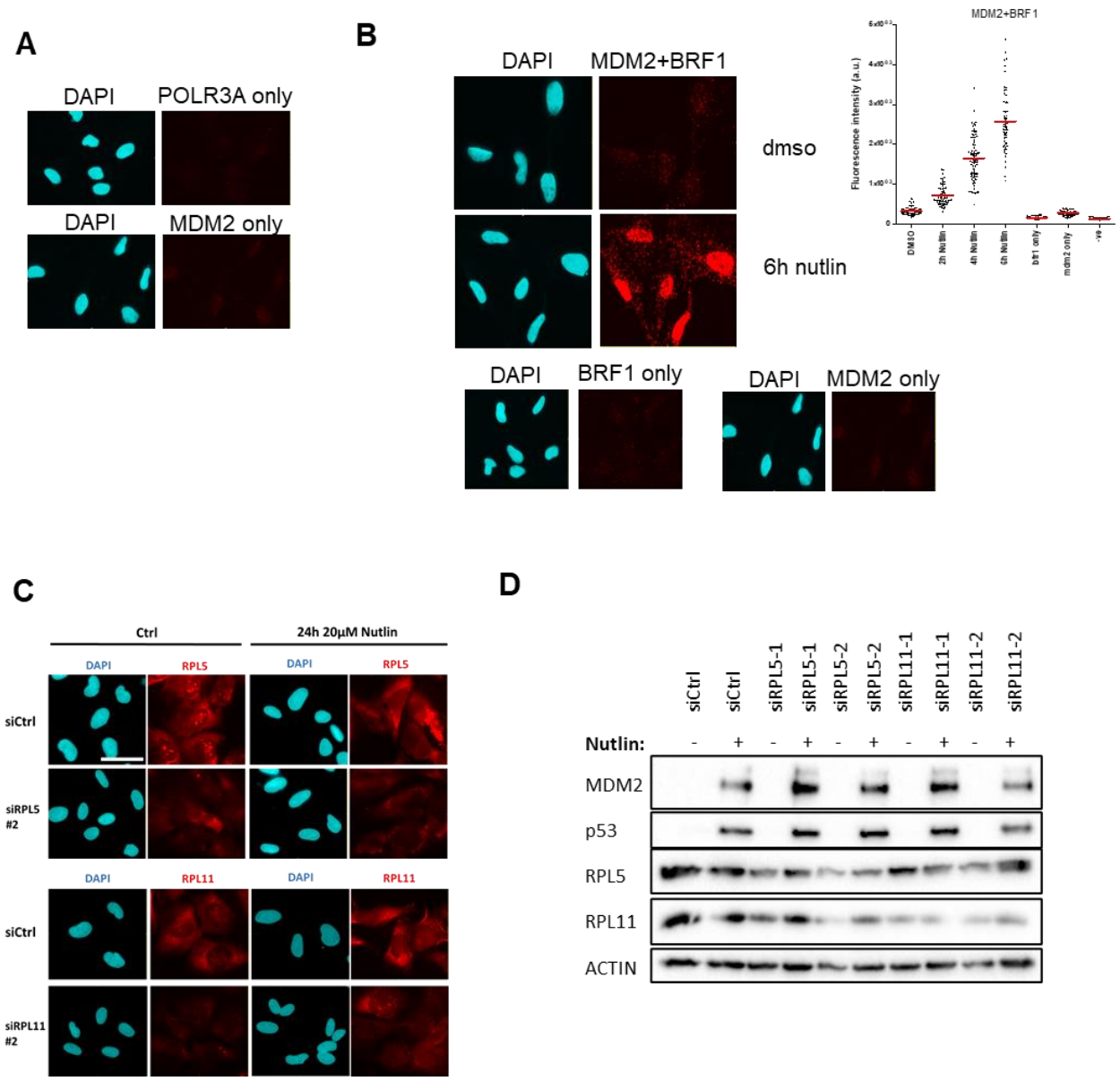

Figure S2: MDM2/RPL5/RPL11 complex is in the proximity of RNA Pol III and leads to its inhibition

A) Negative controls for PLA shown in Fig.1A, where only one of the antibodies was incubated to check for any unspecific binding.
B) SJSA-1 cells were treated with 20μM Nutlin for 6h prior to fixation and performing PLA. MDM2 was shown to be in the proximity of BRF1, a general transcription factor which is part of the RNA Pol III super-complex. Negative controls omitting one of the two antibodies are included (bottom).
C) Immunofluorescence experiments confirmed strong depletion of nuclear RPL5 and RPL11 after siRNA transfection against their respective mRNA (Figure 1C-D). Moreover, p53 activation following Nutlin treatment caused delocalization of both RPs from nucleoli to nucleoplasm.
D) Immunoblot analysis of SJSA-1 cells transfected with RPL5 or RPL11 siRNA (72h), and treated with 20μM Nutlin for 24h prior harvesting.

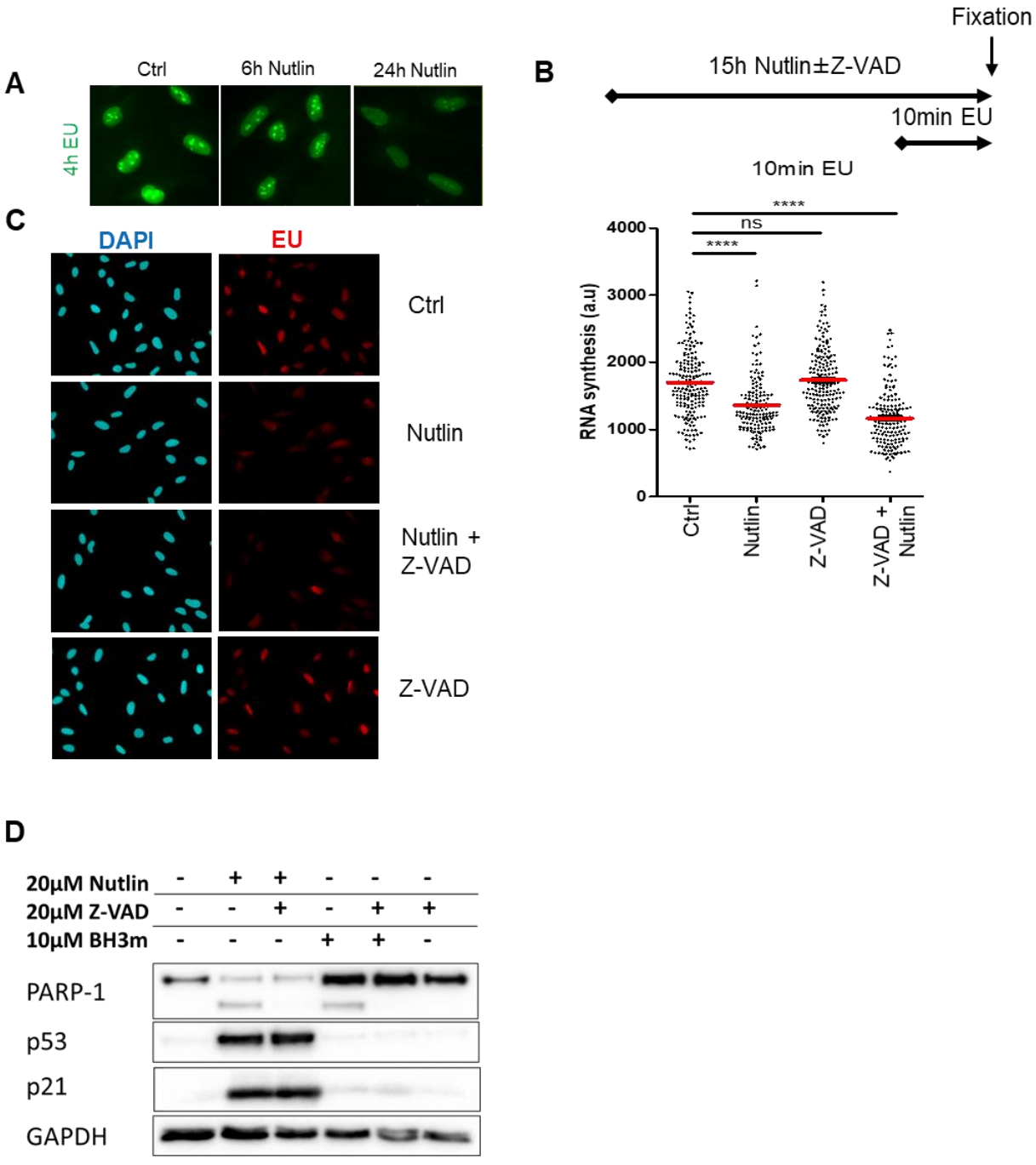

Figure S3: Nutlin treatment leads to global RNA synthesis repression, independent of p21

A) EU assay revealed a slight repression of RNA synthesis after 6h of Nutlin, and this dramatically decreased after 24h treatments.
B) SJSA-1 cells were treated with 20µM Nutlin for 15h, together with DMSO or pan-caspase inhibitor *Z-VAD*-FMK. For detection of nascent RNA, cells were labelled for 10min with EU prior fixation and further processing.
C) Representative images of EU assay performed following Nutlin and/or zVAD treatment. Scatter plots were used to quantify single cell intensities (right panel).

D) Cells were treated for 24h with either Nutlin-3a, zVAD or BH3 mimetic ABT-737 as control for caspase activation. Immunoblot analysis of proteins were used to confirm caspase inhibition by zVAD, by visualizing PARP1 cleavage, and p53 induction by Nutlin.

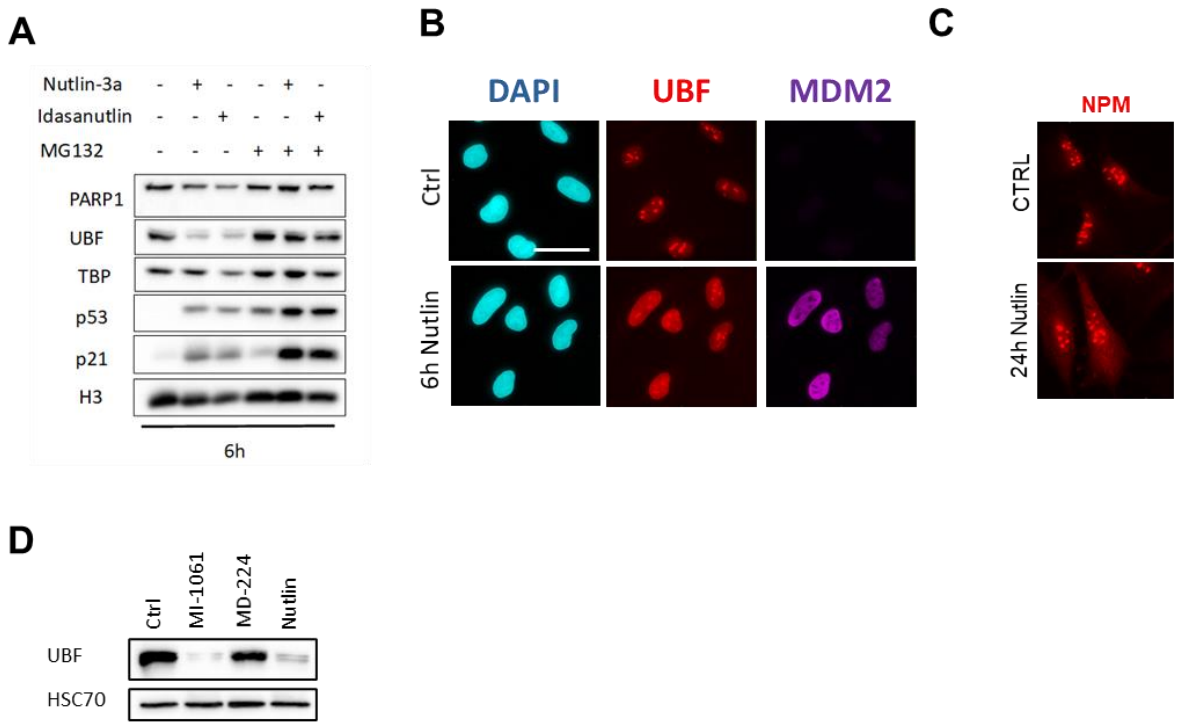

Figure S4: p53 induction leads to Pol 1 complex disruption and defects in ribosome biogenesis

A) SJSA-1 cells were treated for 6h with either 20µM Nutlin-3a or 1µM Idasanutlin, and together with 10µM of MG-132 proteasome inhibitor in the last 4h prior protein harvesting and western blot.
B) Immunofluorescence images show UBF displacement in the nucleoplasm after 6h oof Nutlin treatment. Scale bar= 40µm.
C) NPM was observed to localize to the cytoplasm following a 24h Nutlin treatment.
D) Depletion of MDM2 via MD-224 leads to a rescue in UBF protein levels.

2.5 METHODS

Treatments and transfections

Cells were treated with Nutlin-3a (#B0084-425358, BOC Sciences), MI-1061 (#HY-125858, Hölzel), MD-224 (HY-114312, Hölzel), BMH-21 (#S7718, Selleckchem), MG-132 (#474791, Millipore), Z-VAD-FMK (# ALX-260-020-M005, Enzo Life Sciences), Idasanutlin (#S7205, Selleckchem), ABT-737 (BH3 mimetic, #S1002 Selleckchem).

siRNA transfections were performed using Lipofectamine 3000 (Life Technologies), as described by manufacter. Cells were reverse transfected with final siRNA concentration of 10 nM siRNA. Medium was refreshed after 24 h and cells harvested 48 h post-transfection.

Immunoblot analysis

Cells were harvested in protein lysis buffer (20 mM Tris-HCl pH 7.5, 10 mM NaCl, 1 mM NaCl, 10mM EDTA, 1% Triton-X 100, 1% deoxycholate salt, 0.1% SDS, 2 M urea, protease inhibitors (pepstatin, leupeptin hemisulfate, aprotinin, AppliChem). The samples were sonicated for a short time to disrupt DNA-protein complexes. Total protein concentration was measured using a BCA protein assay kit (Thermo Fisher Scientific). The samples were then boiled in Laemmli buffer at 95°C for 5 min and equal amounts of proteins were separated by SDS-PAGE. Subsequently, proteins were transferred onto a nitrocellulose membrane, blocked in 5% (w/v) non-fat milk in TBS containing 0.1% Tween-20 for 1 h and incubated with the following primary antibodies at 4 °C overnight: MDM2 (IF2, Calbiochem), p53 DO-1 (#sc126, Santa Cruz), Parp1 (#ab137653, Abcam), p21 (#2947S, Cell Signaling), beta actin (#ab6276, Abcam), GAPDH (#ab8245, Abcam), HSC70 (sc7298 Santa Cruz), POLR3A (#PA5-58170, ThermoFisher), TFIIIA/GTF3A (#A303-621A, ThermoFisher), POLR1A (#24799, Cell signalling), RRN3 (HPA049837-100UL), UBF (#sc-13125, Santa Cruz), NPM (#3542 S, Cell Signaling), FBL (#sc-166001, SantaCruz), RPL5 (#51345S, Cell Signaling), RPL11 (#18163S, Cell Signaling), H3 (#ab1791, Abcam).

Membranes were then incubated with peroxidase-conjugated secondary antibodies (donkey anti-mouse or donkey anti-rabbit IgG, Jackson Immunoresearch) and the proteins were detected using either Super Signal West Femto Maximum Sensitivity Substrate (Thermo Fisher Scientific) or Immobilion Western Substrate (Millipore).

RNA isolation and qPCR

RNA was isolated from 6 well plates using the TRIzol reagent, following manufacter instructions. Prior cDNA synthesis, samples were treated with DNAse to remove residual genomic DNA. The following scheme was followed:

RNA	2-3µg
10x Reaction Buffer with MgCl2	2µl
DNase I, RNase-free (1 U/µL)	2µl
RNase Inhibitor (40 U/µL)	0.5µl
Nuclease-free water to 20 µL	Tot volume 20µl

Samples were incubated at 37°C for 30min, followed by addition of 2µl 50mM EDTA per sample and incubation for 10min at 65°C. Subsequentially, cDNA synthesis was performed using random nonamers primers (Promega). RT-qPCR was used to assess and quantify RNA expression levels using the SYBR green dye.

Immunofluorescence

Cells were grown in 8-well permanox slides (#177445, Nunc) fixed with 3.7% PFA in PBS for 30 min before being permeabilized with 0.5% Triton-X-100 in PBS for 30 min. Cells were then blocked with 10% FCS in 0.1% Tween-PBS for 10min at room temperature, followed by incubation with primary antibodies at 4°C, overnight: MDM2 (Calbiochem #OP46), FBL (sc-166001, Santa Cruz), POLR1A (#24799, Cell Signaling Technologies), NPM (#3542 S, Cell Signaling), UBF (#sc-13125, Santa Cruz).

After washing with PBS (3x10min), slides were incubated with secondary antibody (Alexa Flour 488 anti-mouse #A11029, Alexa Flour 647 anti-mouse #A-21235, Alexa Flour 546 anti-rabbit #A10040, ThermoFisher) and 4',6-diamidino-2-phenylindole (DAPI) for 1h at room temperature. Following washes in PBS (3x10min), the chambers were removed, and slides were mounted onto coverslips using fluorescent mounting medium (DakoCytomation, #S302380-2). Images were acquired using a Zeiss Axio Scope.A1 fluorescence microscope equipped with an Axio Cam MRc/503 camera using a 40x magnification, and further analysed with ImageJ. The DAPI signal was used to create binary images (segmentation) to define the nuclear area as region of interest (ROI). These ROIs were then used to quantify the nuclear signal of the other channels. Single nuclei mean gray values were visualized on dot plots, and statistical testing was performed using Graph Pad Prism v.6 unpaired Student's t-test.

Proximity Ligation Assay

Cells were grown in 12-well slides (#81201, Ibidi) and following treatment or transfection, cells were fixed and permeabilized as described above, and subjected to the PLA assay using the Duolink In Situ Detection Reagents Orange (#DUO92007, Sigma-Aldrich) in a humidity chamber according to the manufacturer's instructions. Briefly, plastic wells were removed from the chamber slides prior to blocking and incubation with primary antibodies and PLA probes

(Duolink™ In Situ PLA® Probe Anti-Mouse PLUS #DUO92001, Duolink™ In Situ PLA® Probe Anti-Rabbit MINUS #DUO92005) for 1 h, at 37°C while shaking. Ligase was then added to hybridized PLA probes to generate a closed circle (60min at 37°C) before DNA amplification for 100 min at 37°C while shaking. After the PLA protocol, cells were then counter stained with DAPI, plastic chambers were removed and slides were mounted onto coverslips using fluorescent mounting medium (DakoCytomation, #S302380-2). Images were acquired and analysed as described above.

Ethynyl Uridine nascent RNA assay

To visualize nascent RNA, cells were labelled with the uridine analogue 5- ethynyluridine (5-EU) followed by a copper-catalyzed azide-alkyne cycloaddition reaction named “click chemistry”. Cells were seeded on an 8-well chamber in a volume of 200 µL per well and, after acertain treatment duration, labelled with 1 mM EU for 10-15 min (to detect nascent RNA) or 4 h (to detect steady-state RNA). Next, the cells were fixed in 4% PFA in PBS for 30 min. After two washes with PBS, the cells were permeabilized by adding 0.5%triton X-100 in PBS for 30 min while shaking. the click chemistry reaction was performed by adding freshly prepared click chemistry mixture , followed by an incubation for 1 h shaking:

Component	**Volume (tot 200µl)**
Na-Phosphate buffer (100 mM, pH 7)	198.2 µL
Alexa Fluor® 594-Picolyl-Azide (5 mM)	0.2 µl
CuSO4(100 mM):THPTA(250 mM) premix	0.6 µl
Na-Ascorbate (1M)	1µl

After washing with PBS (3x 5min), slides were either used for further immunofluorescence applications, or stained with DAPI for nuclei visualization. Slides were then mounted using the DAKO fluorescence mounting medium, sealed with nail polish, stored at 4 °C and imaged within one month.

Pre-rRNA analysis by northern blotting

Total RNA was extracted from human cells using TRI reagent (Sigma-Aldrich) according to the manufacturer’s instructions. Total RNA was separated by denaturing agarose (glyoxal) gel electrophoresis, RNAs hydrolysed insituby treatment with 0.1 M NaOH and transferred to a nylon membrane by vacuum blotting. Alternatively, total RNAs were separated by electrophoresis on denaturing acrylamide (urea) gels and transferred to nylon membranes by electroblotting. RNAs were crosslinked to membranes, which were pre-hybridised in SES1 buffer (0.25 M sodium phosphate pH 7.0, 7% SDS, 1 mM EDTA) at 37°C for >1 h. 5’ [32P]-

labelled DNA oligonucleotides complementary to specific rRNA sequences(Table 1)were added and incubated for >14h at 37°C. Probes were removed and membranes were washed for 30 min each at 37°C in 6x SSC (150 mM NaCl, 15 mM sodium citrate) and then 2x SSC supplemented with 0.1% SDS. Membranes were exposed to phosphorimager screens and signals detected using a Typhoon FLA950.

Pulse-chase metabolic labelling of nascent RNAs

Experiments were performed as previously described (Sloan et al., 2013a).Cells treated with Nutlinfor the indicated times were grown in phosphate-free DMEM for 1 h and then for a further 1 h in phosphate-free DMEM supplemented with 15 μCi/mL [32P]-labelled orthophosphate. The labelled media was removed, cells were washed with PBS and then growth for afurther 3 h in unlabelled DMEM containing phosphate. Total RNA was extracted and separated by denaturing agarose/acrylamide gel electrophoresis as described above. Polyacrylamide gels were dried and directly exposed to phosphorimager screens whereas RNAs separated in agarose gels were first transferred to nylon membranes. [32P]-labelled RNAs were detected using a Typhoon FLA9500.

Cell viability assay

Cells were seeded in 96well plates (Corning) 24h prior start of treatments. Cell viability was measured using CellTiter-Glo® Luminiscent assay from Promega (Cat. #G7570) based on detectable ATP, following manufacturer's instructions and in triplicates.

Table 1. DNA oligonucleotide probes used for northern blotting

Probe	Sequence 5'-3'	Reference
ETS1	CGGAGGCCCAACCTCTCCGACGACAGGTCGCCAGAG GACAGCGTGTCAGC	Memet et al., 2017
5'ITS1	CCTCGCCCTCCGGGCTCCGTTAATGATC	Sloan et al., 2013b
ITS2	GCTCTCTCTTTCCCTCTCCGTCTTCC	Choudhury et al. ,2020
Actin mRNA	AGGGATAGCACAGCCTGGATAGCAAC	Memet et al., 2017
U6 snRNA	GAACGCTTCACGAATTTGCGTGTC	Warda et al., 2017
5S rRNA	CCGAGATCAGACGAGATCGGGCGCGTTCAGGGTGGT ATGG	Sloan et al. 2013a

Table 2. qPCR primers

Primer	Sequence
36B4	5’ GATTGGCTACCCAACTGTTG 3’ 3’ CAGGGGCAGCAGCCACAAA 5’
GAPDH	5’ CTATAAATTGAGCCCGCAGCC 3’ 3’ ACGACCAAATCCGTTGACTC 5’
P21	5’ TAGGCGGTTGAATGAGAGG 3’ 3’ AAGTGGGGAGGAGGAAGTAG 5’
MDM2	5’ TCAGGATTCAGTTTCAGATCAG 3’ 3’ CATTTCCAATAGTCAGCTAAGG 5’
PUMA	5’ GCCAGATTTGTGAGACAAGAGG 3’ 3’ CAGGCACCTAATTGGGCTC 5’
rDNA 18S	5’ AAACGGCTACCACATCCAAG 3’ 3’ CCTCCAATGGATCCTCGTTA 5’
rDNA 28S	5’ TGGGTTTTAAGCAGGAGGTG 3’ 3’ AACCTGTCTCACGACGGTCT 5’
rDNA 5S pre-rRNA	5’ CGGGCCTGGTTAGTACTTG 3’ 3’ CTGTAGATAACTCCCATACTTTAGGAC 5’
tRNA Leu-CAA	5’ GTCAGGATGGCCGAGTGGTC 3’ 3’ GTCAGAAGTGGGATTCGAAC 5’

Table 3: Chemicals and reagents used in this study

Chemical	Company	Catalog number
0.05 % Trypsin/EDTA	Invitrogen	25300054
AF594-Picolyl-Azide		CLK-1296-1
Ammonium sulfate	Roth	2SO4 9218.1
Ammonium peroxodisulfate (APS)	Roth	9592.2
Ampicillin,	AppliChem	A0839
Bromphenol blue	Sigma	B0126
Chloroform	Roth	3313.1
cOmpleteTM Protease Inhibitor Cocktail	Roche	5056489001
CuSO4 - Copper(II)-Sulphate	Jena Bioscience	CLK-MI004-50
dATP, stock solution (100 mM)	Primetech	1202.4
dCTP, stock solution (100 mM)	Primetech	1203.4

dGTP, stock solution (100 mM)	Primetech	1204.4
dTTP, stock solution (100 mM)	Primetech	1205.4
Dimethyl sulfoxide (DMSO) for cell culture	AppliChem	A3672,0100
Disodium phosphate dihydrate	Roth	3580.1
Dithiotreit (DTT), > 99 % p.a.	Roth	6908.4
Trehalose dihydrate	Roth	5151.3
Dulbecco's Modified Eagle's DMEM, powder, low glucose, pyruvate	Life Technologies	31600-091
Ethanol (EtOH) absolute, 99.9 %	ChemSolute	2246.2500
Ethylene diamine tetraacetic acid (EDTA)	Roth	8040.1
Ethylene glycol tetraacetic acid (EGTA)	Roth	3054.2
Fetal bovine serum (FBS) superior	Merck	S0615
Formaldehyde solution, 37 % (PFA)	Sigma	F1635-500ML-D
Glycine	Roth	3908.3
HEPES	Roth	9105.4
Hydrochloric acid, 25 %	Th Geyer	825.2511
Immobilon Western HRP Substrate	Merck Millipore	WBKLS0500
Isopropanol	Roth	6752.4
Kanamycin sulfate	AppliChem	A1493
L-glutamine, 200 mM solution	Life technologies	25030123
Lipofectamine 3000 (LPF 3000)	Invitrogen	L3000015
Magnesium chloride (MgCl2) solution, 1 M	Sigma	M M1028 Sigma
Methanol (MetOH), 99 %	Roth	8388.6
Milk powder, blotting grade	Roth	T145.4
Na-Ascorbate	Jena Bioscience	CLK-MI005-1G
NonidetTM P-40 substitute (NP-40)	Sigma	Sigma
Nuclease-free water	Ambion	AM9939
PageRuler prestained protein ladder	Thermo Scientific	26617
Pefabloc® SC-Protease-Inhibitor	Roth	A154.2
Penicilin/streptomycin	Gibco	15140130
Phosphate-buffered saline (PBS) tablets	Gibco	18912014
Ponceau-S	Roth	5938.1
Potassium chloride (KCl)	Roth	P017.1
Protein-G SepharoseTM 4	GE Healthcare	17061805
Rotiphorese® Gel 30 (37,5:1) acrylamide	Roth	3029.1

RPMI 1640 mit HEPES ohne L-Glutamin	Life Technologies	42401042
Sodium chloride (NaCl)	Roth	3957.2
Sodium deoxycholate (NaDOC)	Sigma	30970-100G
Sodium dodecyl sulfate (SDS)	Roth	CN30.3
SpectraTM Multicolor High Range Protein Ladder	Thermo Scientific	26625
SuperSignalWest Femto Maximum Sensitivity	Thermo Scientific	34095
SYBR Green	Life Technologies	S7567
TEMED	AppliChem	A1148,0025
Tris Pufferan, ≥ 99.9 %	Roth	4855.3
Tris(3-hydroxypropyltriazolylmethyl)amine (THPTA)	Sigma	762342
Triton X-100	AppliChem	A1388
TRIzol TM	Life technologies	15596018
Tryptone/Peptone	Roth	8952.2
Tween-20	AppliChem	A4974,0500
Urea, ≥ 99.5 %	Roth	3941.1
Yeast extract 2363.2	Roth	2363.2

Table 4: Solutions, Buffers and Media used in this study

Solution	**Composition**
10x PBS, pH 7.4	24 mM NaCl 0.27 mM KCl 0.81 mM Na2HPO4 0.15 mM KH2PO4 in H2O
10x TBS, pH 7.4	0.5 M Tris 1.54 M NaCl in H2O
10x SDS running buffer	250 mM Tris 1.92 M glycine 34.7 mM SDS
6x Laemmli buffer	0.35 M Tris, pH 6.8 30 % Glycine

	10 % SDS (w/v) 9.3 % DTT (w/v) 0.02 % Bromphenol blue (w/v)
CoIP buffer	300 mM NaCl 50 mM Tris-HCl, pH 7.5 1 % NP-40 in H2O
Click chemistry phosphate buffer	
RIPA-based cell lysis buffer for protein harvesting	2/3 RIPA lysis buffer 1/3 8 M urea Protease inhibitors: 10 µM Pefabloc 1 µg/ml Pepstatin A 1 µg/ml Leupeptin
Ponceau-S solution	0.5 % Ponceau-S (w/v) 1 % Acetic acid in H2O
1x TBS-T	1x TBS-T 10 % 10x TBS 0.1% Tween-20
Self-made 10x qPCR mix	750 mM Tris-HCl, pH 8.8 200 mM (NH4)2SO4 0.1 % Tween-20 in H2O, sterile filtrate (0.2 µm)
Self-made 2x qPCR Master Mix	1x self-made 10x qPCR mix 5.18 mM MgCl2 518 mM Trehalose in 10 mM Tris, pH 8.0 0.43 % Triton X-100 1:22,400 SYBR Green 0.345 mM dNTPs 34.54 U/ml Taq Polymerase

Table 5. Primary and secondary antibodies used in this study

Primary Antibodies for Immunoblot				
Antibody	**Source**	**Dilution**	**Producer**	**Catalog**
P53 DO-1	Mouse	1:1000	Santa Cruz	Sc126

MDM2	Mouse	1:300	CalBiochem	OP46-100UG
B-actin	Mouse	1:40000	Abcam	Ab6276-100
P21	rabbit	1:1000	Cell Signaling	2947 S
Histone H3	rabbit polyclonal	1:5000	abcam	ab1791
PARP1	Rabbit polyclonal	1:500	Abcam	Ab137653
UBF	Mouse mono	1:100	Santa cruz	sc-13125
POLR1A	Rabbit	1:1000	Cell Signaling	24799
RRN3	Rabbit	1:500	Merck	HPA049837-100UL
GAPDH	Mouse	1:5000	Abcam	Ab8245
Fibrillarin (FBL)	mouse	1:400	Santa Cruz	sc-166001
Nucleophosmin (NPM)	Mouse	1:500	Cell Signaling	3542S
POLR3A	Rabbit		Thermo Fisher	PA5-58170
TFIIIA	Rabbit	1:200	Bethyl Laboratories	A303-621A
HSC70	Mouse	1:5000	Santa Cruz	sc7298
RPL5	Rabbit	1:500	Cell Signaling	51345S
RPL11	Rabbit	1:500	Cell Signaling	18163S
TBP	Mouse	1:1000	Diagenode	C15200002

Secondary Antibodies for Immunoblot				
Antibody	**Source**	**Dilution**	**Producer**	**Cat. #**
HRP-coupled AffiniPure F(ab')2 fragment, anti mouse IgG (H+L)	Donkey	1:10000	Jackson Immuno Research	715-036-150
HRP-coupled AffiniPure F(ab')2 fragment, anti rabbit IgG (H+L)	Donkey	1:10000	Jackson Immuno Research	711-036-152

Primary Antibodies for Immunofluorescence				
Antibody	**Source**	**Dilution**	**Producer**	**Catalog**
Fibrillarin (B-1)	mouse	1:50 – 1:100	Santacruz	sc-166001
MDM2	mouse	1:200	Calbiochem	OP46
MDM2	Rbb	1:200	Abcam	ab226939
P53	mouse	1:400	Santacruz	Fl-393
P53 (DO-1)	Mouse	1:200	Santacruz	Sc126
P21	mouse	1:500	Santacruz	Sc-6246
POLR1A	Rabbit	1:200	Cell signaling	24799
FBL	Mouse	1:100	Santa Cruz	sc-166001
UBF	Mouse	1:100	Santa Cruz	sc-13125
NPM	Rabbit	1:100	Cell Signaling	3542S
RPL5	Rabbit	1:200	Cell Signaling	51345S
RPL11	Rabbit	1:200	Cell Signaling	18163S

Secondary Antibodies (Alexa)					
Antibody	**Source**	**Reactivity**	**Dilution**	**Producer**	**Cat. #**
Alexa Flour 647	Goat	Mouse	1:500	ThermoFisher	A-21235
Alexa Flour 546	Goat	mouse	1:500	ThermoFisher	A11003
Alexa Flour 488	Donkey	Rabbit	1:500	ThermoFisher	A32790

Primary Antibodies for PLA				
Antibody	**Source**	**Dilution**	**Producer**	**Cat. #**
MDM2	mouse	1:200	Calbiochem	A-21235
POLR3A	Rabbit	1:150	Thermofisher	PA5-58170
BRF1	Rabbit	1:300	Abcam	Ab264191

Table 6 Small interfering RNA

Target	**ID**	**Producer**	**Cat. #**
P53	s605	Ambion	4390824
Mdm2 #1	Customer Select	Ambion	4390828
Mdm2 #2	s8630	Ambion	4390224

RPL5 #1	s12151	Ambion	4392420
RPL5 #2	s12152	Ambion	4392420
RPL11 #1	s12168	Ambion	4392420
RPL11 #2	s12169	Ambion	4392420
P21	s416	Ambion	4390824
PUMA #1	s25842	Ambion	4392420
PUMA #2	s25841	Ambion	4392420

Acknowledgments

V. Manzini was a member of the IMPRS/MSc./PhD program Molecular Biology at Göttingen during this work. We thank Prof. A. Papantonis for the tRNA Leu-CAA primer sequence and helpful advice. This work was kindly supported by the Deutsche Krebshilfe, the Deutsche Forschungsgemeinschaft, the Wilhelm Sander Stiftung, and the Else Kröner-Fresenius-Stiftung.

3. MANUSCRIPT 2

MDM2 binds and ubiquitinates PARP1

to enhance DNA replication fork progression

Celeste Giansanti[1,6], Valentina Manzini[1,6], Antje Dickmanns[1], Achim Dickmanns[2], Maria Dilia Palumbieri[3], Andrea Sanchi[3], Simon Maria Kienle[4], Sonja Rieth[5], Martin Scheffner[4], Massimo Lopes[3], Matthias Dobbelstein[1,7]

[1]Institute of Molecular Oncology, Göttingen Center of Molecular Biosciences (GZMB), University Medical Center Göttingen, Justus-von-Liebig-Weg 11, D-37077, Göttingen, Germany

[2]Department of Molecular Structural Biology, Institute of Microbiology & Genetics, GZMB, Georg-August-University Göttingen, Justus-von-Liebig-Weg 11, 37077 Göttingen, Germany

[3]Institute of Molecular Cancer Research, University of Zurich, Winterthurerstrasse 190, 8057 Zurich, Switzerland

[4]Department of Biology, University of Konstanz, 78457 Konstanz, Germany

[5]Department of Chemistry, University of Konstanz, 78457 Konstanz, Germany

[6]These authors contributed equally to this work and are equal first authors

[7]Lead contact

Status: under revision in *Cell Reports*

Own contribution: Figure 1A except F, H and J, Figure 2 except A and C. Figure 5 H, G and I, Figure S1 all except F, Figure S2 all except A, F and G, Figure S5 D and Figure S6 C and D. Involved in editing and revising the manuscript.

SUMMARY

The MDM2 oncoprotein antagonizes the tumor suppressor p53 by physical interaction and ubiquitination. However, it also sustains the progression of DNA replication forks, even in the absence of functional p53. Here we show that MDM2 binds, ubiquitinates and destabilizes Poly(ADP-Ribose) Polymerase 1 (PARP1), a multifunctional regulator that also acts on DNA replication fork stability. When cellular MDM2 levels were increased, as observed in cancer, this led to accelerated progression of DNA replication forks, much like the pharmacological inhibition of PARP1. Conversely, overexpressed PARP1 restored normal fork progression despite elevated MDM2. Strikingly, MDM2 profoundly reduced the frequency of fork reversal, revealed as four-way junctions through electron microscopy. The depletion of RECQ1 as well as the primase/polymerase PRIMPOL each reverted the MDM2-mediated acceleration of the nascent DNA elongation rate. In conclusion, high MDM2 levels phenocopy PARP inhibition in the modulation of fork restart, representing a potential vulnerability of cancer cells.

3.1 INTRODUCTION

The tumor suppressor protein p53 is a stress-inducible transcription factor. It induces the expression of genes that promote cell cycle arrest, DNA repair, or programmed cell death (Kastenhuber and Lowe, 2017; Levine, 2020). One of the most strongly p53-responsive genes is the Mouse double minute 2 homolog (MDM2). MDM2 is an E3 ubiquitin-protein ligase that targets p53 for proteasome-mediated degradation, giving rise to a regulatory feedback loop (Picksley and Lane, 1993). MDM2 thus acts as an oncogene, and it is overexpressed in a variety of human tumors, most notably in sarcomas (Rayburn et al., 2005). In addition to its role in regulating p53, additional functions of MDM2 have been described, compatible with a role of MDM2 as an effector, not only a regulator, of tumor suppression by p53 (Levine, 2020). MDM2 interacts with the Polycomb Repressor Complex 2 and mediates histone modifications (Wienken et al., 2016, 2017). Moreover, MDM2 binds and deactivates the Mre11-Rad50-Nbs1 (MRN) complex, delaying DNA repair (Alt et al., 2005). Finally, MDM2 can support the processivity of DNA replication forks, in cooperation with its association partner MDM4 as well as another histone ubiquitin ligase, RNF2 (Klusmann et al., 2016, 2018; Wohlberedt et al., 2020). Since MDM2 relies on p53 for its full expression, this might also explain why the presence of p53 enhances DNA replication fork processivity (Klusmann et al., 2016). However, a clear mechanistic understanding of how MDM2 affects DNA replication forks upon p53 activation remains to be provided.

Poly(ADP-Ribose) Polymerase 1 (PARP1) is an emerging player in the regulation of DNA replication. PARP1 binds to perturbed DNA replication forks and to damaged DNA, and this triggers its catalytic activity. It then covalently attaches ADP-ribose units to a number of target proteins, including PARP1 itself (Chambon et al., 1963; Kun et al., 2004; Langelier et al., 2011, 2014). PARP1 polymerizes these ADP-ribose units to form linear or branched Poly(ADP-ribose) (PAR) chains, in a reaction termed PARylation. PARylation of proteins regulates their function, localization and stability (Gibson and Kraus, 2012). In this way, PARP1 controls DNA repair and chromatin remodelling (Jungmichel et al., 2013; Ray Chaudhuri and Nussenzweig, 2017), and PARP inhibitors represent established drugs to treat tumors with DNA repair deficiencies (Helleday, 2011). Importantly, PARP1 controls DNA replication, and its inhibition leads to enhanced progression of replication forks (Maya-Mendoza et al., 2018). Correspondingly, most PARylation activity is detected during S-phase at sites of DNA replication. This is at least partially triggered by the processing of Okazaki fragments, which can be carried out by a PARP1- and XRCC1-dependent pathway, as an alternative to the canonical FEN1- and LIG1-driven pathway (Hanzlikova et al., 2018). Moreover, PARP1 delays the restart of reversed DNA replication forks. Fork reversal is a replication fork remodeling

process by which a canonical three-way replication fork is converted to a four-way junction by reannealing of parental DNA strands and coordinated annealing of newly synthesized strands (Bétous et al., 2012; Higgins et al., 1976). This happens during replication in response to genotoxic agents, but also when replication forks hit endogenous obstacles, e.g. repetitive DNA forming secondary structures (Follonier et al., 2013; Zellweger et al., 2015). Fork reversal contributes to the temporal arrest of replication, thus allowing repair or bypass of DNA damage (Berti et al., 2013; Neelsen and Lopes, 2015; Quinet et al., 2017).

When active, PARP1 stabilizes DNA replication forks in the regressed state and limits fork restart by inhibiting the activity of the helicase RECQ1 (Berti et al., 2013). Conversely, PARP1 inhibition accelerates replication forks and antagonizes fork reversal (Berti et al., 2013; Maya-Mendoza et al., 2018; Ray Chaudhuri and Nussenzweig, 2017). When PARP1 activity is diminished, alternative DNA Damage Tolerance (DDT) mechanisms become prominent. These include Translesion Synthesis (TLS) and repriming of DNA synthesis downstream of the replication block, by the action of the primase and DNA polymerase PRIMPOL (Genois et al., 2021; Quinet et al., 2020). Thus, PARP1 activity determines how replication forks cope with obstacles. Importantly, however, it remains largely unknown how PARP1 activity itself is regulated during replication. Recently, the methyl transferase CARM1 was found to support PARP1 activity at replication forks (Genois et al., 2021), but additional factors might well be involved in the regulation of PARP1 activity in this context.

On top of its role in DNA synthesis and repair, PARP1 is widely known for its cleavage during apoptosis. In this context, caspases cleave PARP1 into fragments that are readily detectable by immunoblot analysis. This study was initiated by the surprising observation that p53 activity not only induced the cleavage of PARP1 into fragments, but also led to the degradation of PARP1 altogether, even when apoptosis was blocked. This raised the questions whether the most prominent p53-inducible ubiquitin ligase, i.e. MDM2, might mediate PARP1 degradation, and how this would affect the DNA replication process.

Strikingly, we observed that MDM2 destabilizes PARP1, by physically binding and ubiquitinating it. Consequently, MDM2 promotes the progression of DNA replication forks. This increase of the DNA elongation rate requires RECQ1 as well as PRIMPOL, and it coincides with suppression of fork reversal. Thus, MDM2 not only counteracts p53 activity but also antagonizes PARP1. It thus promotes DNA replication fork progression via RECQ1-driven resumption of reversed replication forks and PRIMPOL-mediated re-priming of DNA synthesis.

3.2 RESULTS

MDM2 ubiquitinates PARP1, triggering its proteasomal degradation

We were initially studying p53-induced apoptosis, using an inhibitor of MDM2. The pharmacological MDM2 antagonist Nutlin-3a (Vassilev et al., 2004), referred to as Nutlin from here on, binds to a hydrophobic pocket domain of MDM2, disrupting its interaction with p53. This impairs MDM2-driven ubiquitination of p53, leading to the accumulation of p53 and to enhanced expression of its target genes, including the pro-apoptotic effector BBC3/PUMA, but also MDM2 itself. We had studied apoptosis in the osteosarcoma cell line SJSA-1, characterized by wild type TP53 and MDM2 amplification (Bi et al., 2016). When treating SJSA-1 cells with Nutlin, PARP1 cleavage by caspases resulted in the characteristic fragment visualized by immunoblot analysis (Soldani et al., 2001) (Figure 1A). Surprisingly, Nutlin also reduced the levels of full-length PARP1 (Figures 1A, 1B), not only in SJSA-1 cells, but also in the non-transformed Retinal Pigment Epithelium (RPE) cells (Figure S1A). Previous studies reported that Nutlin induces PARP1 degradation in the human breast cancer cell line MCF-7, in a MDM2- and proteasome-dependent fashion (Kobayashi et al., 2020; Nagai et al., 2012), which was confirmed in our experiments (Figures S1B, S1C). However, the underlying molecular mechanisms have remained elusive. To assess whether the suppression of PARP1 levels results from apoptosis-associated caspase activity, we depleted the pro-apoptotic p53 target gene product PUMA using siRNAs (Figure S1D). As expected, PUMA knockdown prevented the formation of the caspase-dependent PARP1 fragment in response to Nutlin. However, overall PARP1 levels were still suppressed in SJSA-1 cells upon depletion of PUMA (Figure 1A) and in MCF-7 cells that were co-treated with a caspase inhibitor (Figure S1E). In contrast, a proteasome inhibitor restored PARP1 levels in Nutlin-treated SJSA-1 cells (Figure 1B), arguing that PARP1 degradation in response to p53 requires the proteasome rather than caspases. MDM2 is by far the most well-characterized ubiquitin ligase that can be induced by p53 (Sane and Rezvani, 2017). We therefore tested whether MDM2 degrades PARP1 in the context of p53 activation. We used a proteolysis targeting chimera (PROTAC), MD-224, composed of two active domains connected by a linker. One domain, termed, MI-1061, binds MDM2 like Nutlin and displaces p53. The other domain binds the Cereblon-associated E3 ubiquitin ligase (Figure 1C). Thus, MD-224 recruits Cereblon to ubiquitinate and degrade MDM2, while p53 remains active (Li et al., 2019). MI-1061 alone was also included in the experiment as control. As expected, both MD-224 and MI-1061 induced the accumulation of p53 and its target gene product p21, whereas MDM2 levels went up with MI-1061 but not with MD-224 (Figure 1D). Importantly, the MDM2-antagonist MI-1061 decreased PARP1 levels similarly to Nutlin, but the MDM2 PROTAC MD-224 did not (Figure 1D). Consistently, far less

pronounced PARP1 degradation in response to Nutlin was also observed when MDM2 was depleted by two independent siRNAs, and the degree of PARP1 levels rescue correlated with knockdown efficiency (Figure 1E). Similar results were obtained when treating the non-transformed RPE cells with the MDM2-directed PROTAC in comparison to Nutlin or MI-1061 (Figure 1F). This indicates that MDM2 is necessary for PARP1 degradation upon p53 activation. To test whether MDM2 is also sufficient to diminish PARP1 levels even in the absence of p53, we transiently overexpressed MDM2 in the $TP53^{-/-}$ lung cancer cell line H1299 and detected PARP1 by immunofluorescence analysis. Here again, the PARP1-derived signal was significantly reduced upon MDM2 overexpression, indicating that enhanced MDM2 levels are sufficient for PARP1 degradation (Figure 1G).

Correspondingly, purified MDM2 was sufficient for PARP1 ubiquitination *in vitro.* In this assay, the ubiquitination of p53 by MDM2 served as positive control (Figure S1F). When PARP1 was exposed *in vitro* to MDM2, along with the E2 ubiquitin-conjugating enzyme UbcH5b and ubiquitin, a smear was observed ranging from mono-ubiquitinated forms to presumably polyubiquitinated forms of PARP1 (Figures 1H, S1F). These higher molecular weight forms of PARP1 could not be caused by autoPARylation, since the reaction was carried out in the absence of the essential PARP1 substrate NAD+. Our result thus demonstrates that MDM2 is capable of transferring ubiquitin onto PARP1, as it does on p53.

Since PARP1 accounts for most of the cellular PARylation (Kamaletdinova et al., 2019), we investigated whether the drop in PARP1 levels in response to MDM2 was affecting the cellular PAR content. In this experiment, PAR was stabilized by inhibiting Poly(ADP-ribose) glycohydrolase (PARG) using the small molecule, PDD 00017273, thus facilitating its detection. Accumulation of MDM2 correlated with reduced PAR levels, as shown by immunofluorescence analysis of H1299 cells (Figure 1I). This included cells displaying ongoing DNA synthesis, as visualized by 5-Ethynyl-2′-deoxyuridine (EdU) incorporation, meaning that MDM2-mediated decrease of PAR was also visible during S-phase, when most of the endogenous PARP1 PARylation activity is known to be detected (Figure 1I) (Hanzlikova et al., 2018). Moreover, Nutlin reduced PAR levels in SJSA-1 cells (Figure 1J), arguing that p53-induced MDM2 not only mediates the degradation of PARP1 but also diminishes *Poly*(*ADP*-ribosyl)ation.

Taken together, these results indicate that MDM2 directly ubiquitinates PARP1 and thereby mediates its degradation via the proteasome, leading to reduced cellular PAR levels.

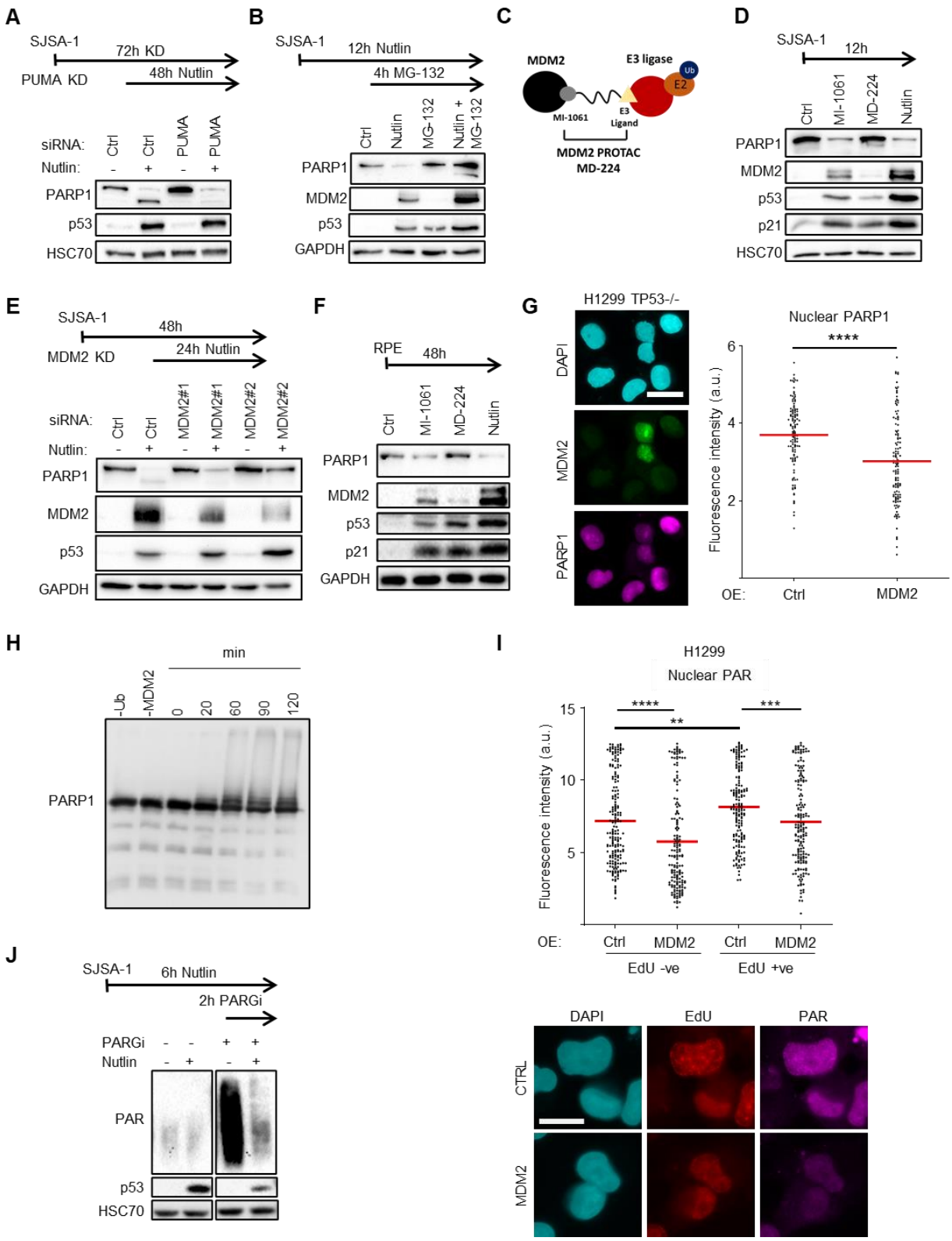
A
SJSA-1
72h KD
PUMA KD
48h Nutlin
siRNA: Ctrl Ctrl PUMA PUMA
Nutlin: - + - +
PARP1
p53
HSC70
B
SJSA-1
12h Nutlin
4h MG-132
Ctrl Nutlin MG-132 Nutlin + MG-132
PARP1
MDM2
p53
GAPDH
C
MDM2
E3 ligase
Ub
E2
MI-1061
E3 Ligand
MDM2 PROTAC MD-224
D
SJSA-1
12h
Ctrl MI-1061 MD-224 Nutlin
PARP1
MDM2
p53
p21
HSC70
E
SJSA-1
48h
MDM2 KD
24h Nutlin
siRNA: Ctrl Ctrl MDM2#1 MDM2#1 MDM2#2 MDM2#2
Nutlin: - + - + - +
PARP1
MDM2
p53
GAPDH
F
RPE
48h
Ctrl MI-1061 MD-224 Nutlin
PARP1
MDM2
p53
p21
GAPDH
G
H1299 TP53-/-
DAPI
MDM2
PARP1
Nuclear PARP1
****
Fluorescence intensity (a.u.)
6
4
2
OE: Ctrl MDM2
H
min
-Ub
-MDM2
0 20 60 90 120
PARP1
I
H1299
Nuclear PAR
****
**
***
Fluorescence intensity (a.u.)
15
10
5
OE: Ctrl MDM2 Ctrl MDM2
EdU -ve
EdU +ve
DAPI
EdU
PAR
CTRL
MDM2
J
SJSA-1
6h Nutlin
2h PARGi
PARGi - - + +
Nutlin - + - +
PAR
p53
HSC70

Figure 1. MDM2 ubiquitinates PARP1, triggering its proteasomal degradation

A) Immunoblot analysis of SJSA-1 cells 72h after transfection of siRNA against PUMA and upon treatment with Nutlin (20µM, 48h).

B) SJSA-1 cells were treated with 20µM Nutlin for 12h. During the last 4h, the proteasome inhibitor MG-132 (10µM) was added, followed by immunoblot analysis. The efficacy of proteasome inhibition is demonstrated by accumulation of p53, MDM2 and PARP1.

C) Mechanism of targeted protein degradation via proteolysis-targeting chimeras (PROTACs). MD-224 is composed of two active domains connected by a linker. One domain is a MDM2 ligand (MI-1061) that disrupts the MDM2-p53 interaction. A second domain recruits an E3 ubiquitin ligase machinery (Cereblon). This leads to the ubiquitination and proteasomal degradation of MDM2, while p53 remains active.

D) SJSA-1 cells were treated with either 1µM MDM2 PROTAC (MD-224), 1µM MI-1061 (ligand control), or 20µM Nutlin for 12h, followed by immunoblot analysis. Treatment with MD-224 induced a p53 response comparable to MI-1061, as shown by p21 levels, while leading to MDM2 degradation.

E) Immunoblot analysis of SJSA-1 cells transfected with two different siRNAs to knock down MDM2 or control siRNA for 48h and treated with Nutlin (20µM, 24h). PARP1 full-length protein levels were restored to different degrees, depending on the efficacy of the MDM2 knockdown.

F) RPE cells were treated with 1µM MDM2 PROTAC (MD-224), 1µM MI-1061 (ligand control) or 10µM Nutlin for 48h to reveal MDM2-dependent loss of PARP1 levels.

G) H1299 cells were transfected either with a control empty vector (pCMV-CTRL) or with a MDM2 overexpressing plasmid (pCMV-MDM2) for 48h. The nuclear fluorescence intensity of PARP1 was quantified specifically in cells expressing medium/high levels of MDM2 (right panel). The same number of cells were randomly selected for quantification from the Ctrl sample (n=122). Red lines represent mean values for each plot. Left panel: representative images; scale bar, 50µm.

H) Ubiquitination of PARP1 by MDM2 *in vitro*. Purified recombinant MDM2 was incubated with PARP1 for up to 120 min. Additional negative controls without ubiquitin (-Ub) or without MDM2 (-MDM2) were included. At the indicated time points, the samples were subjected to immunoblot analysis. PARP1 was ubiquitinated by MDM2, as shown by accumulation of high molecular weight bands with increasing intensities at increasing incubation times.

I) H1299 cells were transfected with either empty vector (pCMV-CTRL) or the pCMV-MDM2 plasmid for 48h, and nuclear levels of PAR were quantified in both EdU positive cells (i.e. cells undergoing S-phase) and EdU negative cells. DAPI was used to identify the location of nuclei. Cells were treated for 2h with 20µM of PARGi to stabilize the PAR chains. Top panel: quantification of single nuclear intensities; red lines represent the mean values for each plot. A range of 150-210 cells was quantified for each condition. Bottom panel: representative images; scale bar, 20µm.

J) Western blot analysis of SJSA-1 cells treated with 20µM Nutlin for 6h and/or 10µM PARGi for 2h. PAR became visible upon PARG inhibition, but was found reduced upon p53 induction. Bands relative to different conditions have been cropped.

MDM2 forms a complex with PARP1 *in vitro* and *in vivo*

Given the ubiquitination of PARP1 by MDM2, we tested whether the two proteins physically interact. Co-immunoprecipitation (co-IP) of purified MDM2 and PARP1 demonstrated that PARP1 directly binds MDM2 (Figure 2A). In addition, bacterially expressed MDM2 was fused

to Glutathione S-Transferase (GST) and coupled to glutathione-sepharose beads, followed by incubation with purified PARP1. In these assays, PARP1 associated with GST-MDM2 but not with GST alone, confirming that MDM2 is indeed capable of physically binding PARP1 (Figure S2A). The interaction was recapitulated in cells, by co-IP and by Proximity Ligation Assay (PLA). First, we transiently overexpressed MDM2 and PARP1 in H1299 cells. When PARP1 was captured by an antibody for immunoprecipitation, we observed coprecipitation of MDM2 as well (Figure 2B). The association was also observed between endogenous PARP1 and MDM2 in Nutlin-treated SJSA-1 cells (Figure 2C), also when using an antibody to MDM2 for precipitation (Figure S2B). PLA confirmed that PARP1 and MDM2 are in a complex, both upon overexpression in H1299 (Figure 2D) and when detecting endogenous proteins in Nutlin-treated SJSA-1 cells (Figure 2E). The PLA signal was also observed when overexpressing MDM2 alone in H1299 cells, in agreement with its binding to endogenous PARP1 (Figure S2C). Controls omitting one of the two antibodies ensured signal specificity from the interacting MDM2 and PARP1 proteins (Figures S2C-E).

We next tested whether the interaction of MDM2 and PARP1 is influenced by the presence of PAR. To this end, we inhibited PARylation through a 24h pre-treatment with the PARP1/2 inhibitor Olaparib (Figure S2F). This did not impair the co-precipitation of MDM2 with PARP1 (Figure 2B). Conversely, inducing the accumulation of PARylated PARP1 by treatment with PARG inhibitor (PDD 00017273) did not increase the co-precipitation and the co-localization of PARP1 and MDM2, but rather reduced them (Figures 2B-D, S2F, S2G). We concluded that the interaction of MDM2 with PARP1 is not mediated, but in fact partially compromised by PAR accumulation.

To map the PARP1-interacting domain(s) on MDM2, we tested the capability of five different MDM2-derived mutants and fragments to co-localize with PARP1, as revealed by PLA (Figures 2F, S2H). Removing the central domain mutant (Δ222-325) in MDM2 significantly decreased the PLA signal arising from the co-localization of MDM2 and PARP1, indicating that this domain is required for the association (Figure 2G).

These findings indicate that PARP1 is a novel and direct interaction partner of MDM2 *in vitro* and *in vivo*. Binding of PARP1 to MDM2 does not require PARylation and does not involve the p53 binding site of MDM2, but rather the acidic/central domain.

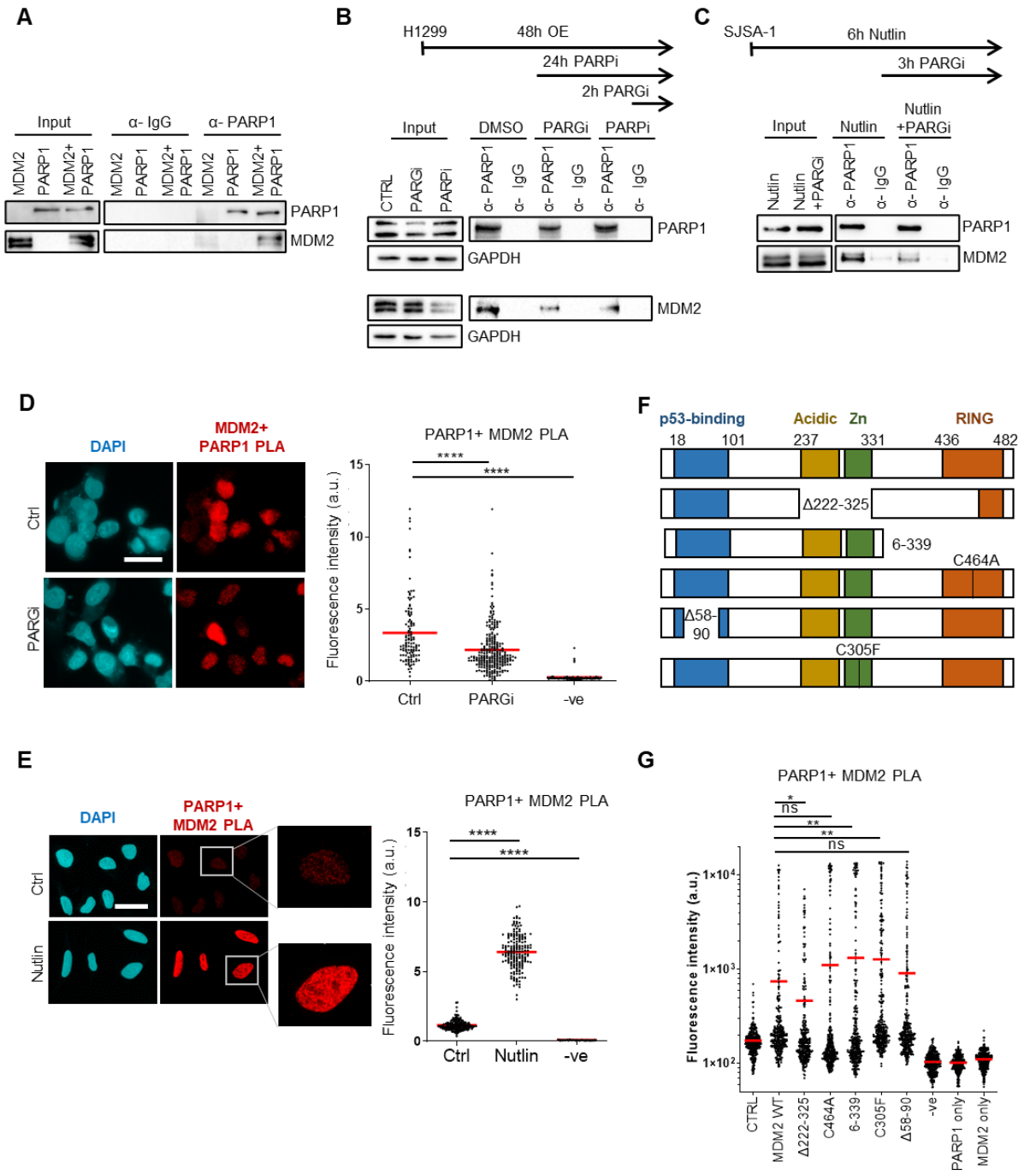

Figure 2. MDM2 forms a complex with PARP1 *in vitro* and *in vivo*

A) Co-immunoprecipitation (Co-IP) of purified MDM2-PARP1. IP using anti-rabbit IgG antibody was used as a negative control.

B) Physical association between MDM2 and PARP1 in H1299 cells, shown by co-IP upon overexpression of both proteins for 48h. Since this cell line is TP53$^{-/-}$, and thus cannot express MDM2, the MDM2 construct was overexpressed 9-fold in excess compared to PARP1. IP was performed with anti-PARP1 antibody, followed by detection of both proteins by immunoblot analysis. Where indicated, the cells were treated with 20μM of PARG inhibitor (PARGi) 2h prior to harvest, or with 10μM PARP inhibitor (PARPi) for 24h. IP using anti-rabbit IgG antibody was used as a negative control.

C) Co-IP revealed physical interaction between endogenous MDM2 and PARP1 in SJSA-1 cells upon Nutlin treatment for 6h (20µM). Where indicated, cells were co-treated with 10µM of PARGi for 3h prior to harvest.

D) Left panel: representative images from the Proximity Ligation Assay (PLA) that was used to determine the interaction of PARP1 and MDM2 in H1299 cells upon overexpression of both proteins for 48h. Scale bar, 20µm. Right panel: quantification of nuclear fluorescence intensity of the PLA signal. DAPI was used to identify nuclei. A negative control (-ve) was obtained by omitting the primary antibodies. The red line represents the mean for each sample.

E) Left panel: representative images of the PLA to determine the interaction of PARP1 and MDM2 in SJSA-1 cells, upon treatment with either DMSO (Ctrl) or 20µM Nutlin for 6h. Scale bar, 30µm. Right panel: quantification of the nuclear PLA signal.

F) Schematic representation of the MDM2 mutants used in this study. Five different MDM2 mutants were overexpressed in H1299 cells together with PARP1. These MDM2 mutants contain deletions in either the central domain (Δ222-325), the RING domain (6-339) or the hydrophobic pocket that binds p53 (Δ58-90). We also included two point mutants, either in the RING domain (C464A) or in the zinc finger (Zn) domain (C305F).

G) H1299 cells were transfected for 48h, either with empty vector (pCMV CTRL) or expression plasmids for MDM2 WT or MDM2 mutants. Negative controls included only one of the two antibodies ("PARP1 only" and "MDM2 only"), or neither of them (-ve).

MDM2 enhances the elongation rate of DNA synthesis, which is abolished by PARP1 overexpression

We and others have previously reported an increase of replication fork processivity upon p53 activation (Klusmann et al., 2016; Yeo et al., 2016). Conversely, MDM2 depletion in a p53-deficient background reduces replication fork progression (Klusmann et al., 2016, 2018). Now, we asked whether the increased levels of MDM2 in the context of p53 activation are actually responsible for enhanced fork progression. To assess this, we took advantage of the MDM2-targeting PROTAC, MD-224, and the corresponding MDM2 antagonist, MI-1061 as control. Upon treatment of SJSA-1 cells with these compounds, the lengths of labelled tracks representing newly synthetized DNA were determined by DNA fiber assays (Figure 3A), as described earlier (Kopper et al., 2013). When treating SJSA-1 cells with Nutlin or MI-1061, the levels of p53 and the p53-target gene products p21 and MDM2 were increased as expected (Figure 3B); remarkably, this doubled the track lengths of newly synthetized DNA (Figures 3C, 3D; Table S1). Strikingly, despite comparable p53 activation, the PROTAC MD-224 had much less potency than Nutlin or MI-1061 to increase DNA track lengths (Figures 3B-D). Moreover, in the non-transformed RPE cells, Nutlin and MI-1061 still enhanced the progression of replication forks, whereas the PROTAC MD-224 did not (Figures S3A-D). This demonstrates that MDM2, rather than p53 itself or other p53-target gene products, is directly causing the observed increase in replication fork progression upon activation of p53.

Next, we asked whether the interaction of MDM2 and PARP1 might form the mechanistic basis for MDM2-dependent enhancement of DNA replication fork progression. This was further motivated by previous reports describing enhanced fork progression upon PARP1 inhibition (Maya-Mendoza et al., 2018). As a first step to address this, we tested how simultaneous MDM2 induction and PARP1 inhibition affect DNA replication. We combined the PARP1 inhibitor, Olaparib, with Nutlin in SJSA-1 cells (Figure 3A). We confirmed the enhanced fork progression with the PARP inhibitor (Maya-Mendoza et al., 2018) as well as Nutlin individually; however, the simultaneous addition of Nutlin and Olaparib did not further increase the lengths of the tracks (Figures 3C, 3D). This suggests an epistatic relationship between enhanced MDM2 expression and PARP inhibition. Since MDM2 antagonizes PARP1 in response to Nutlin, it is conceivable that PARP1 inhibition does not further increase fork progression above the level seen with Nutlin. At the same time, PARP1 inhibition alone still accelerated fork progression as much as the drug combination, suggesting that targeting PARP1 is the predominant mechanism by which MDM2 increases fork speed.

A similar increase of nascent DNA elongation was found in the TP53$^{-/-}$ H1299 cells upon plasmid-based overexpression of MDM2, and also in the presence of the topoisomerase I inhibitor camptothecin (CPT) (Figures 3G, 3H, S3E-H). Importantly, the simultaneous overexpression of PARP1 along with MDM2 significantly attenuated the increase in DNA track lengths (Figures 3E-H), also in the presence of CPT (Figures S3I-K). This strongly suggests that antagonizing PARP1 by MDM2 represents the predominant mechanism by which MDM2 accelerates the progression of DNA replication forks.

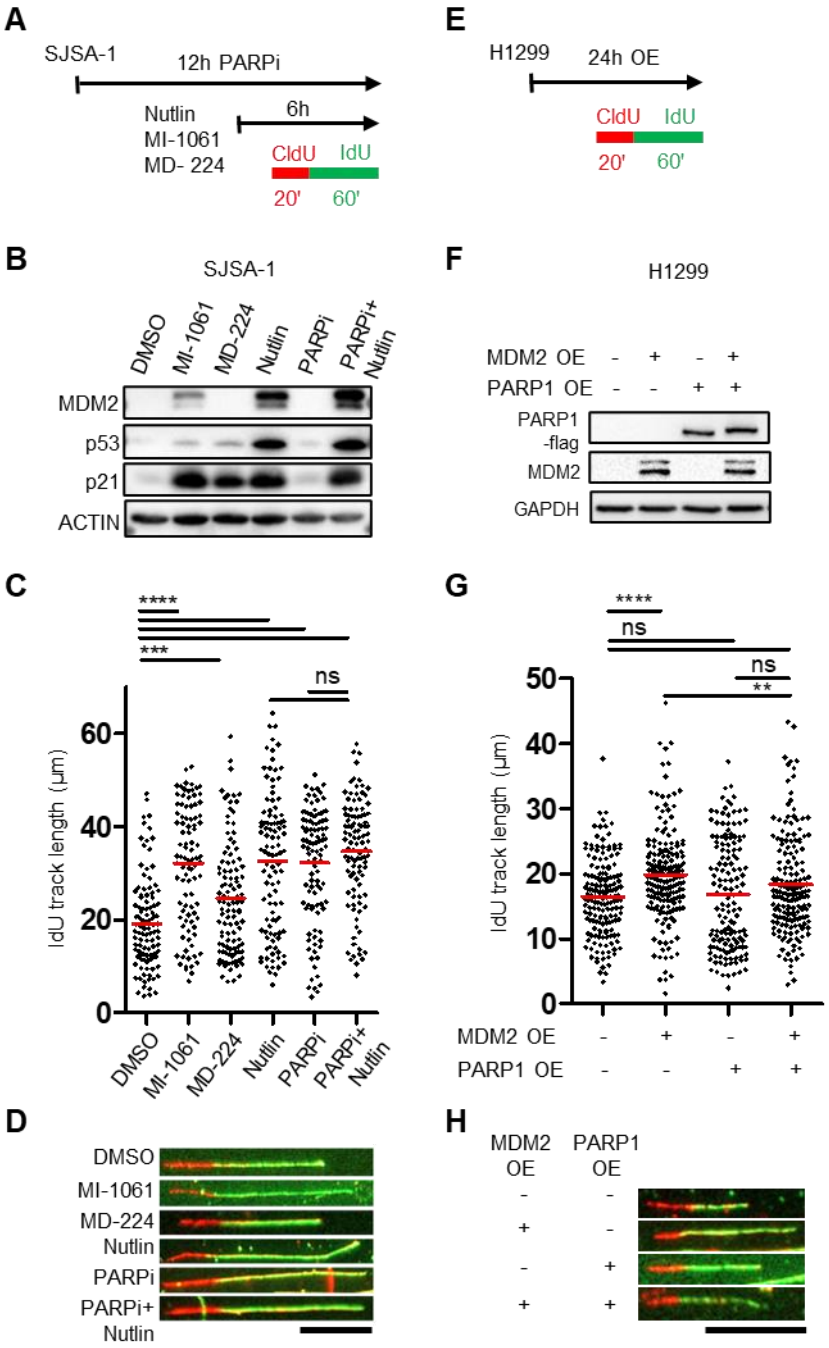

Figure 3. MDM2 enhances the elongation rate of DNA synthesis, which is abolished by PARP1 overexpression

A) Treatment scheme. SJSA-1 cells were treated with Nutlin (20µM, 6h), MI-1061 (1µM, 6h), MD-224 (1µM, 6h), and the PARP inhibitor (PARPi), Olaparib, (10µM, 12h). DNA fiber assays were performed sequentially labeling newly synthetized DNA with CldU (25µM, 20 min) and IdU (25µM, 60 min).

B) Immunoblot analysis of SJSA-1 cells treated as delineated in A, confirming comparable p53 activation by MI-1061, MD-224, and Nutlin, as shown by p21 accumulation, while MD-224 specifically depleted MDM2.

C) DNA fiber assay following treatment shown in A. Only fibers containing both labels were considered for quantification. The mean track length of the second label (IdU) is shown as a red line for each condition. A minimum of 100 fibers was quantified from each sample in three

independent experiments with similar results. Mann-Whitney U test, two sided, was used for statistical analysis: ns, not significant; **p-value≤0.01, ***p-value≤0.001, ****p-value < 0.0001.

D) Representative images of DNA fibers obtained upon treatment as shown in A. Scale bar, 20µm.

E) Protocol used for DNA fiber assays. H1299 cells were subjected to plasmid transfection for overexpression (OE) of MDM2 and/or PARP1 (control plasmid pCMV, expression plasmids pCMV-MDM2 and/or pCMV-PARP1).

F) Immunoblot analysis of H1299 cells transfected as shown in E, confirming MDM2 as well as PARP1 overexpression.

G) DNA fiber assay performed upon MDM2-PARP1 overexpression in H1299 cells.

H) Representative images of DNA fibers analyzed after transfection according to the scheme shown in E. Scale bar, 20µm.

MDM2-mediated PARP1 degradation induces nascent DNA elongation through RECQ1

We next investigated the mechanisms by which the MDM2-mediated degradation of PARP1 increases the progression of DNA replication forks. PARP1 was previously found to inhibit DNA helicase RECQ1, thereby avoiding premature restart of reversed replication forks (Berti et al., 2013). We thus hypothesized that RECQ1 might become active and favour replication fork progression when MDM2 accumulates to antagonize PARP1. To test this, we depleted RECQ1 from SJSA-1 cells (Figures 4A, 4B). Whereas the treatment with Nutlin or the PARP inhibitor Olaparib enhanced the lengths of newly synthesized DNA tracks, this was reverted by the depletion of RECQ1 (Figure 4C). Moreover, upon plasmid-driven overexpression of MDM2 in H1299 cells, depleting RECQ1 prevented the MDM2-induced increase in the elongation rate of nascent DNA (Figures 4D-F). This was still observed when treating the cells with camptothecin (CPT) (Figures S4A-C), which is known to promote replication fork reversal (Ray Chaudhuri et al., 2012). Taken together, this strongly suggests that RECQ1 mediates unrestrained fork progression in response to MDM2 accumulation.

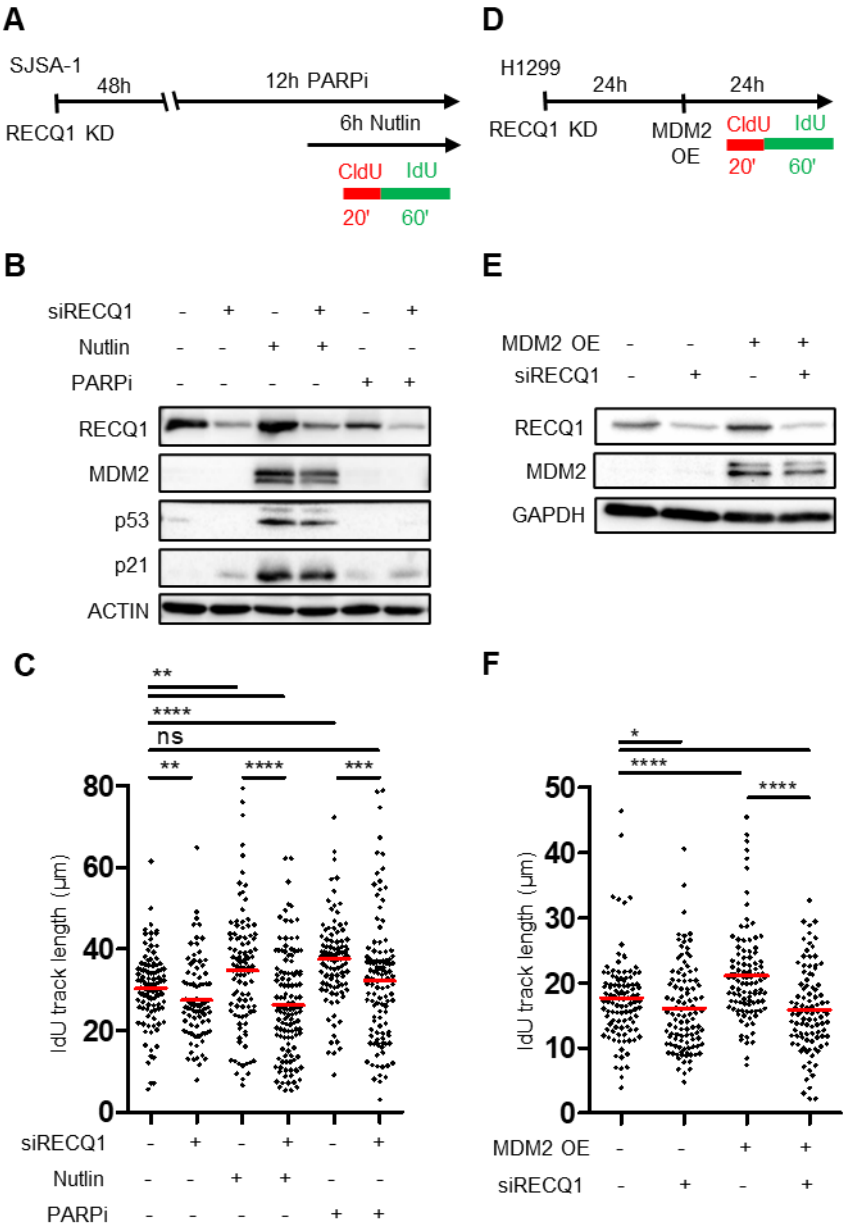

Figure 4. MDM2-mediated PARP1 degradation induces nascent DNA elongation through RECQ1

A) Transfection and treatment protocol. SJSA-1 cells were transfected with siRNAs against RECQ1 and treated with Nutlin (20µM, 6h) or the PARPi Olaparib (10µM, 12h). For DNA fiber assays, sequential labeling of newly synthetized DNA with CldU (25µM, 20 min) and IdU (25µM, 60 min) was performed.

B) Immunoblot analysis after transfection and the treatments described in A, confirming the depletion of RECQ1 by siRNA and the accumulation of p53, p21, and MDM2 upon Nutlin treatment.

C) DNA fiber assay using SJSA-1 cells treated as shown in A. The mean track lengths of the second label (IdU), within bicolored fibers, are shown as red lines. For each condition, a minimum of 100 fibers was quantified in two independent experiments with similar results. Mann-Whitney U test, two sided, was used for statistical analysis: ns, not significant; *p-value≤0.05, **p-value≤0.01, ***p-value≤0.001, ****p-value < 0.0001.

D) Transfection scheme. H1299 cells were transfected with siRNAs against RECQ1 and subjected to plasmid transfection (control plasmid pCMV, expression plasmid, pCMV-MDM2) 24h later.

E) Immunoblot analysis upon treatment as indicated in D, confirming MDM2 overexpression and RECQ1 knockdown.

F) DNA fiber assay analyzing H1299 cells upon transfection as shown in D.

MDM2 accumulation favors PRIMPOL-mediated fork progression and accumulation of DNA damage

We then sought to investigate whether DNA Damage Tolerance (DDT) pathways are supported by MDM2 via degradation of PARP1, thus further explaining enhanced DNA elongation. As one emerging DDT pathway, repriming of DNA synthesis by PRIMPOL resumes DNA elongation at stalled replication forks (Berti et al., 2013; Mourón et al., 2013).

We thus investigated whether accelerated progression of replication forks upon MDM2 accumulation might require PRIMPOL. Indeed, the depletion of PRIMPOL counteracted the enhancement of fork progression in Nutlin-treated SJSA-1 cells (Figures 5A-C) and upon MDM2 overexpression in H1299 cells (Figures 5D-F). This was still seen when replication fork stalling was induced by CPT treatment (Figures S5A-C). PRIMPOL knockdown also attenuated the increase of replication fork progression caused by treatment of SJSA-1 cells with the PARP inhibitor Olaparib (Figure 5B), further corroborating the induction of PRIMPOL repriming activity by PARP1 inhibition (Genois et al., 2021; Quinet et al., 2020).

RECQ1-mediated fork restart can overcome the pausing of replication in the presence of a damaged leading strand template (Berti et al., 2013). Moreover, repriming through PRIMPOL leaves behind gaps of single stranded DNA (Mourón et al., 2013). We thus expected the MDM2-mediated enhancement of fork progression to induce a DNA damage response. Indeed, we observed an MDM2-driven increase of the DNA damage marker γH2AX, both in H1299 and SJSA-1 cells (Figures 5G, 5H). In contrast, depletion of MDM2 via the PROTAC MD-224 failed to induce γH2AX in SJSA-1 cells despite p53 activation (Figure 5H). Intriguingly, the MDM2-driven increase of γH2AX was only visible in H1299 cells that had incorporated the label EdU (Figures 5G, S5D), i.e. in cells undergoing S phase, indicating that MDM2 specifically causes DNA damage accumulation in the context of DNA replication. In order to test to which extent PRIMPOL and RECQ1 contributed to DNA damage accumulation, we depleted each of them upon of MDM2 accumulation. Of note, the Nutlin-induced increase in γH2AX levels was attenuated upon depletion of PRIMPOL but not RECQ1 (Figures 5I, S5E), suggesting that PRIMPOL-induced gaps in the newly synthesized DNA strand are the predominant cause of DNA damage accumulation upon MDM2 induction. Thus, in addition to

RECQ1, PRIMPOL is another essential mediator of increased fork progression upon MDM2 induction, and PRIMPOL activity is causing DNA damage in this context.

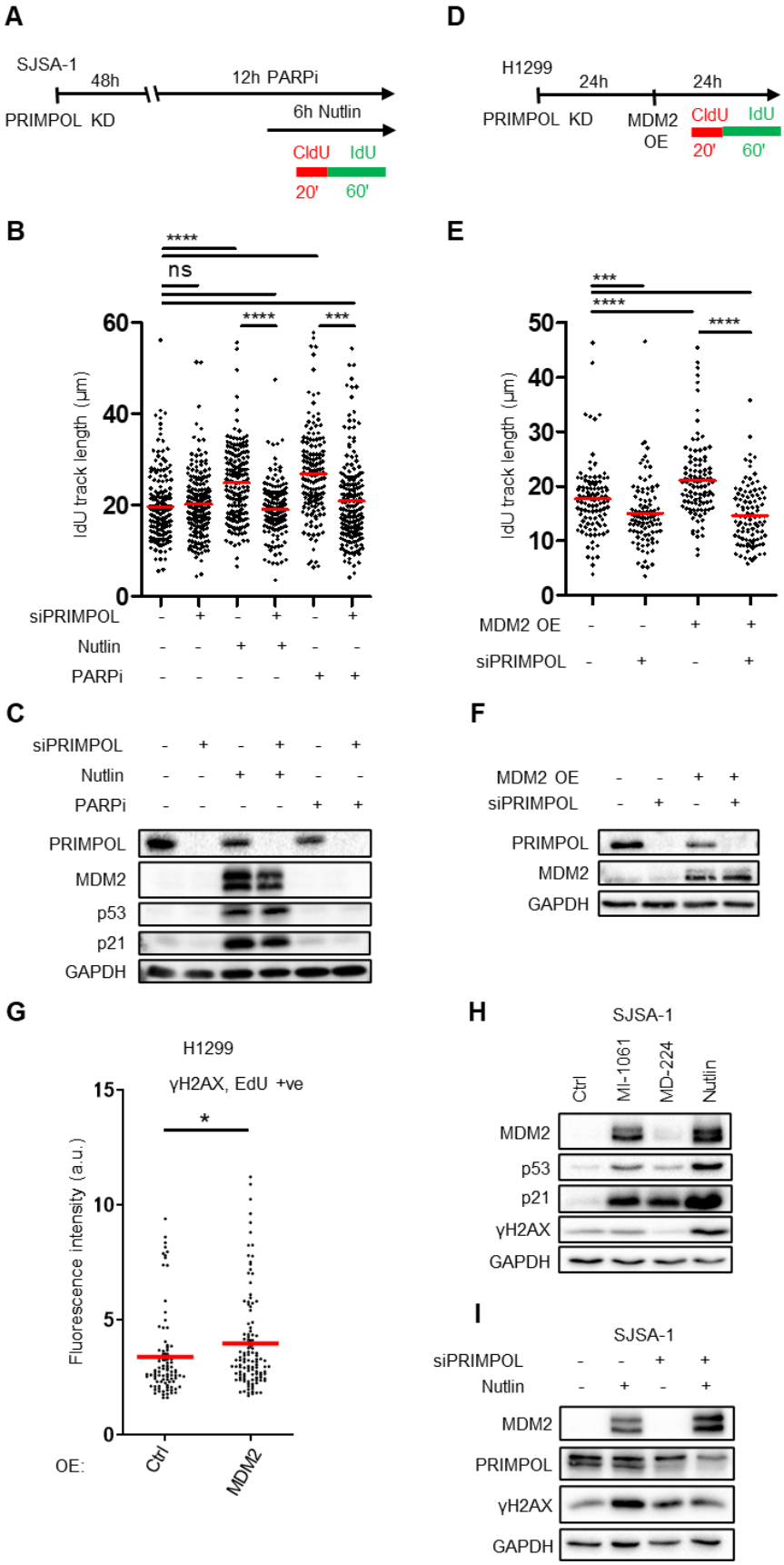

Figure 5. MDM2 accumulation favors PRIMPOL-mediated fork progression and accumulation of DNA damage

A) Transfection and treatment protocol. SJSA-1 cells were transfected with siRNAs against PRIMPOL and treated with Nutlin (20µM, 6h) or the PARPi Olaparib (10µM, 12h). For fiber assays, newly synthetized DNA was labeled with CldU (25µM, 20 min) and IdU (25µM, 60 min) as indicated.

B) DNA fiber assay following transfection and treatment as depicted in A. Mean track lengths of the second label (IdU) in bicolored fibers are indicated as red lines. A minimum of 100 fibers per sample was quantified in two independent experiments with similar results. Mann-Whitney U test, two sided, was used for statistical analysis: ns, not significant; ***p-value≤0.001, ****p-value < 0.0001.

C) Immunoblot analysis after transfection and treatment, as described in A, indicates the depletion of PRIMPOL and the regulation of p53 and MDM2 by Nutlin.

D) Transfection scheme. H1299 cells were transfected with siRNA against PRIMPOL and, after 24h, subjected to plasmid transfection (control plasmid pCMV, expression plasmid, pCMV-MDM2).

E) DNA fiber assay following treatment shown in D.

F) Immunoblot analysis upon treatment as indicated in D, confirming MDM2 overexpression and PRIMPOL knockdown.

G) Quantitative immunofluorescence analysis of phosphorylated Histone 2AX (γH2AX) in H1299 cells upon overexpression of MDM2. The analysis was restricted to cells in S phase, identified by EdU incorporation. Red lines represent the mean values. Ctrl n= 92, MDM2 n=116.

H) Immunoblot analysis of SJSA-1 cells treated with MDM2-binding compounds (Nutlin, 20µM, MI-1061, 1µM) or the MDM2 PROTAC (MD-224, 1µM) for 12h. MD-224 induced comparable p53-activation as MI-1061, as shown by p21 accumulation, while depleting MDM2.

I) Immunoblot analysis upon 12h-treatment with 20µM Nutlin, with or without PRIMPOL depletion via siRNA, revealing the drop in DNA damage response in the absence of PRIMPOL.

MDM2 accumulation antagonizes replication fork reversal

PRIMPOL-mediated fork repriming and fork reversal represent two alternative mechanisms by which cells ensure proper replication when hitting obstacles on the parental DNA (Bai et al., 2020; Quinet et al., 2020). We therefore asked whether MDM2, while promoting RECQ1-mediated fork restart and PRIMPOL- dependent repriming of DNA synthesis, might repress fork reversal. Specifically, we tested whether MDM2 accumulation reduces the proportion of reversed replication forks, visualized as four-way junctions using electron microscopy (EM) (Zellweger and Lopes, 2018) (Figure 6A). MDM2 accumulation was achieved by treating SJSA-1 cells with Nutlin, or by overexpression of MDM2 in H1299 cells. The topoisomerase inhibitor CPT was used at concentrations that reduced fork progression and induced replicative stress (Figure S6A-D), thus enhancing fork reversal to detectable levels. Strikingly, the proportion of reversed forks was strongly reduced by Nutlin in SJSA-1 cells, and even diminished to a quarter of its original frequency by MDM2 overexpression (Figure 6B). Thus,

MDM2 strongly represses DNA replication fork reversal, while enhancing fork restart and repriming.

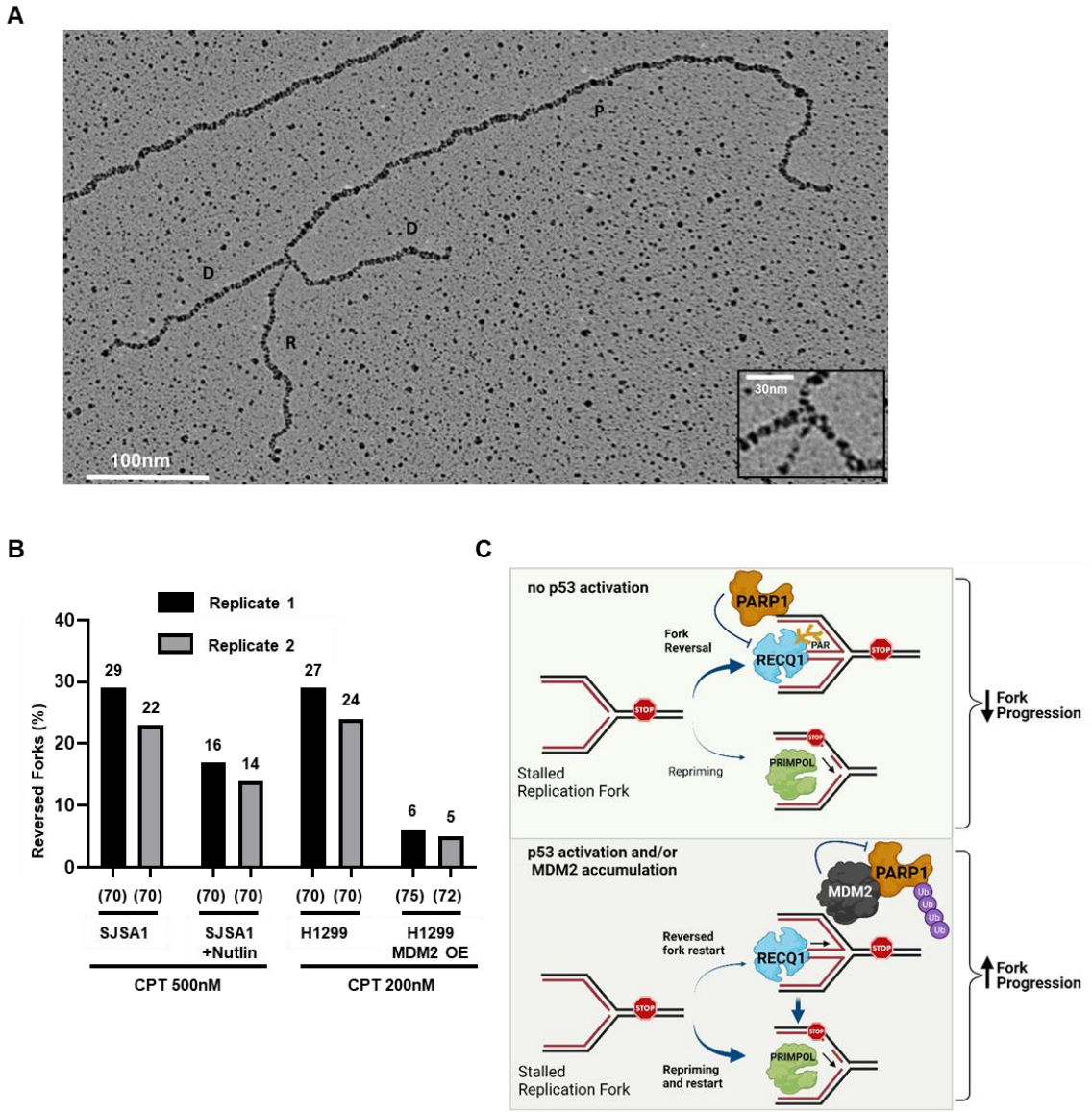

Figure 6. MDM2 accumulation antagonizes replication fork reversal

A) Representative electron microscopy image of reversed replication fork (4-ways). D, daughter strand; P, parental strand; R, reversed arm. The relevant portions of the molecules are magnified in the inset.

B) Frequency of fork reversal in SJSA-1 cells subjected to Nutlin treatment (20µM, 6h) and H1299 cells that were transfected with plasmids (control plasmid pCMV, expression plasmid pCMV-MDM2), each treated with CPT as indicated.

C) Model of PARP1 regulation by MDM2 at stalled DNA replication forks. Obstacles to replication can lead to fork reversal. When MDM2 levels are low, PARP1 antagonizes RECQ1 by PARylation, thus delaying the re-initiation of replication (top). When MDM2 is induced, e.g. by p53 activation, PARP1 is degraded, allowing RECQ1 to resolve reversed forks and PRIMPOL to reprime DNA synthesis downstream the replication obstacle (bottom). Created with BioRender.com.

3.3 DISCUSSION

Our results reveal a functional interaction of MDM2 with PARP1, resulting in PARP1 degradation and enhanced replication fork progression. When MDM2 antagonizes PARP1, the activities of the helicase RECQ1, as well as the primase/polymerase PRIMPOL, become preponderant, with suppression of fork reversal and consequent acceleration of fork progression (Figure 6C).

We found both RECQ1 and PRIMPOL necessary for replication fork acceleration in the context of elevated MDM2. However, these factors perform different functions. RECQ1 is a helicase that mainly acts by resolving reversed replication forks (Berti et al., 2013; Debnath and Sharma, 2020). In contrast, PRIMPOL acts by re-priming DNA synthesis on uncoupled forks, to continue replication. This leaves gaps of single stranded DNA behind, which then need to be repaired by post-replicative gap filling (Mourón et al., 2013; Quinet et al., 2020). Since PARP1 PARylates and antagonizes RECQ1, and since the increase of fork progression upon PARP inhibition requires both RECQ1 (Figure 4) and PRIMPOL (Figure 5) (Quinet et al., 2020), we propose that PARP1 opposes each way of fork restart, while MDM2 promotes both by counteracting PARP1. In this way MDM2 might confer enhanced vulnerability towards DNA damaging agents, which might be clinically relevant when MDM2 levels are increased in tumors, e.g. through gene amplification in sarcomas.

PARP1 and p53 each form part of the Fork Speed Regulatory Network (FSRN), an integrated molecular machinery that regulates the velocity of DNA replication forks, as proposed (Merchut-Maya et al., 2019) based on the observation of PARP1 as a regulator of replication forks (Maya-Mendoza et al., 2018). Our results further expand and corroborate this model by the mechanism of PARP1 degradation through p53-induced MDM2.

Antagonizing p53 was the first function of MDM2 that was discovered (Oliner et al., 1993). Moreover, targeted disruption of TP53 and/or MDM2 in mice revealed essentiality of MDM2, but only in the presence of p53 (de Oca Luna et al., 1995). This might lead to the assumption that antagonizing p53 is the only relevant function of MDM2, despite many p53-independent functions of MDM2 reported in the meantime (Alt et al., 2005; Fåhraeus and Olivares-Illana, 2014; Wienken et al., 2016, 2017). However, it should be noted that animals lacking p53 cannot upregulate MDM2 in response to stress. This may well obscure any functions of MDM2 as an effector, rather than a negative regulator of p53 (Dobbelstein and Levine, 2020). We propose that MDM2 supports DNA replication as part of a p53-response, in agreement with

our earlier findings that p53 as well as MDM2 can support DNA replication (Klusmann et al., 2016; Klusmann et al., 2018).

Previous reports suggested a role for p53 in supporting DNA synthesis upon replication stress (Hampp et al., 2016; Klusmann et al., 2016; Roy et al., 2018; Yeo et al., 2016). Some of them describe a direct role for p53 in DNA replication, independent of its function as a transcription factor. For instance, p53 interacts with the DNA polymerase iota (POLI), inducing idling cycles that slow down replication and induce fork reversal (Hampp et al., 2016; Khare and Eckert, 2002). On the other hand, p53 enhances fork progression and facilitates translesion synthesis by the formation of p21-POLI complexes (Ihle et al., 2021). The choice between these opposing phenotypes depends on the differentiation status of the cell (Ihle et al., 2021). Such a scenario is entirely compatible with our findings that indicate a transcriptional function of p53 in DNA replication, i.e. enhancing the levels of MDM2 and thereby destabilizing PARP1. We propose that p53 can exert its impact on DNA replication in multiple ways, involving mechanisms that do or do not depend on its function as a transcription factor, possibly in a cell type-specific manner.

On top of its interaction with MDM2, PARP1 can associate with additional regulatory factors. These include the Histone PARylation factor 1 (HPF1) (Gibbs-Seymour et al., 2016; Palazzo et al., 2018) and the methyl transferase CARM1 (Genois et al., 2021). Both of them are activators of PARP1, while MDM2 acts as a negative regulator according to our results. Moreover, the E3 ubiquitin ligases CHFR (Kashima et al., 2012), RNF146/Iduna (Kang et al., 2011) and TRIP12 (Gatti et al., 2020) act on PARP1. Unlike these E3 ligases, the interaction of MDM2 with PARP1 does not require PAR. MDM2 binds PARP1 directly as demonstrated by the co-immunoprecipitation of the purified proteins (Figure 2A, S2A), and the interaction is counteracted by increased PAR levels rather than depending on them (Figures 2B-D). Conceivably, PARylation upon replication fork stalling might first delay the interaction of PARP1 and MDM2, thus allowing the stabilization of PARP1 and reversed forks. Conversely, when PAR is degraded upon DNA damage repair or resolution of replication obstacles, this might trigger MDM2-mediated PARP1 degradation and replication restart.

PARP inhibitors, a major class of cancer therapeutics, often exert their activity by trapping PARP1 on chromatin, as exemplified by Olaparib (Pratt et al., 2018). Interestingly, wild type p53 renders cancer cells resistant towards PARP inhibitors (Ireno et al., 2014). This protective effect of p53 towards PARP inhibitors might at least partially be due to MDM2-mediated PARP1 degradation, which would prevent cytotoxic PARP1 trapping on the chromatin.

Fork reversal and PRIMPOL-mediated repriming are two alternative mechanisms by which cells cope with obstacles to the leading DNA strand synthesis. Our results strongly suggest

that MDM2 accumulation is tilting the balance towards repriming. In the context of repeated genotoxic stress, in a BRCA deficient background, PRIMPOL activity protects replication forks against DNA degradation (Quinet et al., 2020), and MDM2 might then support this protective function. Furthermore, PRIMPOL expression is induced by the kinase ATR (Quinet et al., 2020), a principal transducer of a replication stress signal (Saldivar et al., 2017) . At the same time, ATR might promote repriming via p53 phosphorylation and consequent MDM2 induction (Tibbetts et al., 1999). PRIMPOL activation by p53 and MDM2 could thus explain the lengthening of labeled DNA tracks in TP53 wild type cells compared to their TP53 null counterparts upon DNA damage (Yeo et al., 2016).

On top of providing negative feedback on p53, MDM2 emerges as a determinant of genome dynamics. By antagonizing the predominant Poly (ADP-Ribose) Polymerase, it tips the balance between fork reversal and progression towards the latter, thus acting as a central switch to govern the DNA replication machinery.

3.4 SUPPLEMENTARY DATA

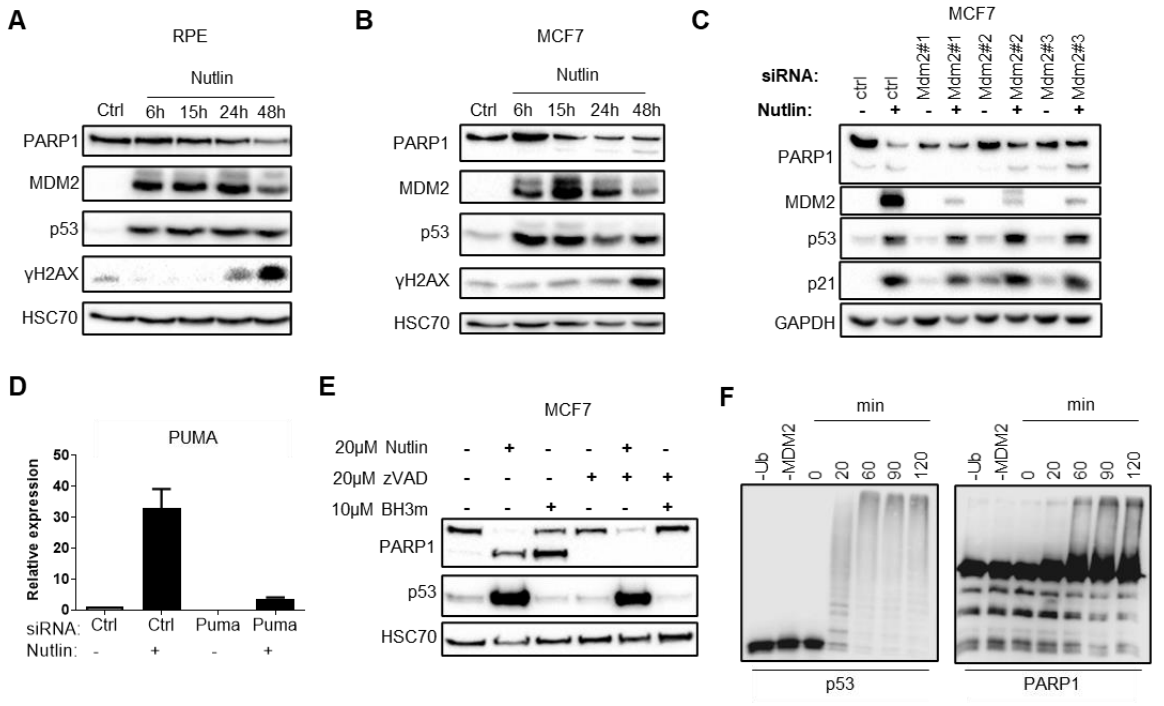

Figure S1. MDM2 ubiquitinates PARP1, triggering its proteasomal degradation

A) RPE cells were treated with 10μM Nutlin and harvested at the indicated time points for immunoblot analysis. Reduction of PARP1 levels was observed starting at 24h of Nutlin treatment and became more prominent at 48h.

B) MCF7 cells were treated with 20μM Nutlin for the indicated periods, and immunoblot analysis was performed.

C) MCF7 cells were treated with 3 separate siRNAs against MDM2 for 48h. Prior to harvest and immunoblot analysis, cells were treated with 20μM Nutlin for 24h.

D) RT-qPCR analysis of PUMA mRNA levels in SJSA-1 cells. P53 activation by Nutlin induced PUMA gene expression, as expected, while siRNA transfection led to depletion of PUMA mRNA, confirming the efficacy of the knock down (n= 2).

E) MCF7 cells were treated with either 20μM Nutlin, 20μM of the caspase inhibitor zVAD, or 10μM of the BH3 mimetic (BH3m) ABT-737. ABT-737 induces caspase activation independent of p53 and was used as control. PARP1 was degraded specifically in the presence of Nutlin but not ABT-737. In both cases, the caspase inhibitor zVAD prevented PARP1 cleavage; however, a loss of full length PARP1 was observed in the presence of Nutlin but not ABT-737, and this loss could not be rescued by zVAD.

F) Ubiquitination of PARP1 by MDM2 *in vitro*. Purified recombinant MDM2 was incubated either with PARP1 (right side) or with p53 (positive control, left side). Additional negative controls without ubiquitin (-Ub) or without MDM2 (-MDM2) were included. MDM2 was incubated with the target protein for up to 120 min. At indicated time points, the samples were subjected to immunoblot analysis. Both p53 and PARP1 were ubiquitinated by MDM2, as shown by accumulation of proteins at high molecular weight with increasing intensities at increasing incubation time. A shorter exposure for PARP1 is shown in Figure 1H.

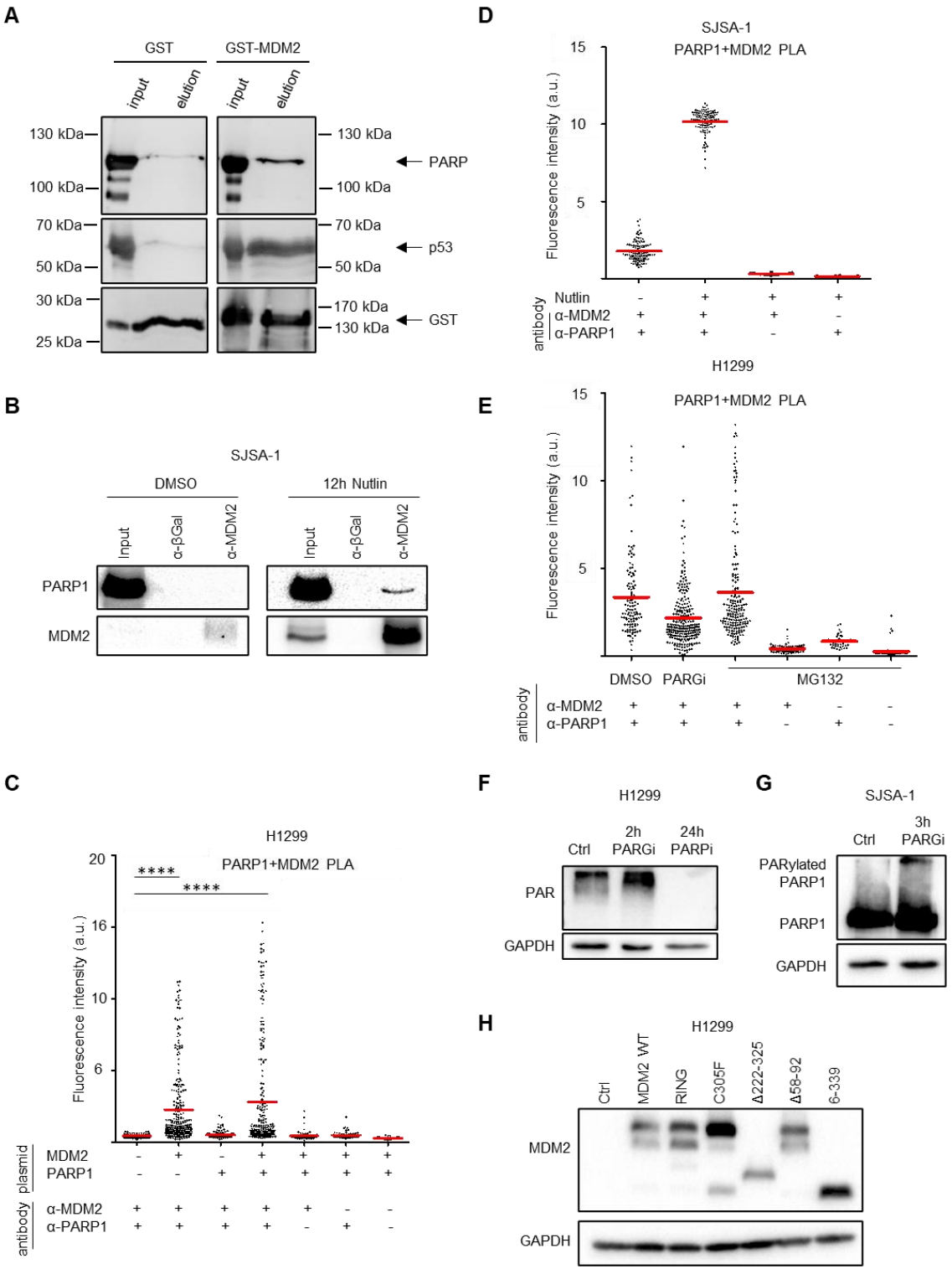

Figure S2. MDM2 forms a complex with PARP1 *in vitro* and *in vivo*

A) GST pull-down assay indicating PARP1 association with GST-MDM2. GST or GST-MDM2 fusion protein were coupled to glutathion beads and incubated with purified PARP1 or p53, followed by washes and elution. Immunoblots were probed to detect PARP1, p53, and GST.

The images to the left (GST) and right (GST-MDM2) were each taken from the same blot with the same exposure time.

B) Immunoblot analysis following immunoprecipitation (IP) of MDM2, upon treatment with 20µM Nutlin for 12h. The IP was performed using an antibody against MDM2 to confirm a physical interaction between MDM2 and PARP1 in SJSA-1 cells. An antibody targeting β-Galactosidase (β-Gal) was used as a negative control.

C) Technical controls of the PLA shown in Figure 2D for H1299 cells. Each antibody was tested individually to assess the background signal of the assay. Note that negative controls were performed under conditions where high levels of both proteins are expected (e.g. when overexpressing both MDM2 and PARP1). Additionally, single over-expressions of either MDM2 or PARP1 were performed by plasmid transfection, to reveal that overexpressed MDM2 associates with endogenous PARP1 as well.

D) Technical controls of the PLA shown in Figure 2E for SJSA-1 cells. Negative controls were performed in cells treated with Nutlin for 6h to enhance MDM2 levels.

E) Technical controls of the PLA shown in Figure 2D. H1299 cells were either treated with PARGi (2h, 20µM), or with the proteasome inhibitor MG132 (10µM, 4h) to increase protein levels.

F) Immunoblot analysis of input samples used for Co-IP (Figure 2B). The PAR signal becomes stronger upon PARGi (20µM, 2h) treatment. PARP1i treatment (Olaparib, 10µM, 24h) completely abolished PARylation.

G) Immunoblot analysis of input samples used for Co-IP (Figure 2C). AutoPARylated PARP1 becomes visible upon PARGi treatment (10µM, 3h).

H) Immunoblot analysis of MDM2 mutants (Figure 2G).

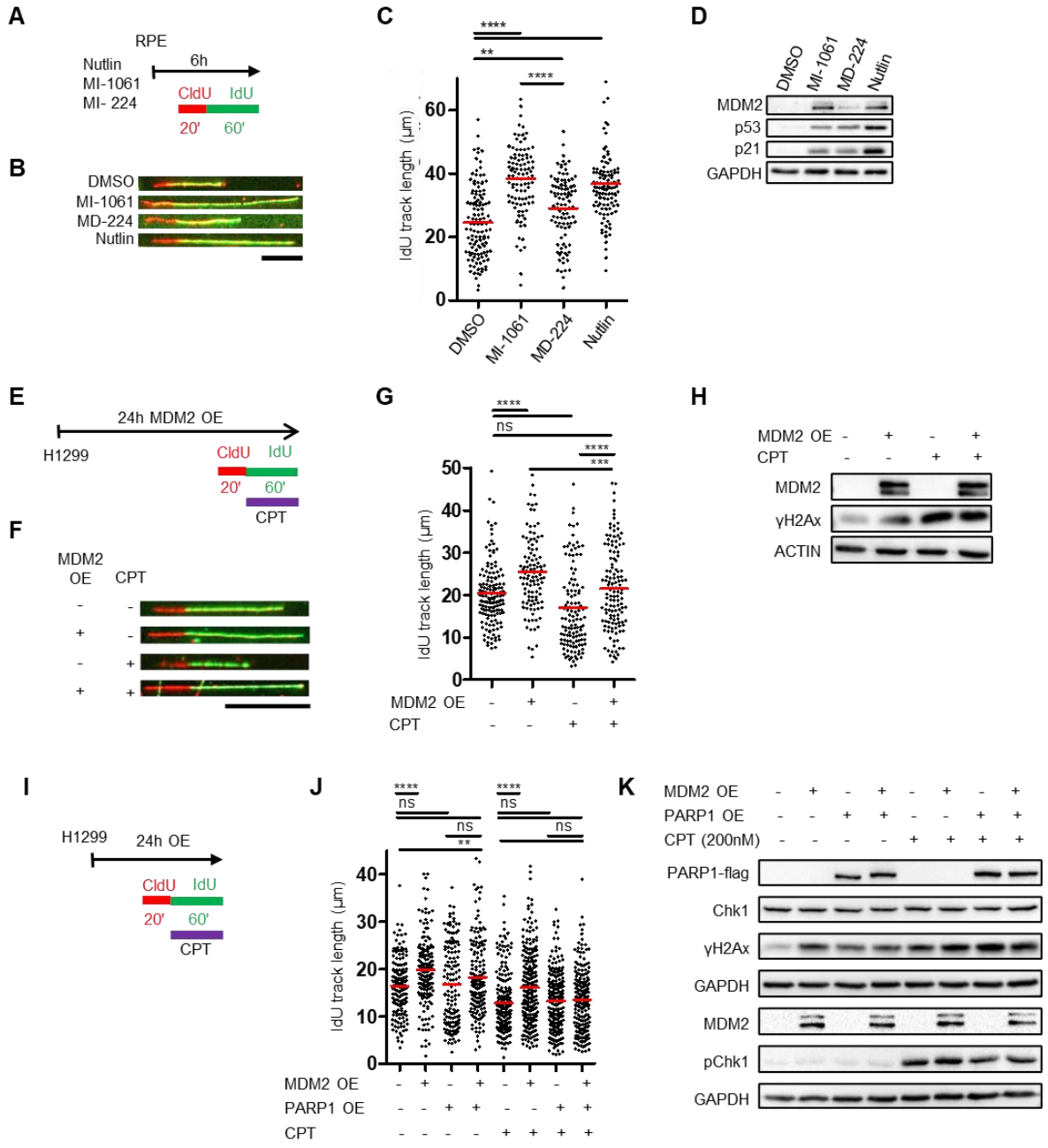

Figure S3. MDM2 enhances the elongation rate of DNA synthesis, which is abolished by PARP1 overexpression

A) Treatment protocol. RPE cells were treated with Nutlin (20µM, 6h), MI-1061 (1µM, 6h), or MD-224 (1µM, 6h). DNA fiber assays were performed by sequential labeling of newly synthetized DNA with CldU (25µM, 20 min) and IdU (25µM, 60 min).

B) Representative images of DNA fibers detected upon treatment shown in A. Scale bar=20µm.

C) DNA fiber assay following treatment shown in A. Mean IdU track lengths, within bicolored fibers, are indicated by red lines. A minimum of 100 fibers was quantified in three independent experiments with similar results. Mann-Whitney U test, two sided, was used for statistical analysis: **p-value≤0.01, ****p-value < 0.0001.

D) Immunoblot analysis of RPE cells treated following the protocol shown in A.

E) Transfection and treatment schedule. H1299 cells were subjected to plasmid transfection (control plasmid pCMV, expression plasmid pCMV-MDM2). Treatment with CPT (200nM) was performed 1h prior to harvest. For DNA fiber assays, the newly synthetized DNA was labeled with CldU (25μM, 20 min) and then IdU (25μM, 60 min).

F) Representative images of DNA fibers upon transfection and treatment depicted in E. Scale bar=20μm.

G) DNA fiber assay following transfection and treatment of H1299 cells as indicated in E.

H) Immunoblot analysis upon treatment as indicated in E, confirming MDM2 overexpression and DNA damage (γH2AX) induced by CPT treatment.

I) Protocol used for DNA fiber assays. H1299 cells were subjected to plasmid transfection (control plasmid pCMV, expression plasmid pCMV-MDM2 and/or pCMV-PARP1), followed by CPT treatment and fiber assays as in E.

J) Fiber assay analysis of H1299 cells transfected and treated as depicted in I.

K) Immunoblot analysis upon transfection and treatment as indicated in I.

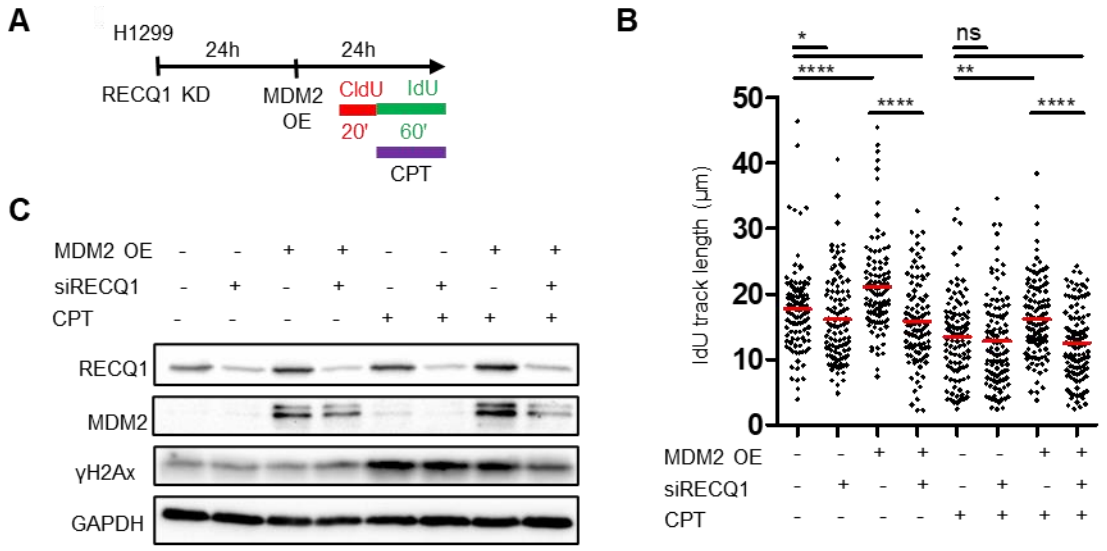

Figure S4. MDM2-mediated PARP1 degradation induces nascent DNA elongation through RECQ1

A) Transfection and treatment schedule. H1299 cells were subjected to plasmid transfection (control plasmid pCMV, expression plasmid pCMV-MDM2) and RECQ1 depletion via siRNA. For DNA fiber assay the cells were labeled with CldU (25μM, 20 min) and then IdU (25μM, 60 min). CPT (200nM) was added 1h prior harvest.

B) DNA fiber assays following transfection of H1299 cells as indicated in A. A minimum of 100 fibers was quantified in two independent experiments with similar outcome.

C) Immunoblot analysis upon treatment as indicated in A.

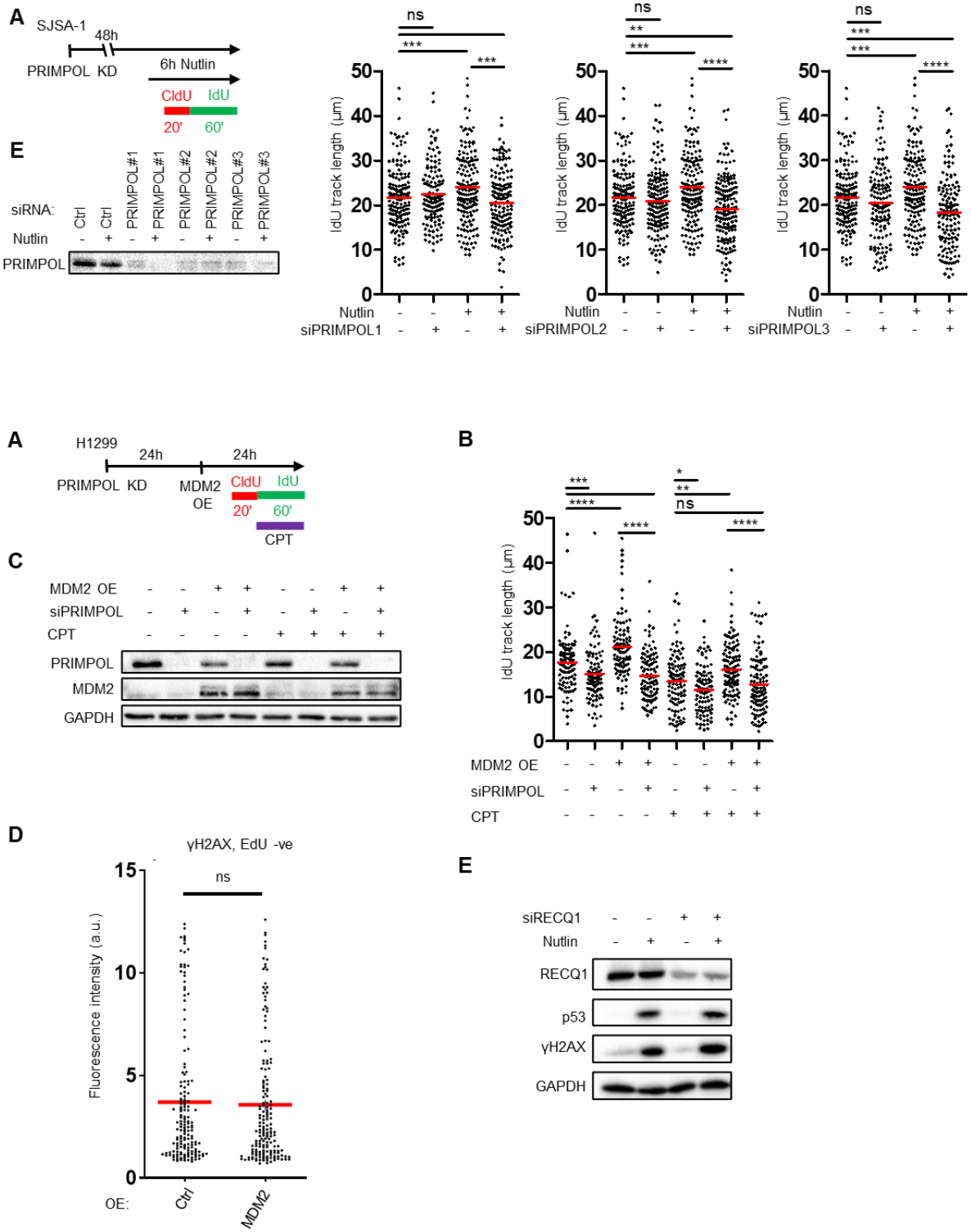

Figure S5. MDM2 accumulation favors PRIMPOL-mediated fork progression and accumulation of DNA damage

A) Transfection and treatment protocol. H1299 cells were transfected with plasmids (control plasmid pCMV, expression plasmid pCMV-MDM2) and siRNA to deplete PRIMPOL. For DNA fiber assays, the nascent DNA was labeled with CldU (25µM, 20 min) and then IdU (25µM, 60 min).

B) DNA fiber assay following transfection and treatment of H1299 cells as indicated in A. A minimum of 100 fibers for each sample was quantified in two independent experiments with similar outcome.

C) Immunoblot analysis upon transfection and treatment as indicated in A, confirming MDM2 overexpression and PRIMPOL depletion.

D) Quantitative immunofluorescence analysis of γH2AX in H1299 cells upon overexpression of MDM2. Unlike in Figure 5G, EdU negative, i.e. cells that did not undergo DNA replication, were subjected to quantification. This indicated that MDM2 did not induce DNA damage in cells out of S-phase.

E) Immunoblot analysis of SJSA-1 cells upon treatment with 20μM Nutlin for 12h, with or without RECQ1 depletion via siRNA, revealing no change in the DNA damage response by Nutlin treatment in the absence of RECQ1.

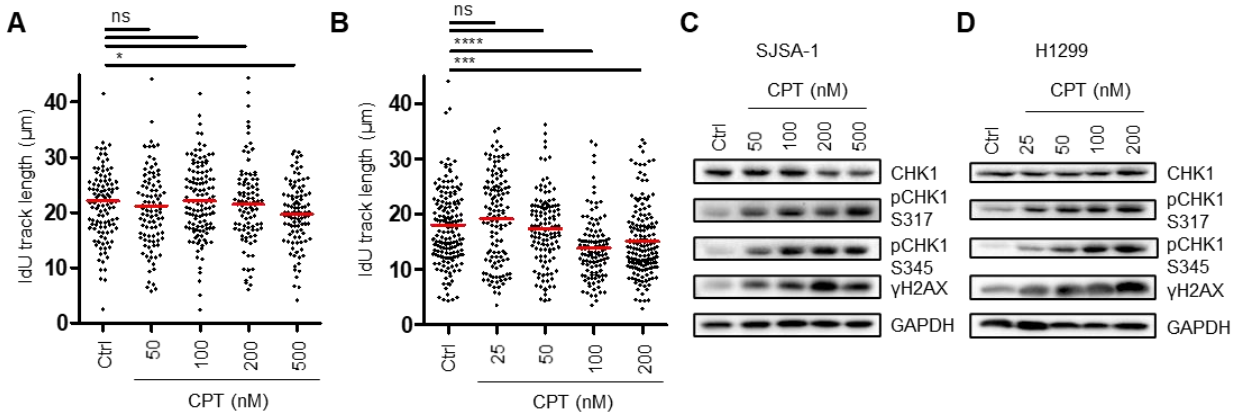

Figure S6. MDM2 accumulation antagonizes replication fork reversal

A, B) Fiber assay analysis of SJSA-1 and H1299 cells, respectively, treated with the indicated concentrations of CPT for 1h. More than 100 fibers for each sample were quantified in two independent experiments with similar outcome.

C, D) Immunoblot analysis of SJSA-1 and H1299 cells treated with indicated concentrations of CPT for 1h.

3.5 METHODS

Cell culture

The human non-small cell lung cancer cell line H1299, the human osteosarcoma cell line SJSA-1, and the human breast cancer cell line MCF-7 were maintained in Dulbecco's modified Eagle's medium (DMEM, 31600091, Thermo Fisher Scientific) supplemented with 10% Fetal Bovine Serum (ACSM0190, Anprotec), 50U/ml Penicillin, 50μg/ml Streptomycin (15140122, GIBCO) and 2mM Glutamine (25030024, GIBCO). The non-tumorigenic human retinal pigment epithelial RPE cells were cultured in DMEM as above, supplemented with 10μg/ml Hygromycin (10687010, Thermo Fisher Scientific) for hTERT activation. Hygromycin was

removed from culturing medium 24h prior to experiments. All cell lines were cultured at 37°C with 5% CO2 and routinely tested for mycoplasma contamination.

Cells were treated with Nutlin-3a (B0084-425358, BOC Sciences), Camptothecin (C9911, Sigma), PDD 00017273 (5952, Tocris), MI-1061 (HY-125858, Hölzel), MD-224 (HY-114312, Hölzel), Olaparib (S1060, Selleckchem), MG-132 (474791, Millipore), ABT-737 (S1002, Selleckchem) and zVAD (ALX-260-020-M005, Enzo Life Sciences).

siRNA transfections were performed using Lipofectamine 3000 (Life Technologies). Cells were reverse transfected with final siRNA concentration of 10 nM siRNA against PRIMPOL (s47417, Thermo Fisher Scientific), RECQ1 (s11903, Thermo Fisher Scientific), MDM2 (#1 s8629, #2 s224037, #3 4390828 Thermo Fisher Scientific), PUMA (s25841 Thermo Fisher Scientific) or scrambled siRNA controls (#4390844, #4390847, Thermo Fisher Scientific). Medium was refreshed after 24 h, and cells were harvested 48 h post-transfection or differently when indicated. For plasmid-mediated overexpression, 2.5 µg of plasmids were forward transfected using Lipofectamine 3000. Cells were transfected to overexpress the following plasmids: pCMV6-XL5 empty control (Origene, #PCMV6XL5), pCMV MDM2 (Oliner et al., 1993), pCMV-PARP1-3xFlag-WT (Addgene, #111575), pcHDM Δ222-325 (Chen et al., 1993), pcHDM Δ58-90 (Chen et al., 1993), pCMV MDM2 mtRING (Roth et al., 1998), pCMV MDM2 C305F (Meng et al., 2015), pCMV MDM2 6-339 (Chen et al., 1993). Medium was refreshed after 6 h, and cells were harvested for experiments 24 and 48h post-transfection.

DNA fiber assay

DNA fiber assays were carried out as previously described (Köpper et al., 2013). Newly synthetized DNA was labeled with 5-chloro-2-deoxyuridine (CldU, 25 µM, Sigma-Aldrich) for 20 min, followed by 5-iodo-2-deoxyuridine (IdU, 25 µM, Sigma-Aldrich) for 1 h. Cells were lysed by spreading buffer (200 mM Tris pH 7.4, 50 mM EDTA, 0.5% SDS), and DNA fibers were spread on glass slides prior to fixation in a solution of methanol and acetic acid (Roth). After DNA denaturation by 2.5 M HCl (Sigma-Aldrich), CldU- and IdU-labelled tracts were detected by immunostaining, using antibodies that were originally developed against BrdU. These were mouse anti-BrdU (B44, BD) and rat anti-BrdU (BU1/75, ICR1, Abcam). Then, Alexa Fluor 488-conjugated goat anti-mouse IgG and Alexa Fluor 555-conjugated goat anti-rat IgG (Thermo Fisher Scientific) were used as secondary antibodies. DNA fibers were visualized by fluorescence microscopy (Axio Scope A1 microscope, Zeiss) and analyzed with ImageJ. Fiber length in pixel was converted in micrometers using the conversion factor: 1 pixel=5.7 µm, as previously described (Köpper et al., 2013). Fiber length in micrometers can be converted to kb using the conversion factor 1 µm =2.59 kb (Henry-Mowatt et al., 2003).

Statistical testing was performed using GraphPad Prism. Statistical significance was determined by Mann–Whitney U test.

Immunoblot analysis

Cells were harvested in protein lysis buffer, i.e. 20 mM Tris-HCl pH 7.5, 10 mM NaCl, 1 mM NaCl, 10mM EDTA, 1% Triton-X 100, 1% deoxycholate salt, 0.1% SDS, 2 M urea, and protease inhibitors (pepstatin, leupeptin hemisulfate, aprotinin, AppliChem). The samples were briefly sonicated to disrupt DNA-protein complexes. Total protein concentration was measured using a BCA protein assay kit (Thermo Fisher Scientific). The samples were boiled in Laemmli buffer at 95°C for 5 min, and equal amounts of proteins were separated by SDS-PAGE. Subsequently, proteins were transferred onto a nitrocellulose membrane, blocked in 5% (w/v) non-fat milk (Roth) in TBS containing 0.1% Tween-20 (AppliChem) for 1 h and incubated with the primary antibodies at 4 °C overnight.

Membranes were then incubated with peroxidase (HRP)-conjugated secondary antibodies (Jackson ImmunoResearch) and the proteins were detected using either Super Signal West Femto Maximum Sensitivity Substrate (Thermo Fisher Scientific) or Immobilion Western Substrate (Millipore).

Co-Immunoprecipitation (Co-IP)

For *in vitro* co-IP, purified proteins were incubated at 4°C overnight on a rotator in co-IP buffer (50 mM Tris, pH 7.5, 300 mM NaCl, 1% NP-40), followed by overnight incubation with 2µg anti-PARP1 antibody and 30 minutes incubation with Protein G Sepharose (GE Healthcare) (4°C). Beads were washed 5 times with co-IP buffer.

For *in vivo* Co-IP, cells were washed with cold PBS followed by lysis in Co-IP Buffer (50 mM Tris, pH 7.5, 300 mM NaCl, 1% NP-40), supplemented with protease inhibitors (11836153001, Roche). Homogenized cell lysate was precleared with Protein G Sepharose (GE Healthcare), followed by overnight incubation with 2 µg of the precipitating antibody. Samples were then incubated with Protein G Sepharose for coupling with the primary antibody for 2h (4°C) and then washed 8 times with Co-IP Buffer.

For both *in vitro* and *in vivo* co-IP, beads were re-suspended in 3x Laemmli Buffer and boiled for 10 min at 95°C to release precipitated protein. Immunoprecipitates were subjected to SDS-PAGE and immunoblot analysis. The following antibodies were used for all precipitations: PARP1 (ALX-210-302-R100, Enzo Life Sciences), MDM2 (IF2 OP46, Merck), IgG rabbit (ab171870, Abcam), β-galactosidase mouse (Z378B, Promega).

RNA extraction, reverse transcription, and real time quantitative PCR

Total RNA was extracted from cells using TRIzol® (Invitrogen). mRNA was reverse-transcribed using oligo-dT and random nonamers as primers, followed by qRT-PCR analysis using SYBR Green (Invitrogen). Gene expression levels were normalized to the mRNA from the gene 36B4, and the analysis was conducted using the ΔΔCt method.

Immunofluorescence

Cells were grown in 8-well permanox slides (177445, Nunc) fixed with 3.7% PFA in PBS for 30 min before being permeabilized with 0.5% Triton-X-100 in PBS for 30 min. Cells were then blocked with 10% FCS in 0.1% Tween-PBS for 10min at room temperature, followed by incubation with primary antibodies at 4°C, overnight. After washing with PBS (3x10 min), slides were incubated with secondary antibody and 4',6-diamidino-2-phenylindole (DAPI, Sigma-Aldrich) for 1h at room temperature. Following washes in PBS (3x10 min), the chambers were removed, and slides were mounted onto coverslips using fluorescent mounting medium (S302380-2, DakoCytomation). Images were acquired using a Zeiss Axio Scope.A1 fluorescence microscope equipped with an Axio Cam MRc/503 camera using a 40x magnification, and further analysed with ImageJ. The DAPI signal was used to create binary images (segmentation) to define the nuclear area as region of interest (ROI). These ROIs were then used to quantify the nuclear signal of the other channels. Single nuclei mean gray values were visualized on dot plots, and statistical testing was performed using Graph Pad Prism v.6 unpaired Student's t-test: ns, not significant; *p-value≤0.05; **p-value≤0.01; ***p-value≤0.001; ****p-value < 0.0001.

Proximity Ligation Assay

Cells were grown in 12-well slides (81201, Ibidi) and following treatment or transfection, cells were fixed and permeabilized as described above, and subjected to the PLA assay using the Duolink In Situ Detection Reagents Orange (DUO92007, Sigma-Aldrich) in a humid chamber. Briefly, plastic wells were removed from the chamber slides prior to blocking and incubation with primary antibodies (1:200 MDM2 IF-2, 1:200 PARP1 ab227244) overnight at 4°C. This was followed by incubation with PLA probes (Duolink™ In Situ PLA® Probe Anti-Mouse PLUS DUO92001, Duolink™ In Situ PLA® Probe Anti-Rabbit MINUS DUO92005) for 1 h, at 37°C while shaking. Ligase was then added to hybridized PLA probes to generate a closed circle (60 min at 37°C) before DNA amplification for 100 min at 37°C while shaking. After performing the PLA protocol, cells were counterstained with DAPI, the plastic chambers were removed

and the slides were mounted onto coverslips using fluorescent mounting medium (S302380-2, DakoCytomation). Images were acquired and analysed as described above.

EdU incorporation

EdU (5-ethynyl-2‘-deoxyuridine) was purchased from Thermo-Fisher Scientific (A10044) and diluted in DMSO to a final concentration of 10 mM. Cells were grown and transfected in 8-well permanox slides (177445, Nunc) and EdU was added to growing cultures to a final concentration of 10 µM for 30 min. Following fixation and permeabilization, the following reagents were added to 100 mM Na-phosphate buffer (pH 7) in order to perform the click chemistry reaction: 5 µM AlexaFlour594 picolyl-azide (Jena Biosciences, #CLK-1296-1), 100 µM CuSO4 (Jena Biosciences, #CLK-MI004) in 500 µM Tris(3-hydroxypropyltriazolylmethyl)amine (THPTA; Sigma-Aldrich, #762342), 5 mM Na-Ascorbate (Jena Biosciences, #CLK-MI005). Click chemistry was performed at RT, for 1h, followed by 3x 10 min washes in PBS. Immunofluorescence was consecutively carried on as described above.

Electron Microscopy

Asynchronous and subconfluent H1299 cells were transfected with the empty vector pCMV-XL5 (control) or the expression plasmid pCMV-MDM2 WT. After 24h, the cells were treated with 200 nM of CPT (Sigma-Aldrich) for 1h. Asynchronous and subconfluent SJSA-1 cells were treated with Nutlin (20uM, BOC Sciences) or DMSO for 6h. CPT was then added at the concentration of 500nM for 1h. Cells were collected, resuspended in ice-cold PBS and crosslinked with 4,5′,8-trimethylpsoralen (10 µg/ml final concentration), followed by irradiation pulses with 365 nm monochromatic UV light (UV Stratalinker 1800; Agilent Technologies). For DNA extraction, cells were lysed (1.28 M sucrose, 40 mM Tris-HCl [pH 7.5], 20 mM MgCl2, and 4% Triton X-100; Qiagen) and digested (800 mM guanidine–HCl, 30 mM Tris-HCl [pH 8.0], 30 mM EDTA [pH 8.0], 5% Tween-20, and 0.5% Triton X-100) at 50 °C for 2 h in the presence of 1 mg/ml proteinase K. The DNA was purified using chloroform/isoamyl alcohol (24:1) and precipitated in 0.7 volume of isopropanol. Finally, the DNA was washed with 70% EtOH and resuspended in 200 µl TE (Tris-EDTA) buffer. 100 U of restriction enzyme (PvuII high fidelity, New England Biolabs) were used to digest 6 µg of mammalian genomic DNA for 5 h. RNase A (R5503, Sigma–Aldrich) to a final concentration of 250 ug/ml was added for the last 2 h of this incubation. The digested DNA was purified using the Silica Bead DNA Gel Extraction Kit (Thermo Fisher Scientific). The Benzyldimethylalkylammonium chloride (BAC) method was used to spread the DNA on the water surface and then load it on carbon-coated 400-mesh nickel grids (G2400N, Plano Gmbh). Subsequently, DNA was coated with platinum using a High Vacuum Evaporator BAF060 (Leica). The grids were scanned using a transmission

electron microscope (Tecnai G2 Spirit; FEI; LaB6 filament; high tension ≤120 kV) and images were acquired with a side mount charge-coupled device camera (2600 × 4000 pixels; Orius 1000; Gatan, Inc.) and processed with DigitalMicrograph Version 1.83.842 (Gatan, Inc.). For each experimental condition at least 70 replication fork molecules were analyzed in two different biological replicates by using ImageJ.

GST pull-down assay

For *in vitro* MDM2-PARP1 binding assays, 1.5 µM of GST-SUMO tagged HA-MDM2 or GST (as control) were incubated 10 min on ice in binding buffer (2 mM $MgCl_2$ and 1 mM DTT) with 2 µM of recombinant PARP1 prior to the addition of 10 µl Glutathion-Sepharose® 4B (17-0756-01, Cytiva,) pre-equilibrated in binding buffer. The mixtures were incubated for 3 h at room temperature in an overhead shaker, followed by 4 washing steps with 200 µl washing buffer (1x PBS, 1 mM DTT) . Bound proteins were eluted twice by incubating beads with 25 µl elution buffer (1x PBS and 40 mM GSH pH 7.6). Eluates were combined and electrophoresed on 10% SDS gels followed by western blot analysis against p53 (DO-I Calbiochem Cat: OP43-20UG (ASK07) Lot: 489202-25), GST (SAB5300159, Sigma-Aldrich) or PARP1 (ALX-804-211-R050, F1-23 Enzo Life Sciences). For generation of recombinant PARP1, His-tagged PARP1 was expressed and purified as previously described (Kruger et al., 2020; Langelier et al., 2011).

***In vitro* Ubiquitination Assay**

0.25 µM p53 or PARP1 were incubated with 100 nM UBA1, 0.5 µM UbcH5b, 0.35 µM MDM2 in 25 mM Tris- HCl pH 7.5, 50 mM NaCl, 1 mM DTT, 2 mM ATP, 2 mM $MgCl_2$ at 37°C for the times indicated. Reactions were started by the addition of 39 µM Ub and stopped by the addition of 5x Laemmli stop buffer. Reaction mixtures were subjected to SDS-PAGE followed by Western blot analysis against p53 (DO-I Calbiochem, OP43-20UG (ASK07) Lot: 489202-25) or PARP1 (ALX-804-211-R050, F1-23 Enzo Life Sciences).

4. DISCUSSION

MDM2 is a E3 ubiquitin ligase and the major negative regulator of the tumour suppressor p53; it is therefore considered an oncogene, and its overexpression is observed in several cancer types. In this study, we have investigated two novel non-canonical functions of the oncoprotein MDM2. We found that MDM2, when in a complex with RPL5 and RPL11, can negatively regulate RNA Pol III activity and affect ribosome biogenesis (Manuscript 1). Moreover, we identified PARP1 as a new direct interactor of MDM2, and MDM2-dependent ubiquitination of PARP1 enforces the restart of reversed replication forks (Manuscript 2).

4.1 MDM2, together with RPL5 and RPL11, inhibits RNA Pol III activity

The 5S-RNP, composed of RPL5, RPL11 and 5S rRNA, presents some unique characteristics that differentiate it from other RNPs. First, mammalian cells contain a large pool of free 5S-RPL5 RNPs, representing up to 50% of total 5S rRNA (Madru et al., 2015; Steitz et al., 1988). None of the other RPs or rRNA are expressed in such excess, which suggests extra-ribosomal functions, and the necessity of a fast-responding mechanism upon stress. Both RPL5 and RPL11 can directly interact with the 5S rRNA, and therefore might act as sensors for problems that arise in ribosome biogenesis (Chakraborty et al., 2011). And finally, the 5S RNP was shown previously to interact with MDM2, directly linking ribosome biogenesis to the p53 pathway, to further strengthen the concept of the 5S-RNP as a detector of stresses.

Our study revealed that MDM2 is recruited to the proximity of RNA Pol III, and this depends on the presence of both RPL5 and RPL11 (Manuscript 1, Figure 2C). However, it's unclear how the MDM2-5S RNP localizes in proximity of POLR3A, the catalytic subunit of RNA Pol III. RPL5 has been shown to be necessary for the proper processing of 5S rRNA by binding and stabilizing it co-transcriptionally (Sloan et al., 2013). It is tempting to speculate that MDM2, together with RPL11, might be recruited in the proximity of RNA Pol III by RPL5 binding nascent 5S rRNA. The IF results shown in Manuscript 1 (Manuscript 1, Figure S2C) suggest higher nucleoplasmic levels of free RPL5 protein levels compared to RPL11 in unstressed cells, and this was also confirmed by sucrose gradient experiments (Appendix, Figure 1). RPL11 was shown to accumulate in the ribosome-free fraction only upon MDM2 accumulation *via* Nutlin, indicating that RPL11 is recruited (or sequestered) to the nucleoplasm, possibly by the MDM2-RPL5-5S complex (Appendix, Figure 1). In the future, immunoprecipitation of MDM2 in unstressed cells will help us understanding whether it can interact with RPL5-5S even without p53 induction or presence of ribosomal stress. Interaction between MDM2 and RPL11 could then be analysed upon different Nutlin points, to identify the exact time point

RPL11 joins the complex. Moreover, analysis of the MDM2-RPL5-RL11 *via* native gels, which allows investigation of folded proteins and macromolecular complexes, could further shed light on the dynamics of the complex formation.

In our study, depletion of either RPL5 or RPL11 not only rescued 5S rRNA synthesis upon Nutlin treatment, but also led to accumulation of unprocessed 5S in the absence of p53 activation (Manuscript 1, Figure 2D). This was surprising, since an incorrect stoichiometry of rRNA and RPs is known to induce cell cycle arrest and cytotoxicity which would inhibit RNA synthesis as a result (Delgado-Román and Muñoz-Centeno, 2021). We hypothesize that both these proteins are involved in processing of the 5S rRNA. However, since processing of the 5S rRNA involves cleavage of only 2-3 nt, and it's not completely understood in humans (Ciganda and Williams, 2011), it is difficult to distinguish between mature and pre- 5S rRNA *via* qPCR. This question would better be answered by metabolic pulse-labelling of RNA and detection of global nascent 5S rRNA via northern blotting. If both RPL5 and RPL11 are necessary for processing of the 5S rRNA, depletion of either of them would cause an accumulation of longer, unprocessed 5S rRNA and a decrease in processed 5S rRNA. To further confirm our qPCR results, we investigated the role of MDM2 using the MD-224 degrader strategy (Manuscript 1, Figure 1A). MD-224 is a small compound composed of two domains: one targeting the hydrophobic pocket of MDM2, thus disrupting its interaction with p53, and the other one recruits the E3 ubiquitin ligase machinery Cereblon. This way, p53 is activated, MDM2 is induced transcriptionally but its immediately degraded by the proteasome. This proteolysis targeting chimera (PROTAC) strategy allow us to study MDM2 functions in the context of p53 activation, in proliferating cells. Our study shows that both RPL5 and RPL11 are required for inhibition of RNA Pol III by MDM2, since depletion of any of these proteins rescue 5S pre-rRNA levels (Manuscript 1, Figure 1E, 2D). This is not surprising, since it has been shown that depletion of any of the components of the 5S RNP abolishes the binding of the others, explaining why RPL5 and RPL11 might be dependent on each other (Bursać et al., 2012; Donati et al., 2013), and why depletion of one of them might cause the entire complex to destabilize.

4.2 MDM2 is an inhibitor of transcription

MDM2 has been previously shown to inhibit RNA Pol II-dependent transcription, either by inhibiting transcription factors (Biderman et al., 2012) or by chromatin modifications (Riscal et al., 2016; Wienken et al., 2016). The Tjian laboratory showed, through *in vitro* studies, that MDM2 can repress gene expression, also in the absence of p53 (Thut et al., 1997). Our results further corroborate this, showing for the first time that MDM2 can also affect transcription of non-coding RNA. Nutlin treatment caused repression of both RNA Pol III and RNA Pol I transcription, although RNA Pol III inhibition preceded inhibition of RNA Pol I inhibition by a few hours (Manuscript 1, Figure 1 and 5). Moreover, depletion of MDM2 by proteasomal degradation using the PROTAC MD-224 led to a complete rescue of both 5S and tRNA (Leu-CAA) pre-RNA, arguing that inhibition of RNA Pol III is directly caused my MDM2 and not by downstream signalling (Manuscript 1, Figure 1E). Already two decades ago, p53 was thought to inhibit activity of RNA Pol III, since fibroblasts derived from $p53^{-/-}$ mice lines showed a increase in Pol III transcriptional activity (Cairns, 1998). Our results further expand on this, uncovering MDM2 as a mediator of Pol III inhibition.

But how could MDM2 directly affect RNA Pol III activity? RPL5 and RPL11 seem to be important for both inhibition of RNA Pol III and localization of MDM2 in the proximity of RNA Pol III (Manuscript 1, Figure 1C, D), arguing that presence of the MDM2/RPL5/RPL11 is essential for repression of 5S and tRNA transcription observed by Nutlin treatment. Ribosomal proteins L5 and L11 might be recruiting MDM2 at the site of Pol III transcription, however we don't know the exact mechanism of inhibition yet. Two different scenarios are possible; first, MDM2 could affect the chromatin landscape of RNA Pol III-dependent genes by ubiquitination of H2A, which generally represses gene expression (Cao and Yan, 2012). Second, MDM2 could inhibit transcription factors necessary for Pol III activity, such as TFIIIA, BRF1 or BDP1, either by direct interaction or PTMs. MDM2 was detected in proximity of BRF1, so this scenario is possible (Manuscript 1, Figure S2B). Chromatin immunoprecipitation could be employed to answer both these questions either by precipitating MDM2, and detecting its levels at RNA Pol III genes, or by precipitating transcription factors to see whether they are still part of the initiation complex. Either way, both questions remain important since inhibition of RNA Pol III activity might result from a combination of both events.

4.3 P53 activation induces nucleolar stress

A recent study from Frottin *et al.* described the nucleolus as a protein quality control department. Proteins which are prone to aggregation (e.g., intrinsically disordered) were observed to be sequestered in the GC (Granular Component, outermost) phase, which is rich in negatively charged proteins such as Nucleophosmin (NPM) and RNA. Sequestering of misfolded proteins in the GC prevents them to aggregate, allowing Hsp70-mediated refolding or degradation after stress, and this is reversible. However, the nucleolus has a limited capacity to contain misfolded proteins, and when proteotoxic stress is prolonged, the GC turns from liquid to solid state causing loss of functionality and proteins are free to aggregate (Frottin et al., 2019).

MDM2 has large portions of intrinsically disordered domains, its central domain is positively charged and it can bind strongly to RNA, as previously described (Elenbaas et al., 1996). Moreover, MDM2 has been shown to aggregate, together with mutTP53 (Wawrzynow et al., 2018), and also to form oligomers with itself or MDMX (Leslie and Zhang, 2016). Upon p53 induction *via* Nutlin treatment, MDM2 levels increase drastically, especially in cell lines with a *MDM2* amplification, and some MDM2 proteins might as well misfold or form oligomers. It would be interesting to investigate, using confocal STED microscopy for instance, if MDM2 can localize in the nucleolus, as previously suggested (Weber et al., 1999), and in which phase of the nucleolus it accumulates. We have observed MDM2 being localized mainly in the nucleoplasm (Manuscript 1, Figure S4B), however the samples were acquired under a classic epifluorescence microscope. Confocal microscopy would enable the acquisition of images at the exact plane of focus, without background fluorescent light from the cytoplasm or other regions of the specimen and would be more informative for our purpose. We can't exclude for now that a minority of MDM2 protein might indeed localize in the nucleolus.

Our study reveals a stronger disruption of the DFC (Dense Fibrillar Center, middle) rather than the GC, as shown by an extreme delocalisation of FBL (found in the DFC) from the nucleoli to the nucleoplasm, compared to a milder delocalisation of NPM (found in the GC) (Manuscript 1, Figure 4 and Figure S4). However, it has been shown that the disordered domain in both FBL and NPM are required for phase-separation in the nucleoli (Brangwynne et al., 2011; Mangan et al., 2017). Therefore, disruption in FBL localization would also lead to loss of droplet formation in the nucleoli, precipitation of nucleolar proteins and eventually cell death. We observed that, as nucleolar stress and disruption increased, several components and cofactors of the RNA Pol I (such as POLR1A, UBF, RRN3) and RNA Pol III machinery (such as POLR3A, TFIIIA) are degraded in a MDM2-dependent way (Manuscript 1, Figure 2E and 4C). This could be a consequence of nucleolar disruption, or it could depend on the

proteasome and on direct ubiquitination by MDM2. It was shown that several ribosome biogenesis factors, such as nucleolin, NPM, and UBF often shuttle from the nucleolus to the nucleplasm, particurarly in response to stress, (Borer et al., 1989; Khandelwal et al., 2011; Phair and Misteli, 2000; Sirri et al., 2008), making a direct interaction with MDM2 plausible. Answering this question might reveal to be hard, since p53 induction by Nutlin induces dozens of target genes, and unfortunately the MDM2 PROTAC MD-224 could be used only for a limited time frame in our hands (e.g., 6-12h), since longer treatments did not lead to comparable p53 induction with the MI-1061 control (data not shown). Nucleolar stress was only detected upon longer treatments (24h), which makes a rescue experiment difficult to perform due to cell cycle arrest following p21 induction and due to the results difficult to interpret. This could be solved either by screening for a suitable cell line where the MD-224 is functional for longer time points, or testing different MDM2 degraders (Wang et al., 2021), so that a rescue experiment can be performed in proliferating cells. Another experiment that could be very informative is immunoprecipitation of MDM2 in isolated nucleoli and in response to different cellular stresses. This would uncover the MDM2 interactome specifically in nucleoli and reveal if interactions change depending on the type of stress.

$P19^{ARF}$, referred to as ARF from now on, is another important component of the MDM2/p53 network, and has been shown to sequester MDM2 into the nucleolus, thereby allowing p53 accumulation and activation (Weber et al., 1999). However, in our study we found MDM2 predominantly in the nucleoplasm arguing against an ARF-dependent sequestering of MDM2 in the nucleolus (Manuscript 1, Figure S4B). Different types of stress could affect localization of MDM2. Interestingly, inhibition of the proteasome *via* MG-132 treatment led to an increased localization of MDM2 in the nucleoli (Appendix, Figure 2). Further studies are needed to better understand recruitment of MDM2 in this subnuclear organelle and its cellular consequences.

4.4 MDM2 induction and cell death

Many current cancer therapies employ genotoxic chemotherapy, such as alkylating agents (e.g., cisplatin), antimetabolites (e.g., 5-FU, gemcitabine) and alkaloids (e.g., etoposide). These therapies are highly effective by inducing DNA damage and replicative stress (Kitao et al., 2018); however, they increase the chance of cancer formation in untransformed cells. Non-genotoxic strategies are currently under study, with p53 re-activation as being one of the prominent ones (Khoo et al., 2014). Being p53 the most mutated tumour suppressor underlines the importance of this protein in preventing cancer formation. However, a considerable percentage of tumours still retain functional wild type p53 which, however, is kept

inactive by overexpression of its antagonist MDM2. Agents disrupting the p53-MDM2 interaction, such as Nutlins, have been considerably researched but unfortunately haven't been very successful in the clinics with the exception of treatment of a minority of sarcomas and acute myeloid leukaemia (AML) (Wang et al., 2017). In most tumorigenic cell lines tested *in vitro*, Nutlins were observed to induce reversible cell cycle arrest instead of apoptosis, while clinical studies using the derivative RG7112 caused haematological toxicity in patients (Tisato et al., 2017). Moreover, multiple p53 mutations arose within patients following treatment with the derivative SAR40583, suggesting a resistance mechanism (Jung et al., 2016). Therefore, combination therapies are being researched so to induce synergism with Nutlins.

Nutlins can induce cell death mainly in cell lines overexpressing MDM2, with few exceptions (Tovar et al., 2006). Our study confirms this and takes it a step further, by showing that MDM2 levels, and not p53, are responsible for cell death in the osteosarcoma cell line SJSA-1. Depletion of MDM2 and consequent treatment with Nutlin does not affect p53 levels or activity, but it prevents cell death in this cell line (Manuscript 1, Figure 6). Moreover, disruption of the MDM2/RPL5/RPL11 also prevents apoptosis and caspase activation, suggesting that this complex is involved in induction of cell death in response to p53 activation (Manuscript 1, Figure 6). Surprisingly, *PUMA* knockdown was unable to rescue cell death in response to Nutlin, although caspase activation was inhibited, as shown by PARP1 cleavage. Irreversible inhibition of caspases using zVAD was not sufficient to prevent cell death induced by Nutlin (Appendix Figure 3). This suggests two separate scenarios: 1) Nutlin induces caspase-independent cell death and not apoptosis, mediated by MDM2 expression; 2) Cyto-toxicity induced by Nutlin is so extreme that cells die *via* other mechanisms when apoptosis is inhibited. We tested several inhibitors of caspase-independent cell death, and none was capable of rescuing cell death, suggesting the second option as being the most probable (Appendix, Figure 4).

A difficult question that remains to be answered is: what mechanism exactly is mediating cell death in response to Nutlin? Different scenarios are possible. Disruption of ribosome biogenesis might be the cause since the lack of these essentials molecular machines will prevent the cell to function properly. However, ribosomes are extremely stable, and they need to be produced mainly when cells are growing and proliferating; p53 activation in our system would lead to cell cycle arrest quite early on, but cell death induction is too rapid to be caused by a lack of ribosomes (Manuscript 1, Figure 7). It would be tempting to speculate that RNA Pol III inhibition, and consequent nucleolar stress, might be involved. We observe degradation of several components of RNA Pol I and RNA Pol III complexes, including transcription factors, which is directly caused by MDM2 levels (Manuscript 1, Figure 2E, S4A-D). Inhibition of rRNA synthesis would also cause leak of several "orphan" ribosomal proteins, which are quite

unstable when found as free units and need to be degraded by the proteasome (Sung et al., 2016). If the ubiquitin-proteasome system is overwhelmed by the presence of too many proteins to be degraded, it would stop functioning properly, leading to accumulation of toxic misfolded and aggregated proteins; proteotoxicity might then cause cell death, and if the stress is persistent and strong enough, it would kill the cells also independently of caspases as previously described (Iurlaro and Muñoz-Pinedo, 2016).

An important experiment to be performed in the future is combining p53 activation with RNA Pol III inhibition, to understand whether this would be sufficient to induce cell death in cancer cells. Unfortunately, there are currently no available specific and potent RNA Pol III inhibitors to test a possible synergism with Nutlin. However, it would be interesting to test weather partial depletion of POLR3A, for example *via* siRNA, in combination with Nutlin treatment, can induce cell death in cell lines without a MDM2 overexpression, for example in the osteosarcoma U2OS cell line. This cell line retains wild type p53 and harbours low MDM2 levels, and it is known to respond poorly to p53 induction. U2OS was also the only cell line that did not show any depletion of UBF, which is essential for rRNA transcription, in response to Nutlin, while all the other cell lines tested, that respond to Nutlin with cell death, showed some degree of degradation (Appendix, Figure 5). It will be important to also investigate the protein levels of members of the RNA Pol I and RNA Pol III complex. A growing body of research links tRNA levels to inhibition of cytochrome c release, linking RNA Pol III activity to inhibition of apoptosis for the first time (Liu et al., 2016; Mei et al., 2010; Saikia et al., 2014). In these studies, both full length and fragmented tRNAs were shown to directly interact with cytochrome c, preventing it to activate caspases downstream and delaying apoptosis. Further investigations towards this direction will be necessary to understand how RNA Pol III activity affects cell fate.

4.5 MDM2 accumulation increases replication speed

Previous work from the Dobbelstein lab described p53 as a supporter of DNA replication by increasing processivity, and this was linked to reduction of replicative stress in primary cells (Klusmann et al., 2016). Removal of p53 was seen to reduce fork progression, and p53 activity was protecting genome stability by preventing stalling of replication forks. One of the mechanisms allowing p53 to increase fork speed was through expression of MDM2. A follow up study linked the chromatin modifying activity of MDM2 to the prevention of DNA:RNA hybrids, independently of p53 (Klusmann et al., 2018). Such structures, also called R-loops, arise naturally during transcription when a newly synthesised RNA sequence hybridize with DNA, and these pose an obstacle to both transcription and replication (García-Muse and Aguilera, 2019). MDM2 and the ubiquitin ligase component of the PRC1 complex, RNF2, were

shown to act in parallel on DNA replication, and MDM2 overexpression could compensate for RNF2 depletion. H2A ubiquitination by MDM2 and/or RNF2 was necessary to avoid R-loop formation, therefore reducing obstacles to replication and increasing fork speed (Klusmann et al., 2018). H2A ubiquitination by both MDM2 and the PRC1 complex has been linked to transcriptional repression, partially explaining why the presence of these E3 ubiquitin ligases reduce R-loop formation; A reduction in transcription would lead to a decrease in R-loops, and therefore less obstacles for replication.

It is important to remember that the concept of replication stress has evolved over the past few years, with high replication speed being recently described as a cause of fork collapsing and DNA damage. When replication proceeds at speeds that are either too low or too high, this could cause stalling and collapse of the replication fork, with consequent genome instability (Maya-Mendoza et al., 2018; Merchut-Maya et al., 2019; Zeman and Cimprich, 2014). Among other stresses that affect replication speed, excessive heterochromatin formation, repetitive genome sequences, R-loops, DNA damage are some examples (Zeman and Cimprich, 2014). Our results elucidate a new mechanism of replication speed control by MDM2, independent of its transcriptional inhibition activity. DNA replication forks have several ways to deal with replication stress, and it is not surprised that MDM2 is involved in more than one. We focused on the mechanisms of fork reversal, a critical protective mechanism in response to obstacles of replication. We showed that high levels of MDM2 following overexpression or p53 induction cause a decrease in the numbers of four-way DNA structures, as seen by electron microscopy (Manuscript 2, Figure 6). The first indication that this could be explained by a “forced” induction of fork restart by MDM2 came from DNA fiber assays analysis, where high levels of MDM2 were linked to high replication speed (Manuscript 2, Figure 3). The combination of PARP inhibition *via* Olaparib with Nutlin treatment did not farther increase fork speed, suggesting an epistatic effect. PARP1 degradation by Nutlin was described a couple of years back (Kobayashi et al., 2020), therefore making the E3 ubiquitin ligase MDM2 an inviting candidate to investigate in this context. Indeed, we show that MDM2 and PARP1 interact directly, both *in vitro* and *in vivo*, linking two of the most important tumour suppressors, PARP1 and p53. PARP1 role in DNA damage response and replication fork stability has been extensively studied (Hanzlikova et al., 2018; Maya-Mendoza et al., 2018; Ronson et al., 2018; Sugimura et al., 2008), and it was shown that PARP1 can prevent premature restart of reversed forks by inhibiting the activity of the helicase RECQ1 (Berti et al., 2013). Therefore, MDM2 might sequester PARP1 from RECQ1, allowing the helicase to restart fork progression and increasing overall fork speed. Indeed, we could show that depletion of RECQ1 rescues replication fork speed, bringing it back to control levels (Manuscript 2, Figure 4). MDM2 is therefore a newly discovered PARP1 regulator, and acts in

the opposite manner as the previously described CARM1 (Genois et al., 2021). Both these proteins have been shown to affect PARylation levels, with MDM2 inhibiting PARP1 activity while CARM1 induces its activity. As a result, MDM2 increases fork speed while CARM1 slows it down, forming a replication regulatory module through interaction with PARP1 (Genois et al., 2021). Since replication speed must be tightly regulated to prevent genome instability, it is tempting to speculate that many more PARP1 regulators might be present in the cell.

A recent publication described the p53 protein as an inducer of fork reversal in stem cells, independently of its transcription activity and therefore MDM2 expression (Ihle et al., 2021). More precisely, p53 forms a complex with Polι at replication sites, followed by recruitment of the translocase zinc finger ran-binding domain containing 3 (ZRANB3). ZRANB3 is involved in induction of fork reversal upon DNA damage and other replication obstacles (Vujanovic et al., 2017), therefore effectively linking the p53 protein to induction of 4-way junctions. Interestingly, Polι preferentially associates with p21 instead of p53 in differentiated cells, therefore limiting fork reversal (Ihle et al., 2021). These events were also reflected in DNA replication speed, which was slower in stem cells compared to differentiated cells. If p53 can induce fork reversal, its negative regulator MDM2 is also part of this regulatory network by inducing fork restart. Investigation of MDM2 activity, upon induction of stress, in both stem and differentiated cells would be interesting in this context.

4.6 MDM2 and DNA damage

In our study, prolonged induction of MDM2 with Nutlin led to accumulation of γH2AX, a marker of DNA damage (Giglia-Mari et al., 2011), and depletion of MDM2 led to a decrease in this marker even below control levels (Manuscript 2, Figure 5H). DNA damage could be a consequence of 1) high speed progression of the replication fork or 2) PARP1 depletion. In the first case, accelerated fork speed would ignore pre-existing DNA lesions, leading to genome instability. In the second case, DNA insults that stop fork progression to be repaired remain unrecognized since no PARylation is present at the replication machinery. A combination of both events is the most probable scenario.

We observe a strong phosphorylation of H2AX already at 12h Nutlin treatment (Manuscript 2, Figure 5H), which could not be explained by apoptosis induction, therefore suggesting that the DNA damage repair is induced. However, the MDM2 role in DNA damage repair is currently debated. Studies from the Eischen lab have shown that MDM2 can delay DNA repair mechanisms by interacting with and inhibiting NBS1, which is part of the MRN complex (Bouska et al., 2008). However, MDM2 induction and overexpression was shown to induce genome instability in the long term (Wang et al., 2008). Another study has shown that MDM2

overexpression confers resistance to known inhibitors of topoisomerase II by suppressing the levels of DNA double-strand breaks induced by such inhibitors (Senturk et al., 2017). In our study, we only looked at phosphorylation of H2AX, which is a marker for DNA damage repair activation (Manuscript 2, Figure5 H-I); In the future it will be important to distinguish between induction of DNA damage (e.g., DNA double-strand breaks) and activation of DNA damage response (e.g., ATM/ATR activation). For example, performing a comet assay which allows for direct quantification of DNA breaks, might be informative to better understand the role of MDM2 in this context. Interestingly, depletion of the DNA primase PRIMPOL reduced γH2AX levels in response to Nutlin (Manuscript 2, Figure 5I). This enzyme is an error-prone polymerase which is employed to re-prime and restart DNA replication downstream of lesions, particularly in the context of reversed forks (Guilliam et al., 2015; Quinet et al., 2020). We observed a reduction of fork reversal upon MDM2 induction (Figure 6A-B), which could be mediated in part by PRIMPOL activity, and the error-prone activity of this polymerase could explain the activation of the DNA damage response in this context.

4.7 Conclusions and further perspectives

The work described in this thesis has uncovered two novel, non-canonical functions of the MDM2 protein. Over the past few years, MDM2 has been extensively investigated to discover several new interactions and activities, also p53-independent, revealing an increasingly complex network. Although canonically referred to as an oncogene, several tumour suppression functions of MDM2 have been described. For example, MDM2 overexpression was shown to suppress cell proliferation (Brown et al., 1998; Dang et al., 2002), to limit mutant p53 accumulation (Terzian et al., 2008) and to suppress MYC-dependent tumorigenesis by interacting with ribosomal proteins (Macias et al., 2010).

The results presented here further expand on this; on one hand, we show that MDM2 inhibits RNA Pol III activity and might possibly induce cell death, both events suppressing cell growth and proliferation and thus being tumour suppressors; on the other hand, we observe increase of DNA replication speed and DNA damage accumulation, which could lead to genome instability and higher mutational rate, giving tumour cells a growth advantage. These disparate functions might as well be explained by MDM2 interacting with different proteins, both tumour suppressors and inducers. Further studies focusing on the MDM2 interactome will shed light on physiologically relevant functions of this protein, and how these differ in the context of tumorigenesis.

5. APPENDIX

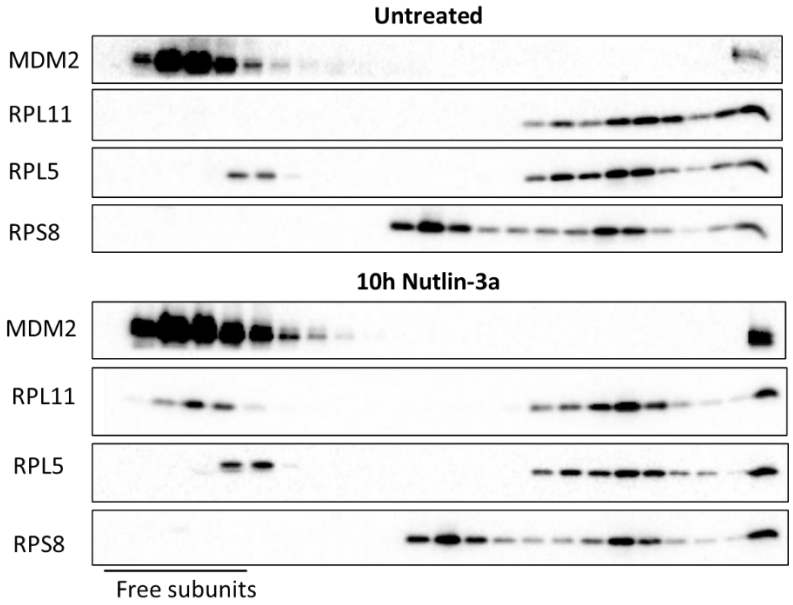

Appendix Figure 1: ribosomal subunits separation using sucrose gradients.

SJSA-1 cells were treated with 20μM of Nutlin or DMSO for 10h prior harvesting and preparation of different fractions. Free subunits can be observed in the left side, while mature ribosomes are found on the right side. RPS8 was included as control for the small ribosomal subunit. MDM2 was not found present at mature ribosomes, as observed for ribosomal proteins L5, L11 and S8. RPL5 was found as a free subunit in both untreated and treated cells, while RPL11 accumulated as a free subunit only after Nutlin treatment.

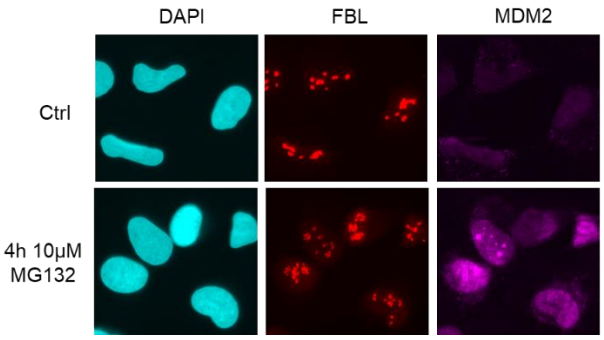

Appendix Figure 2: MDM2 accumulates in the nucleoli after proteasome inhibition

SJSA-1 cells were treated with 10μM of MG132 inhibitor for 4h. FBL was used as a nucleolar marker, and MDM2 was found in the nucleoli following inhibition of the proteasome.

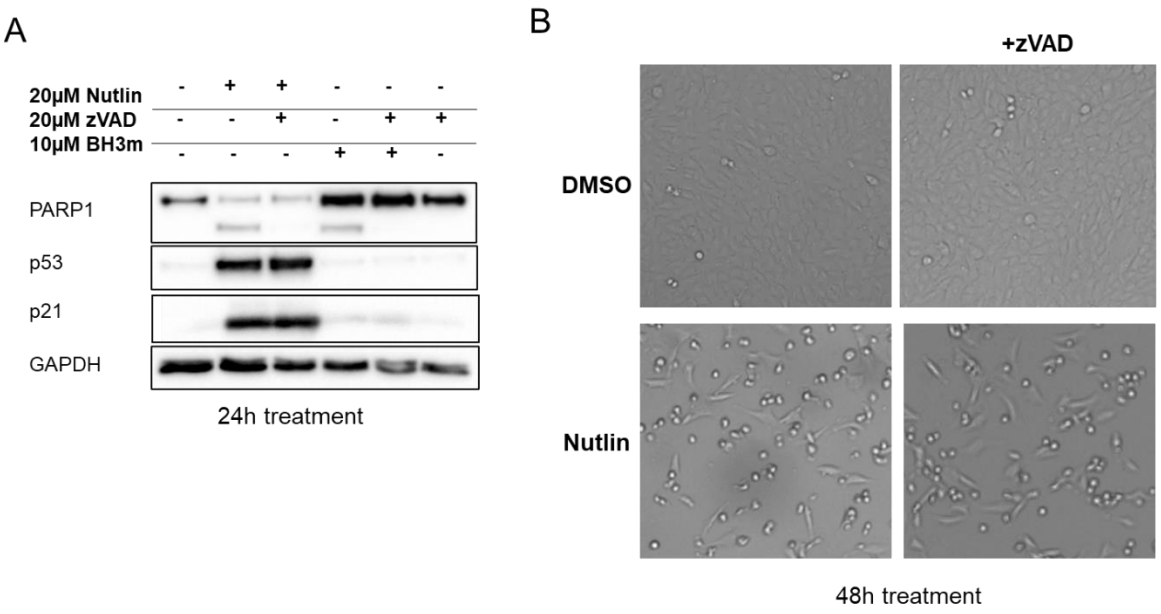

Appendix Figure 3: SJSA-1 cells die after 48h of Nutlin treatment, also when caspases are inhibited

A) Western blot analysis showing that PARP1 is cleaved upon caspase activation by Nutlin and BH3, while cleavage is prevented upon caspase inhibition via zVAD. B) Brightfield images showing cytotoxicity in response to Nutlin which was not rescued upon zVAD treatment.

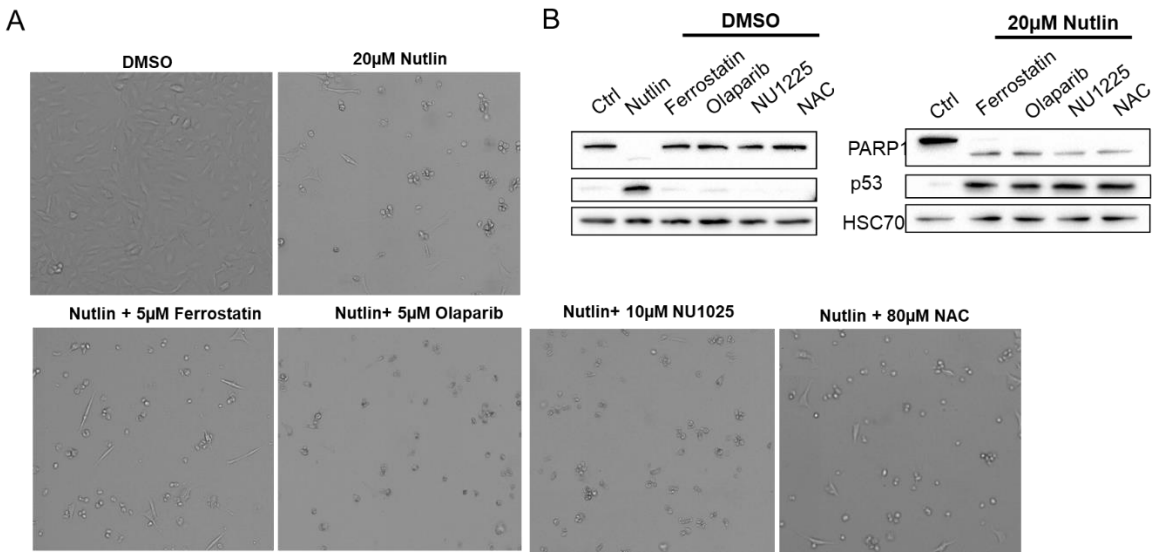

Appendix Figure 4: inhibitors of various types of cell death did not rescue toxicity induced by Nutlin

A) Brightfield images of SJSA-1 cells that were treated with several inhibitors of cell death together with Nutlin, for 48h. Ferrostatin inhibits ferroptosis, Olaparib and NU1225 are PARP1 inhibitors which prevent parthanatos, while N-acetyl cysteine (NAC) inhibits reactive oxygen species (ROS) accumulation. B) Immunoblot analysis shows PARP1 cleavage

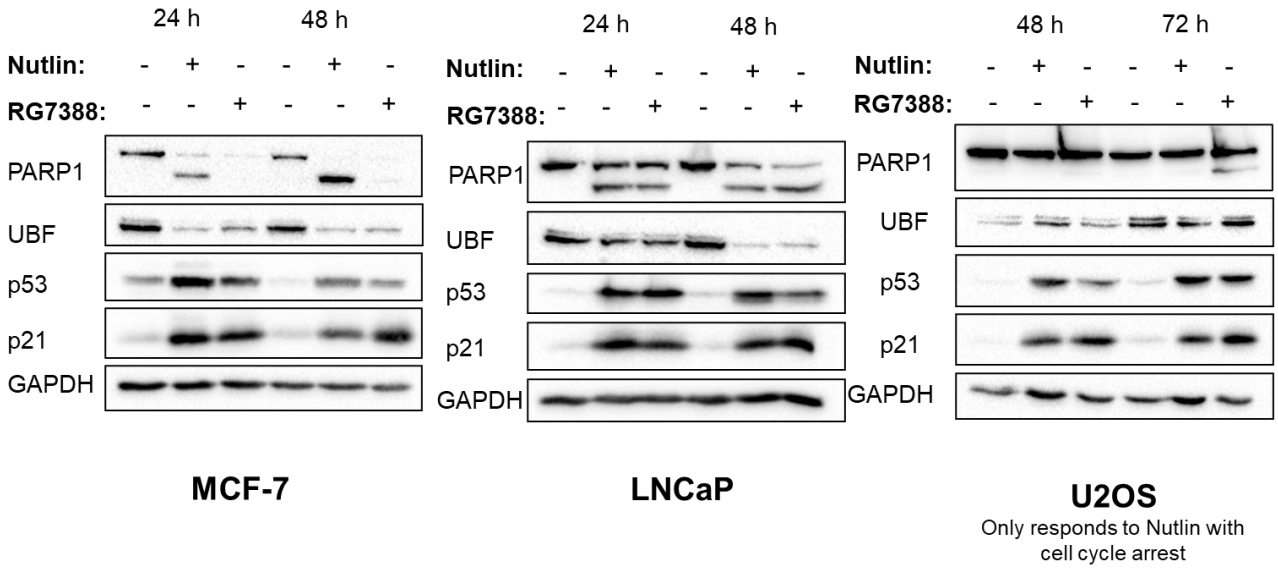

Appendix Figure 5: cell lines responding to Nutlin with cell death also display UBF downregulation

MCF-7 and LNCaP are two cancer cell lines without MDM2 amplification that respond to Nutlin with cell death, while U2OS cells respond poorly to Nutlin and only arrest their proliferation. The first two display UBF downregulation, which was not observed in U2OS.

6. REFERENCES

Ahmad, Y., Boisvert, F.M., Gregor, P., Cobley, A., and Lamond, A.I. (2009). NOPdb: Nucleolar Proteome Database—2008 update. Nucleic Acids Res. *37*, D181–D184.

Alemasova, E.E., and Lavrik, O.I. (2019). Poly(ADP-ribosyl)ation by PARP1: reaction mechanism and regulatory proteins. Nucleic Acids Res. *47*, 3811–3827.

Alt, J.R. (2003). Mdm2 haplo-insufficiency profoundly inhibits Myc-induced lymphomagenesis. EMBO J. *22*, 1442–1450.

Alt, J.R., Bouska, A., Fernandez, M.R., Cerny, R.L., Xiao, H., and Eischen, C.M. (2005). Mdm2 Binds to Nbs1 at Sites of DNA Damage and Regulates Double Strand Break Repair. J. Biol. Chem. *280*, 18771–18781.

Andrysik, Z., Galbraith, M.D., Guarnieri, A.L., Zaccara, S., Sullivan, K.D., Pandey, A., MacBeth, M., Inga, A., and Espinosa, J.M. (2017). Identification of a core TP53 transcriptional program with highly distributed tumor suppressive activity. Genome Res. *27*, 1645–1657.

Artero-Castro, A., Castellvi, J., García, A., Hernández, J., Cajal, S.R.Y., and LLeonart, M.E. (2011). Expression of the ribosomal proteins Rplp0, Rplp1, and Rplp2 in gynecologic tumors. Hum. Pathol. *42*, 194–203.

Arva, N.C., Gopen, T.R., Talbott, K.E., Campbell, L.E., Chicas, A., White, D.E., Bond, G.L., Levine, A.J., and Bargonetti, J. (2005). A chromatin-associated and transcriptionally inactive p53-Mdm2 complex occurs in mdm2 SNP309 homozygous cells. J. Biol. Chem. *280*, 26776–26787.

Aubert, M., O'Donohue, M.-F., Lebaron, S., and Gleizes, P.-E. (2018). Pre-Ribosomal RNA Processing in Human Cells: From Mechanisms to Congenital Diseases. Biomolecules *8*, 123.

Bai, G., Kermi, C., Stoy, H., Schiltz, C.J., Bacal, J., Zaino, A.M., Hadden, M.K., Eichman, B.F., Lopes, M., and Cimprich, K.A. (2020). HLTF Promotes Fork Reversal, Limiting Replication Stress Resistance and Preventing Multiple Mechanisms of Unrestrained DNA Synthesis. Mol. Cell *78*, 1237-1251.e7.

Baugh, E.H., Ke, H., Levine, A.J., Bonneau, R.A., and Chan, C.S. (2018). Why are there hotspot mutations in the TP53 gene in human cancers? Cell Death Differ. *25*, 154–160.

Bennett, M.R. (1999). Mechanisms of p53-induced apoptosis. Biochem. Pharmacol. *58*, 1089–1095.

Berti, M., Ray Chaudhuri, A., Thangavel, S., Gomathinayagam, S., Kenig, S., Vujanovic, M., Odreman, F., Glatter, T., Graziano, S., Mendoza-Maldonado, R., et al. (2013). Human RECQ1 promotes restart of replication forks reversed by DNA topoisomerase I inhibition. Nat. Struct. Mol. Biol. *20*, 347–354.

Bétous, R., Mason, A.C., Rambo, R.P., Bansbach, C.E., Badu-Nkansah, A., Sirbu, B.M., Eichman, B.F., and Cortez, D. (2012). SMARCAL1 catalyzes fork regression and Holliday junction migration to maintain genome stability during DNA replication. Genes Dev. *26*, 151–162.

Biderman, L., Manley, J.L., and Prives, C. (2012). Mdm2 and MdmX as Regulators of Gene Expression. Genes Cancer *3*, 264–273.

Bohlman, S., and Manfredi, J.J. (2014). p53-independent effects of Mdm2. Subcell. Biochem. *85*, 235–246.

Bohnsack, K.E., and Bohnsack, M.T. (2019). Uncovering the assembly pathway of human ribosomes and its emerging links to disease. EMBO J. *38*.

Bouska, A., Lushnikova, T., Plaza, S., and Eischen, C.M. (2008). Mdm2 promotes genetic instability and transformation independent of p53. Mol. Cell. Biol. *28*, 4862–4874.

Brooks, C.L., and Gu, W. (2011). p53 regulation by ubiquitin. FEBS Lett. *585*, 2803–2809.

Brown, C.Y., Mize, G.J., Pineda, M., George, D.L., and Morris, D.R. (1999). Role of two upstream open reading frames in the translational control of oncogene mdm2.

Brown, D.R., Thomas, C.A., and Deb, S.P. (1998). The human oncoprotein MDM2 arrests the cell cycle: elimination of its cell-cycle-inhibitory function induces tumorigenesis. EMBO J. *17*, 2513.

Bursać, S., Brdovčak, M.C., Pfannkuchen, M., Orsolić, I., Golomb, L., Zhu, Y., Katz, C., Daftuar, L., Grabusić, K., Vukelić, I., et al. (2012). Mutual protection of ribosomal proteins L5 and L11 from degradation is essential for p53 activation upon ribosomal biogenesis stress. Proc. Natl. Acad. Sci. U. S. A. *109*, 20467–20472.

Callus, B.A., Moujallad, D.M., Silke, J., Gerl, R., Jabbour, A.M., Ekert, P.G., and Vaux, D.L. (2008). Triggering of Apoptosis by Puma Is Determined by the Threshold Set by Prosurvival Bcl-2 Family Proteins. J. Mol. Biol. *384*, 313–323.

Candau, R., Scolnick, D.M., Darpino, P., Ying, C.Y., Halazonetis, T.D., and Berger, S.L. (1997). Two tandem and independent sub-activation domains in the amino terminus of p53 require the adaptor complex for activity. Oncogene *15*, 807–816.

Cao, B., Fang, Z., Liao, P., Zhou, X., Xiong, J., Zeng, S., Lu, H., Cao, B., Fang, Z., Liao, P., et al. (2017). Cancer-mutated ribosome protein L22 (RPL22/eL22) suppresses cancer cell survival by blocking p53-MDM2 circuit. Oncotarget *8*, 90651–90661.

Carrillo, A.M., Hicks, M., Khabele, D., and Eischen, C.M. (2015). Pharmacologically Increasing Mdm2 Inhibits DNA Repair and Cooperates with Genotoxic Agents to Kill p53-Inactivated Ovarian Cancer Cells. Mol. Cancer Res. *13*, 1197–1205.

Chakraborty, A., Uechi, T., and Kenmochi, N. (2011). Guarding the 'translation apparatus': defective ribosome biogenesis and the p53 signaling pathway. Wiley Interdiscip. Rev. RNA *2*, 507–522.

Chambon, P., Weill, J.D., and Mandel, P. (1963). Nicotinamide mononucleotide activation of a new DNA-dependent polyadenylic acid synthesizing nuclear enzyme. Biochem. Biophys. Res. Commun. *11*, 39–43.

Chen, L., Li, Z., Zwolinska, A.K., Smith, M.A., Cross, B., Koomen, J., Yuan, Z.-M., Jenuwein, T., Marine, J.-C., Wright, K.L., et al. (2010). MDM2 recruitment of lysine methyltransferases regulates p53 transcriptional output. EMBO J. *29*, 2538–2552.

Chène, P. (2001). The role of tetramerization in p53 function. Oncogene *20*, 2611–2617.

Cordenonsi, M., Dupont, S., Maretto, S., Insinga, A., Imbriano, C., and Piccolo, S. (2003). Links between tumor suppressors: p53 is required for TGF-beta gene responses by cooperating with Smads. Cell *113*, 301–314.

Dai, M.S., and Lu, H. (2004). Inhibition of MDM2-mediated p53 Ubiquitination and Degradation by Ribosomal Protein L5 *. J. Biol. Chem. *279*, 44475–44482.

Debnath, S., and Sharma, S. (2020). RECQ1 Helicase in Genomic Stability and Cancer. Genes (Basel). *11*, 622.

Desroches, A., and Denault, J.-B. (2019). Caspase-7 uses RNA to enhance proteolysis of poly(ADP-ribose) polymerase 1 and other RNA-binding proteins. Proc. Natl. Acad. Sci. *116*, 21521–21528.

Dobbelstein, M., and Levine, A.J. (2020). Mdm2: Open questions. Cancer Sci. *111*, 2203–2211.

Donati, G., Peddigari, S., Mercer, C.A., and Thomas, G. (2013). 5S ribosomal RNA is an essential component of a nascent ribosomal precursor complex that regulates the Hdm2-p53 checkpoint. Cell Rep. *4*, 87–98.

Drygin, D., Rice, W.G., and Grummt, I. (2010). The RNA polymerase I transcription machinery: an emerging target for the treatment of cancer. Annu. Rev. Pharmacol. Toxicol. *50*, 131–156.

Edwards, S.J., Hananeia, L., Eccles, M.R., Zhang, Y.F., and Braithwaite, A.W. (2003). The proline-rich region of mouse p53 influences transactivation and apoptosis but is largely dispensable for these functions. Oncogene *22*, 4517–4523.

Fåhraeus, R., and Olivares-Illana, V. (2014). MDM2's social network. Oncogene *33*, 4365–4376.

Feric, M., Vaidya, N., Harmon, T.S., Mitrea, D.M., Zhu, L., Richardson, T.M., Kriwacki, R.W., Pappu, R. V., and Brangwynne, C.P. (2016). Coexisting Liquid Phases Underlie Nucleolar Subcompartments. Cell *165*, 1686–1697.

Ferrándiz, N., Caraballo, J.M., García-Gutierrez, L., Devgan, V., Rodriguez-Paredes, M., Lafita, M.C., Bretones, G., Quintanilla, A., Muñoz-Alonso, M.J., Blanco, R., et al. (2012). p21 as a Transcriptional Co-Repressor of S-Phase and Mitotic Control Genes. PLoS One *7*, e37759.

Follonier, C., Oehler, J., Herrador, R., and Lopes, M. (2013). Friedreich's ataxia–associated GAA repeats induce replication-fork reversal and unusual molecular junctions. Nat. Struct. Mol. Biol. *20*, 486–494.

Fredriksson, S., Gullberg, M., Jarvius, J., Olsson, C., Pietras, K., Gústafsdóttir, S.M., Östman, A., and Landegren, U. (2002). Protein detection using proximity-dependent DNA ligation assays. Nat. Biotechnol. *20*, 473–477.

Fridman, J.S., Hernando, E., Hemann, M.T., De Stanchina, E., Cordon-Cardo, C., and Lowe, S.W. (2003). Tumor Promotion by Mdm2 Splice Variants Unable to Bind p53 1. CANCER Res. *63*, 5703–5706.

Gannon, H.S., Woda, B.A., and Jones, S.N. (2012). ATM Phosphorylation of Mdm2 Ser394 Regulates the Amplitude and Duration of the DNA Damage Response in Mice. Cancer Cell *21*, 668–679.

Gartel, A.L., Serfas, M.S., and Tyner, A.L. (1996). p21--negative regulator of the cell cycle. Proc. Soc. Exp. Biol. Med. *213*, 138–149.

Gatti, M., Imhof, R., Huang, Q., Baudis, M., and Altmeyer, M. (2020). The Ubiquitin Ligase TRIP12 Limits PARP1 Trapping and Constrains PARP Inhibitor Efficiency. Cell Rep. *32*, 107985.

Genois, M.-M., Gagné, J.-P., Yasuhara, T., Jackson, J., Saxena, S., Langelier, M.-F., Ahel, I., Bedford, M.T., Pascal, J.M., Vindigni, A., et al. (2021). CARM1 regulates replication fork speed and stress response by stimulating PARP1. Mol. Cell *81*, 784-800.e8.

Gibbs-Seymour, I., Fontana, P., Rack, J.G.M., and Ahel, I. (2016). HPF1/C4orf27 Is a PARP-1-Interacting Protein that Regulates PARP-1 ADP-Ribosylation Activity. Mol. Cell *62*, 432–442.

Gibson, B.A., and Kraus, W.L. (2012). New insights into the molecular and cellular functions of poly(ADP-ribose) and PARPs. Nat. Rev. Mol. Cell Biol. *13*, 411–424.

Goodfellow, S.J., and Zomerdijk, J.C.B.M. (2013). Basic mechanisms in RNA polymerase I

transcription of the ribosomal RNA genes. Subcell. Biochem. *61*, 211–236.

Gu, J., Kawai, H., Nie, L., Kitao, H., Wiederschain, D., Jochemsen, A.G., Parant, J., Lozano, G., and Yuan, Z.-M. (2002). Mutual Dependence of MDM2 and MDMX in Their Functional Inactivation of p53. J. Biol. Chem. *277*, 19251–19254.

Sen Gupta, A., and Sengupta, K. (2017). Lamin B2 Modulates Nucleolar Morphology, Dynamics, and Function. Mol. Cell. Biol. *37*.

Hampp, S., Kiessling, T., Buechle, K., Mansilla, S.F., Thomale, J., Rall, M., Ahn, J., Pospiech, H., Gottifredi, V., and Wiesmüller, L. (2016). DNA damage tolerance pathway involving DNA polymerase ι and the tumor suppressor p53 regulates DNA replication fork progression. Proc. Natl. Acad. Sci. *113*, E4311–E4319.

Hanzlikova, H., Kalasova, I., Demin, A.A., Pennicott, L.E., Cihlarova, Z., and Caldecott, K.W. (2018). The Importance of Poly(ADP-Ribose) Polymerase as a Sensor of Unligated Okazaki Fragments during DNA Replication. Mol. Cell *71*, 319-331.e3.

Happo, L., Cragg, M.S., Phipson, B., Haga, J.M., Jansen, E.S., Herold, M.J., Dewson, G., Michalak, E.M., Vandenberg, C.J., Smyth, G.K., et al. (2010). Maximal killing of lymphoma cells by DNA damage-inducing therapy requires not only the p53 targets Puma and Noxa, but also Bim. Blood *116*, 5256–5267.

He, X., Li, Y., Dai, M.S., and Sun, X.X. (2016). Ribosomal protein L4 is a novel regulator of the MDM2-p53 loop. Oncotarget *7*, 16217–16226.

Helleday, T. (2011). DNA repair as treatment target. Eur. J. Cancer *47*, S333–S335.

Henras, A.K., Plisson-Chastang, C., O'Donohue, M.F., Chakraborty, A., and Gleizes, P.E. (2015). An overview of pre-ribosomal RNA processing in eukaryotes. Wiley Interdiscip. Rev. RNA *6*, 225–242.

Herdman, C., Mars, J.C., Stefanovsky, V.Y., Tremblay, M.G., Sabourin-Felix, M., Lindsay, H., Robinson, M.D., and Moss, T. (2017). A unique enhancer boundary complex on the mouse ribosomal RNA genes persists after loss of Rrn3 or UBF and the inactivation of RNA polymerase I transcription. PLOS Genet. *13*, e1006899.

Higgins, N.P., Kato, K., and Strauss, B. (1976). A model for replication repair in mammalian cells. J. Mol. Biol. *101*, 417–425.

Holmberg Olausson, K., Nistér, M., and Lindström, M. (2012). p53 -Dependent and -Independent Nucleolar Stress Responses. Cells *1*, 774–798.

Horn, H.F., and Vousden, K.H. (2007a). Coping with stress: multiple ways to activate p53. Oncogene *26*, 1306–1316.

Horn, H.F., and Vousden, K.H. (2007b). Coping with stress: multiple ways to activate p53. Oncogene 2007 269 *26*, 1306–1316.

Ihle, M., Biber, S., Schroeder, I.S., Blattner, C., Deniz, M., Damia, G., Gottifredi, V., and Wiesmüller, L. (2021). Impact of the interplay between stemness features, p53 and pol iota on replication pathway choices. Nucleic Acids Res. *49*, 7457–7475.

Ireno, I.C., Wiehe, R.S., Stahl, A.I., Hampp, S., Aydin, S., Troester, M.A., Selivanova, G., and Wiesmüller, L. (2014). Modulation of the poly (ADP-ribose) polymerase inhibitor response and DNA recombination in breast cancer cells by drugs affecting endogenous wild-type p53. Carcinogenesis *35*, 2273–2282.

Jao, C.Y., and Salic, A. (2008). Exploring RNA transcription and turnover in vivo by using click chemistry. Proc. Natl. Acad. Sci. *105*, 15779–15784.

Jeffers, J.R., Parganas, E., Lee, Y., Yang, C., Wang, J., Brennan, J., MacLean, K.H., Han, J., Chittenden, T., Ihle, J.N., et al. (2003). Puma is an essential mediator of p53-dependent and -independent apoptotic pathways. Cancer Cell *4*, 321–328.

Jiang, L., Kon, N., Li, T., Wang, S.-J., Su, T., Hibshoosh, H., Baer, R., and Gu, W. (2015). Ferroptosis as a p53-mediated activity during tumour suppression. Nature *520*, 57–62.

Jones, S.N., Roe, A.E., Donehower, L.A., and Bradley, A. (1995). Rescue of embryonic lethality in Mdm2-deficient mice by absence of p53. Nature *378*, 206–208.

Jones, S.N., Hancock, A.R., Vogel, H., Donehower, L.A., and Bradley, A. (1998). Overexpression of Mdm2 in mice reveals a p53-independent role for Mdm2 in tumorigenesis. Proc. Natl. Acad. Sci. *95*, 15608–15612.

Julien, O., and Wells, J.A. (2017). Caspases and their substrates. Cell Death Differ. *24*, 1380–1389.

Jungmichel, S., Rosenthal, F., Altmeyer, M., Lukas, J., Hottiger, M.O., and Nielsen, M.L. (2013). Proteome-wide Identification of Poly(ADP-Ribosyl)ation Targets in Different Genotoxic Stress Responses. Mol. Cell *52*, 272–285.

Kalvari, I., Argasinska, J., Quinones-Olvera, N., Nawrocki, E.P., Rivas, E., Eddy, S.R., Bateman, A., Finn, R.D., and Petrov, A.I. (2018). Rfam 13.0: shifting to a genome-centric resource for non-coding RNA families. Nucleic Acids Res. *46*, D335–D342.

Kamaletdinova, T., Fanaei-Kahrani, Z., and Wang, Z.-Q. (2019). The Enigmatic Function of PARP1: From PARylation Activity to PAR Readers. Cells *8*, 1625.

Kanai, M., Hanashiro, K., Kim, S.H., Hanai, S., Boulares, A.H., Miwa, M., and Fukasawa, K. (2007). Inhibition of Crm1–p53 interaction and nuclear export of p53 by poly(ADP-ribosyl)ation. Nat. Cell Biol. 2007 910 *9*, 1175–1183.

Kang, H.C., Lee, Y.-I., Shin, J.-H., Andrabi, S.A., Chi, Z., Gagne, J.-P., Lee, Y., Ko, H.S., Lee, B.D., Poirier, G.G., et al. (2011). Iduna is a poly(ADP-ribose) (PAR)-dependent E3 ubiquitin ligase that regulates DNA damage. Proc. Natl. Acad. Sci. *108*, 14103–14108.

Kannan, K., Kaminski, N., Rechavi, G., Jakob-Hirsch, J., Amariglio, N., and Givol, D. (2001). DNA microarray analysis of genes involved in p53 mediated apoptosis: activation of Apaf-1. Oncogene *20*, 3449–3455.

Kashima, L., Idogawa, M., Mita, H., Shitashige, M., Yamada, T., Ogi, K., Suzuki, H., Toyota, M., Ariga, H., Sasaki, Y., et al. (2012). CHFR Protein Regulates Mitotic Checkpoint by Targeting PARP-1 Protein for Ubiquitination and Degradation. J. Biol. Chem. *287*, 12975–12984.

Kastenhuber, E.R., and Lowe, S.W. (2017). Putting p53 in Context. Cell *170*, 1062–1078.

Khare, V., and Eckert, K.A. (2002). The proofreading 3′→5′ exonuclease activity of DNA polymerases: a kinetic barrier to translesion DNA synthesis. Mutat. Res. Mol. Mech. Mutagen. *510*, 45–54.

Khoo, K.H., Verma, C.S., and Lane, D.P. (2014). Drugging the p53 pathway: understanding the route to clinical efficacy. Nat. Rev. Drug Discov. 2014 133 *13*, 217–236.

Klusmann, I., Rodewald, S., Müller, L., Friedrich, M., Wienken, M., Li, Y., Schulz-Heddergott, R., and Dobbelstein, M. (2016). p53 Activity Results in DNA Replication Fork Processivity. Cell Rep. *17*, 1845–1857.

Klusmann, I., Wohlberedt, K., Magerhans, A., Teloni, F., Korbel, J.O., Altmeyer, M., and Dobbelstein, M. (2018). Chromatin modifiers Mdm2 and RNF2 prevent RNA:DNA hybrids that impair DNA replication. Proc. Natl. Acad. Sci. U. S. A. *115*, E11311–E11320.

Kobayashi, M., Ishizaki, Y., Owaki, M., Matsumoto, Y., Kakiyama, Y., Hoshino, S., Tagawa, R., Sudo, Y., Okita, N., Akimoto, K., et al. (2020). Nutlin-3a suppresses poly (ADP-ribose) polymerase 1 by mechanisms different from conventional PARP1 suppressors in a human breast cancer cell line. Oncotarget *11*, 1653–1665.

Kopper, F., Bierwirth, C., Schon, M., Kunze, M., Elvers, I., Kranz, D., Saini, P., Menon, M.B., Walter, D., Sorensen, C.S., et al. (2013). Damage-induced DNA replication stalling relies on MAPK-activated protein kinase 2 activity. Proc. Natl. Acad. Sci. *110*, 16856–16861.

Kun, E., Kirsten, E., Mendeleyev, J., and Ordahl, C.P. (2004). Regulation of the Enzymatic Catalysis of Poly(ADP-ribose) Polymerase by dsDNA, Polyamines, Mg 2+ , Ca 2+ , Histones H 1 and H 3 , and ATP. Biochemistry *43*, 210–216.

Langelier, M.-F., Planck, J.L., Roy, S., and Pascal, J.M. (2011). Crystal Structures of Poly(ADP-ribose) Polymerase-1 (PARP-1) Zinc Fingers Bound to DNA. J. Biol. Chem. *286*, 10690–10701.

Langelier, M.-F., Riccio, A.A., and Pascal, J.M. (2014). PARP-2 and PARP-3 are selectively activated by 5′ phosphorylated DNA breaks through an allosteric regulatory mechanism shared with PARP-1. Nucleic Acids Res. *42*, 7762–7775.

Levine, A.J. (2020). p53: 800 million years of evolution and 40 years of discovery. Nat. Rev. Cancer *20*, 471–480.

Li, M., He, Y., Dubois, W., Wu, X., Shi, J., and Huang, J. (2012). Distinct Regulatory Mechanisms and Functions for p53-Activated and p53-Repressed DNA Damage Response Genes in Embryonic Stem Cells. Mol. Cell *46*, 30–42.

Li, Y., Yang, J., Aguilar, A., McEachern, D., Przybranowski, S., Liu, L., Yang, C.-Y., Wang, M., Han, X., and Wang, S. (2019). Discovery of MD-224 as a First-in-Class, Highly Potent, and Efficacious Proteolysis Targeting Chimera Murine Double Minute 2 Degrader Capable of Achieving Complete and Durable Tumor Regression. J. Med. Chem. *62*, 448–466.

Lill, N.L., Grossman, S.R., Ginsberg, D., DeCaprio, J., and Livingston, D.M. (1997). Binding and modulation of p53 by p300/CBP coactivators. Nature *387*, 823–827.

Linke, K., Mace, P.D., Smith, C.A., Vaux, D.L., Silke, J., and Day, C.L. (2008). Structure of the MDM2/MDMX RING domain heterodimer reveals dimerization is required for their ubiquitylation in trans. Cell Death Differ. *15*, 841–848.

Liu, Y., Deisenroth, C., and Zhang, Y. (2016). RP–MDM2–p53 Pathway: Linking Ribosomal Biogenesis and Tumor Surveillance. Trends in Cancer *2*, 191–204.

Liu, Y., Tavana, O., and Gu, W. (2019). p53 modifications: exquisite decorations of the powerful guardian. J. Mol. Cell Biol. *11*, 564–577.

Lovato, A., Panasci, L., and Witcher, M. (2012). Is There an Epigenetic Component Underlying the Resistance of Triple-Negative Breast Cancers to Parp Inhibitors? Front. Pharmacol. *0*, 202.

Lushnikova, T., Bouska, A., Odvody, J., Dupont, W.D., and Eischen, C.M. (2011). Aging mice have increased chromosome instability that is exacerbated by elevated Mdm2 expression. Oncogene *30*, 4622–4631.

Macias, E., Jin, A., Deisenroth, C., Bhat, K., Mao, H., Lindström, M.S., and Zhang, Y. (2010). An ARF-Independent c-MYC-Activated Tumor Suppression Pathway Mediated by Ribosomal Protein-Mdm2 Interaction. Cancer Cell *18*, 231–243.

Madru, C., Lebaron, S., Blaud, M., Delbos, L., Pipoli, J., Pasmant, E., Réty, S., and Leulliot, N. (2015). Chaperoning 5S RNA assembly. Genes Dev. *29*, 1432–1446.

Mangan, H., Gailín, M.Ó., and McStay, B. (2017). Integrating the genomic architecture of human nucleolar organizer regions with the biophysical properties of nucleoli. FEBS J. *284*, 3977–3985.

Martin, C., Chen, S., Maya-Mendoza, A., Lovric, J., Sims, P.F.G., and Jackson, D.A. (2009). Lamin B1 maintains the functional plasticity of nucleoli. J. Cell Sci. *122*, 1551–1562.

Maya-Mendoza, A., Moudry, P., Merchut-Maya, J.M., Lee, M., Strauss, R., and Bartek, J. (2018). High speed of fork progression induces DNA replication stress and genomic instability. Nature *559*, 279–284.

Meek, D.W., and Hupp, T.R. (2010). The regulation of MDM2 by multisite phosphorylation—Opportunities for molecular-based intervention to target tumours? Semin. Cancer Biol. *20*, 19–28.

Melnik, S., Deng, B., Papantonis, A., Baboo, S., Carr, I.M., and Cook, P.R. (2011). The proteomes of transcription factories containing RNA polymerases I, II or III. Nat. Methods *8*, 963–968.

Merchut-Maya, J.M., Bartek, J., and Maya-Mendoza, A. (2019). Regulation of replication fork speed: Mechanisms and impact on genomic stability. DNA Repair (Amst). *81*, 102654.

Michalak, E.M., Villunger, A., Adams, J.M., and Strasser, A. (2008). In several cell types tumour suppressor p53 induces apoptosis largely via Puma but Noxa can contribute. Cell Death Differ. *15*, 1019–1029.

Minsky, N., and Oren, M. (2004). The RING domain of Mdm2 mediates histone ubiquitylation and transcriptional repression. Mol. Cell *16*, 631–639.

Mirjolet, J.-F., Barberi-Heyob, M., Didelot, C., Peyrat, J.-P., Abecassis, J., Millon, R., and Merlin, J.-L. (2000). Bcl-2/Bax protein ratio predicts 5-fluorouracil sensitivity independently of p53 status. Br. J. Cancer *83*, 1380–1386.

Morello, L.G., Hesling, C., Coltri, P.P., Castilho, B.A., Rimokh, R., and Zanchin, N.I.T. (2011). The NIP7 protein is required for accurate pre-rRNA processing in human cells. Nucleic Acids Res. *39*, 648–665.

Mourón, S., Rodriguez-Acebes, S., Martínez-Jiménez, M.I., García-Gómez, S., Chocrón, S., Blanco, L., and Méndez, J. (2013). Repriming of DNA synthesis at stalled replication forks by human PrimPol. Nat. Struct. Mol. Biol. *20*, 1383–1389.

Nagai, W., Okita, N., Matsumoto, H., Okado, H., Oku, M., and Higami, Y. (2012). Reversible induction of PARP1 degradation by p53-inducible cis-imidazoline compounds. Biochem. Biophys. Res. Commun. *421*, 15–19.

Neelsen, K.J., and Lopes, M. (2015). Replication fork reversal in eukaryotes: from dead end to dynamic response. Nat. Rev. Mol. Cell Biol. *16*, 207–220.

Nevins, J.R., Leone, G., DeGregori, J., and Jakoi, L. (1997). Role of the Rb/E2F pathway in cell growth control. J. Cell. Physiol. *173*, 233–236.

Nicholson, J., and Hupp, T.R. (2010). The molecular dynamics of MDM2. Https://Doi.Org/10.4161/Cc.9.10.11597 *9*, 1878–1881.

Nicolas, E., Parisot, P., Pinto-Monteiro, C., de Walque, R., De Vleeschouwer, C., and Lafontaine, D.L.J. (2016). Involvement of human ribosomal proteins in nucleolar structure and p53-dependent nucleolar stress. Nat. Commun. *7*, 11390.

Nishimura, K., Kumazawa, T., Kuroda, T., Katagiri, N., Tsuchiya, M., Goto, N., Furumai, R., Murayama, A., Yanagisawa, J., and Kimura, K. (2015). Perturbation of Ribosome Biogenesis Drives Cells into Senescence through 5S RNP-Mediated p53 Activation. Cell Rep. *10*, 1310–

1323.

de Oca Luna, R.M., Wagner, D.S., and Lozano, G. (1995). Rescue of early embryonic lethality in mdm2-deficient mice by deletion of p53. Nature *378*, 203–206.

Oliner, J.D., Pietenpol, J.A., Thiagalingam, S., Gyuris, J., Kinzler, K.W., and Vogelstein, B. (1993). Oncoprotein MDM2 conceals the activation domain of tumour suppressor p53. Nature *362*, 857–860.

Oliner, J.D., Saiki, A.Y., and Caenepeel, S. (2016). The Role of MDM2 Amplification and Overexpression in Tumorigenesis. Cold Spring Harb. Perspect. Med. *6*, a026336.

Onofrillo, C., Galbiati, A., Montanaro, L., and Derenzini, M. (2017). The pre-existing population of 5S rRNA effects p53 stabilization during ribosome biogenesis inhibition. Oncotarget *8*, 4257–4267.

Palazzo, L., Leidecker, O., Prokhorova, E., Dauben, H., Matic, I., and Ahel, I. (2018). Serine is the major residue for ADP-ribosylation upon DNA damage. Elife *7*.

Pelava, A., Schneider, C., and Watkins, N.J. (2016). The importance of ribosome production, and the 5S RNP-MDM2 pathway, in health and disease. Biochem. Soc. Trans. *44*, 1086–1090.

Pelletier, J., Thomas, G., and Volarević, S. (2018). Ribosome biogenesis in cancer: new players and therapeutic avenues. Nat. Rev. Cancer *18*, 51–63.

Peltonen, K., Colis, L., Liu, H., Trivedi, R., Moubarek, M.S., Moore, H.M., Bai, B., Rudek, M.A., Bieberich, C.J., and Laiho, M. (2014). A Targeting Modality for Destruction of RNA Polymerase I that Possesses Anticancer Activity. Cancer Cell *25*, 77–90.

Picksley, S.M., and Lane, D.P. (1993). The p53-mdm2 autoregulatory feedback loop: a paradigm for the regulation of growth control by p53? Bioessays *15*, 689–690.

Pratt, G., Yap, C., Oldreive, C., Slade, D., Bishop, R., Griffiths, M., Dyer, M.J.S., Fegan, C., Oscier, D., Pettitt, A., et al. (2018). A multi-centre phase I trial of the PARP inhibitor olaparib in patients with relapsed chronic lymphocytic leukaemia, T-prolymphocytic leukaemia or mantle cell lymphoma. Br. J. Haematol. *182*, 429–433.

Quinet, A., Lemaçon, D., and Vindigni, A. (2017). Replication Fork Reversal: Players and Guardians. Mol. Cell *68*, 830–833.

Quinet, A., Tirman, S., Jackson, J., Šviković, S., Lemaçon, D., Carvajal-Maldonado, D., González-Acosta, D., Vessoni, A.T., Cybulla, E., Wood, M., et al. (2020). PRIMPOL-Mediated Adaptive Response Suppresses Replication Fork Reversal in BRCA-Deficient Cells. Mol. Cell *77*, 461-474.e9.

Ray Chaudhuri, A., and Nussenzweig, A. (2017). The multifaceted roles of PARP1 in DNA repair and chromatin remodelling. Nat. Rev. Mol. Cell Biol. *18*, 610–621.

Rayburn, E., Zhang, R., He, J., and Wang, H. (2005). MDM2 and human malignancies: expression, clinical pathology, prognostic markers, and implications for chemotherapy. Curr. Cancer Drug Targets *5*, 27–41.

Roth, J. (1998). Nucleo-cytoplasmic shuttling of the hdm2 oncoprotein regulates the levels of the p53 protein via a pathway used by the human immunodeficiency virus rev protein. EMBO J. *17*, 554–564.

Roy, S., Tomaszowski, K.H., Luzwick, J.W., Park, S., Li, J., Murphy, M., and Schlacher, K. (2018). p53 orchestrates DNA replication restart homeostasis by suppressing mutagenic RAD52 and POLθ pathways. Elife *7*.

Russo, A., and Russo, G. (2017). Ribosomal Proteins Control or Bypass p53 during Nucleolar

Stress. Int. J. Mol. Sci. *18*, 140.

Saldivar, J.C., Cortez, D., and Cimprich, K.A. (2017). The essential kinase ATR: ensuring faithful duplication of a challenging genome. Nat. Rev. Mol. Cell Biol. *18*, 622–636.

Sane, S., and Rezvani, K. (2017). Essential Roles of E3 Ubiquitin Ligases in p53 Regulation. Int. J. Mol. Sci. *18*, 442.

Senturk, J.C., Bohlman, S., and Manfredi, J.J. (2017). Mdm2 selectively suppresses DNA damage arising from inhibition of topoisomerase II independent of p53. Oncogene *36*, 6085–6096.

Shen, H., and G. Maki, C. (2011). Pharmacologic Activation of p53 by Small-Molecule MDM2 Antagonists. Curr. Pharm. Des. *17*, 560–568.

Shieh, S.Y., Ikeda, M., Taya, Y., and Prives, C. (1997). DNA damage-induced phosphorylation of p53 alleviates inhibition by MDM2. Cell *91*, 325–334.

Siliciano, J.D., Canman, C.E., Taya, Y., Sakaguchi, K., Appella, E., and Kastan, M.B. (1997). DNA damage induces phosphorylation of the amino terminus of p53. Genes Dev. *11*, 3471–3481.

Simbulan-Rosenthal, C.M., Rosenthal, D.S., Luo, R., and Smulson, M.E. (1999). Poly(ADP-ribosyl)ation of p53 during Apoptosis in Human Osteosarcoma Cells. Cancer Res. *59*.

Sloan, K.E., Bohnsack, M.T., and Watkins, N.J. (2013). The 5S RNP Couples p53 Homeostasis to Ribosome Biogenesis and Nucleolar Stress. Cell Rep. *5*, 237–247.

Smeenk, L., van Heeringen, S.J., Koeppel, M., van Driel, M.A., Bartels, S.J.J., Akkers, R.C., Denissov, S., Stunnenberg, H.G., and Lohrum, M. (2008). Characterization of genome-wide p53-binding sites upon stress response. Nucleic Acids Res. *36*, 3639–3654.

Soldani, C., Lazzè, M.C., Bottone, M.G., Tognon, G., Biggiogera, M., Pellicciari, C.E., and Scovassi, A.I. (2001). Poly(ADP-ribose) Polymerase Cleavage during Apoptosis: When and Where? Exp. Cell Res. *269*, 193–201.

Soussi, T. (2005). The p53 pathway and human cancer. Br. J. Surg. *92*, 1331–1332.

Sriraman, A., Dickmanns, A., Najafova, Z., Johnsen, S.A., and Dobbelstein, M. (2018). CDK4 inhibition diminishes p53 activation by MDM2 antagonists. Cell Death Dis. *9*, 918.

Steitz, J.A., Berg, C., Hendrick, J.P., La Branche-Chabot, H., Metspalu, A., Rinke, J., and Yario, T. (1988). A 5S rRNA/L5 complex is a precursor to ribosome assembly in mammalian cells. J. Cell Biol. *106*, 545–556.

Stępiński, D. (2018). The nucleolus, an ally, and an enemy of cancer cells. Histochem. Cell Biol. *150*, 607–629.

Sullivan, K.D., Galbraith, M.D., Andrysik, Z., and Espinosa, J.M. (2018). Mechanisms of transcriptional regulation by p53. Cell Death Differ. *25*, 133–143.

Szymanski, M. (2002). 5S Ribosomal RNA Database. Nucleic Acids Res. *30*, 176–178.

Terzian, T., Suh, Y.-A., Iwakuma, T., Post, S.M., Neumann, M., Lang, G.A., Van Pelt, C.S., and Lozano, G. (2008). The inherent instability of mutant p53 is alleviated by Mdm2 or p16INK4a loss. Genes Dev. *22*, 1337–1344.

Thut, C.J., Goodrich, J.A., and Tjian, R. (1997). Repression of p53-mediated transcription by MDM2: a dual mechanism. Genes Dev. *11*, 1974–1986.

Tibbetts, R.S., Brumbaugh, K.M., Williams, J.M., Sarkaria, J.N., Cliby, W.A., Shieh, S.-Y., Taya, Y., Prives, C., and Abraham, R.T. (1999). A role for ATR in the DNA damage-induced

phosphorylation of p53. Genes Dev. *13*, 152–157.

Uldrijan, S., Pannekoek, W.J., and Vousden, K.H. (2007). An essential function of the extreme C-terminus of MDM2 can be provided by MDMX. EMBO J. *26*, 102–112.

Vaseva, A. V., Marchenko, N.D., Ji, K., Tsirka, S.E., Holzmann, S., and Moll, U.M. (2012). p53 Opens the Mitochondrial Permeability Transition Pore to Trigger Necrosis. Cell *149*, 1536–1548.

Vassilev, L.T., Vu, B.T., Graves, B., Carvajal, D., Podlaski, F., Filipovic, Z., Kong, N., Kammlott, U., Lukacs, C., Klein, C., et al. (2004). In Vivo Activation of the p53 Pathway by Small-Molecule Antagonists of MDM2. Science (80-.). *303*, 844–848.

Vierna, J., Wehner, S., Höner zu Siederdissen, C., Martínez-Lage, A., and Marz, M. (2013). Systematic analysis and evolution of 5S ribosomal DNA in metazoans. Heredity (Edinb). *111*, 410–421.

Villunger, A., Michalak, E.M., Coultas, L., Müllauer, F., Böck, G., Ausserlechner, M.J., Adams, J.M., and Strasser, A. (2003). p53- and Drug-Induced Apoptotic Responses Mediated by BH3-Only Proteins Puma and Noxa. Science (80-.). *302*, 1036–1038.

Vogelstein, B., Lane, D., and Levine, A.J. (2000). Surfing the p53 network. Nature *408*, 307–310.

Wallace, H., and Birnstiel, M.L. (1966). Ribosomal cistrons and the nucleolar organizer. Biochim. Biophys. Acta - Nucleic Acids Protein Synth. *114*, 296–310.

Wallace, M., Worrall, E., Pettersson, S., Hupp, T.R., and Ball, K.L. (2006). Dual-Site Regulation of MDM2 E3-Ubiquitin Ligase Activity. Mol. Cell *23*, 251–263.

Wang, M., and Lemos, B. (2017). Ribosomal DNA copy number amplification and loss in human cancers is linked to tumor genetic context, nucleolus activity, and proliferation. PLOS Genet. *13*, e1006994.

Wang, P., Lushnikova, T., Odvody, J., Greiner, T.C., Jones, S.N., and Eischen, C.M. (2008). Elevated Mdm2 expression induces chromosomal instability and confers a survival and growth advantage to B cells. Oncogene *27*, 1590–1598.

Weber, J.D., Taylor, L.J., Roussel, M.F., Sherr, C.J., and Bar-Sagi, D. (1999). Nucleolar Arf sequesters Mdm2 and activates p53. Nat. Cell Biol. *20*.

Wienken, M., Dickmanns, A., Nemajerova, A., Kramer, D., Najafova, Z., Weiss, M., Karpiuk, O., Kassem, M., Zhang, Y., Lozano, G., et al. (2016). MDM2 Associates with Polycomb Repressor Complex 2 and Enhances Stemness-Promoting Chromatin Modifications Independent of p53. Mol. Cell *61*, 68–83.

Wienken, M., Moll, U.M., and Dobbelstein, M. (2017). Mdm2 as a chromatin modifier. J. Mol. Cell Biol. *9*, 74–80.

Willis, I.M., and Moir, R.D. (2018). Signaling to and from the RNA Polymerase III Transcription and Processing Machinery. Annu. Rev. Biochem. *87*, 75–100.

Wohlberedt, K., Klusmann, I., Derevyanko, P.K., Henningsen, K., Choo, J.A.M.Y., Manzini, V., Magerhans, A., Giansanti, C., Eischen, C.M., Jochemsen, A.G., et al. (2020). Mdm4 supports DNA replication in a p53-independent fashion. Oncogene *39*, 4828–4843.

Xiong, X., Zhao, Y., He, H., and Sun, Y. (2011). Ribosomal protein S27-like and S27 interplay with p53-MDM2 axis as a target, a substrate and a regulator. Oncogene *30*, 1798–1811.

Yadavilli, S., Mayo, L.D., Higgins, M., Lain, S., Hegde, V., and Deutsch, W.A. (2009). Ribosomal protein S3: A multi-functional protein that interacts with both p53 and MDM2

through its KH domain. DNA Repair (Amst). *8*, 1215–1224.

Yang, K., Yang, J., and Yi, J. (2018). Nucleolar Stress: hallmarks, sensing mechanism and diseases. Cell Stress *2*, 125–140.

Yeganeh, M., and Hernandez, N. (2020). RNA polymerase III transcription as a disease factor. Genes Dev. *34*, 865–882.

Yeo, C.Q.X., Alexander, I., Lin, Z., Lim, S., Aning, O.A., Kumar, R., Sangthongpitag, K., Pendharkar, V., Ho, V.H.B., and Cheok, C.F. (2016). p53 Maintains Genomic Stability by Preventing Interference between Transcription and Replication. Cell Rep. *15*, 132–146.

Zellweger, R., Dalcher, D., Mutreja, K., Berti, M., Schmid, J.A., Herrador, R., Vindigni, A., and Lopes, M. (2015). Rad51-mediated replication fork reversal is a global response to genotoxic treatments in human cells. J. Cell Biol. *208*, 563–579.

Zemp, I., and Kutay, U. (2007). Nuclear export and cytoplasmic maturation of ribosomal subunits. FEBS Lett. *581*, 2783–2793.

Zhang, X., Wang, W., Wang, H., Wang, M.H., Xu, W., and Zhang, R. (2013). Identification of ribosomal protein S25 (RPS25)-MDM2-p53 regulatory feedback loop. Oncogene *32*, 2782–2791.

Zhang, Y., Wang, J., Yuan, Y., Zhang, W., Guan, W., Wu, Z., Jin, C., Chen, H., Zhang, L., Yang, X., et al. (2010). Negative regulation of HDM2 to attenuate p53 degradation by ribosomal protein L26. Nucleic Acids Res. *38*, 6544–6554.

Zhao, R., Gish, K., Murphy, M., Yin, Y., Notterman, D., Hoffman, W.H., Tom, E., Mack, D.H., and Levine, A.J. (2000). The transcriptional program following p53 activation. Cold Spring Harb. Symp. Quant. Biol. *65*, 475–482.

Zhao, Y., Yu, H., and Hu, W. (2014). The regulation of MDM2 oncogene and its impact on human cancers. Acta Biochim. Biophys. Sin. (Shanghai). *46*, 180–189.

Zhu, Y., Poyurovsky, M. V., Li, Y., Biderman, L., Stahl, J., Jacq, X., and Prives, C. (2009). Ribosomal Protein S7 Is Both a Regulator and a Substrate of MDM2. Mol. Cell *35*, 316–326.

7. ACKNOWLEDGMENTS

I am very grateful to Matthias since he gave me the opportunity to do my PhD in his lab and always let me follow my ideas and gave me intellectual freedom. Thank you for believing in me, for the passionate scientific discussions and for always supporting me during up and downs. I hope I have been able to return your kindness and support with my work. I would also like to thank the members of my thesis committee, Prof. Papantonis and Prof. Bohnsack, for the helpful advice and discussions. Next I would like to thank all the members of the Molecular Oncology department. Special thanks to my PhD buddy Luisa Klemke, I can't even begin to describe the amount of support, scientific advice, human warmth and simply awesomeness that Luisa gave me during these past few years. I wouldn't be half the scientist and person without her, and I am truly grateful to have such an amazing person in my life. Secondly, Celeste Giansanti with whom I have worked in very close contact for one of my projects. We had lots of fun together sharing ideas, discussing science, and coming up with sci-fi mechanism to explain our results! It truly made working during a pandemic more bearable. I would like to thank all my students, especially Jennifer and Kester. Jennifer did her master thesis with me, and it was truly a pleasure working together and supervising her. She did an incredible job and helped me a lot, and I am truly amazed by her accuracy and care. Kester did his medical thesis in the lab, and I enjoyed helping and having scientific discussion with him. He is the most hard-working person I ever met, but I really hope he won't keep working 60-70 hours per week in the future! I also want to thank Karina, Christina, Daniel, Camilo which were doing their lab rotation with me. I never thought I would enjoy teaching so much, but supervising students really helped me not only by providing results, but also for finding new motivation and passion for the topic. I want to thank Antje, you are really the lab mom and you are always taking care of all of us. You really helped me a lot during my PhD, and I will be forever grateful. And of course, every member of the molecular oncology department: Kim for the nice talks in the office, Ramona for the scientific discussions, Josephine for the deep talks in the FACS room, the PhD students from the previous and new generations, the lab technicians, and secretaries.

When I started my PhD back in 2017, I thought it was the biggest challenge I ever took on in my life. Little did I know then that I would have need to finish my PhD in a middle of a global pandemic. My friends and family were essential for me to overcome these challenges. I want to thank my sister Giulia, we talk every day and I am so happy to have a big sister that is always there for me. I know that no matter what, we will always have each other back, and I love her very much. I am grateful to my parents, for always believing in me and for giving me the opportunity to have such an international education. I feel very privileged to have such a

supportive family. Daniel is an angel in my life, he has been always by my side with his infinite patience. He always knows when I need a hug, some advice, or a snack. I feel incredibly lucky to have met him, and I hope I can support him during his PhD the same ways he has supported me! My cat Arya is also part of the family, and since I found her in the Romanian countryside back in 2018, she has been very important in my life. My friends Rashi, Salma and Laura. We have been a tight group for the past 6 years, supported each other during the hard times during PhD. We cried, laughed, travelled, got food poisoning together in Delhi…. I can safely say that we have shared quite a lot! Now this journey is ending, but I know they will always be there, no matter where in the world.